Eur. Phys. J. C (2024) 84:818
https://doi.org/10.1140/epjc/s10052-024-12975-4

THE EUROPEAN PHYSICAL JOURNAL C

Regular Article

Search for leptoquark pair production decaying into $te^-\bar{t}e^+$ or $t\mu^-\bar{t}\mu^+$ in multi-lepton final states in pp collisions at $\sqrt{s} = 13$ TeV with the ATLAS detector

ATLAS Collaboration[⋆]

CERN, 1211 Geneva 23, Switzerland

Received: 3 July 2023 / Accepted: 2 June 2024

Abstract A search for leptoquark pair production decaying into $te^-\bar{t}e^+$ or $t\mu^-\bar{t}\mu^+$ in final states with multiple leptons is presented. The search is based on a dataset of pp collisions at $\sqrt{s} = 13$ TeV recorded with the ATLAS detector during Run 2 of the Large Hadron Collider, corresponding to an integrated luminosity of 139 fb^{-1}. Four signal regions, with the requirement of at least three light leptons (electron or muon) and at least two jets out of which at least one jet is identified as coming from a b-hadron, are considered based on the number of leptons of a given flavour. The main background processes are estimated using dedicated control regions in a simultaneous fit with the signal regions to data. No excess above the Standard Model background prediction is observed and 95% confidence level limits on the production cross section times branching ratio are derived as a function of the leptoquark mass. Under the assumption of exclusive decays into te^- ($t\mu^-$), the corresponding lower limit on the scalar mixed-generation leptoquark mass $m_{\mathrm{LQ}^{\mathrm{d}}_{\mathrm{mix}}}$ is at 1.58 (1.59) TeV and on the vector leptoquark mass $m_{\tilde{U}_1}$ at 1.67 (1.67) TeV in the minimal coupling scenario and at 1.95 (1.95) TeV in the Yang–Mills scenario.

Contents

1 Introduction

The similarities in the structure of the lepton and quark sectors of the Standard Model (SM) raise the possibility of an existing underlying symmetry connecting the two sectors. Consequently, many extensions of the SM of particle physics contain leptoquarks (LQ) [1–7], hypothetical particles that carry non-zero baryon and lepton quantum numbers and are charged under all SM gauge groups. In particular, LQs are triplets with respect to the strong interaction, and have fractional electric charge. A LQ state can have either spin 0 (scalar LQ) or spin 1 (vector LQ), and both are considered in this paper. Due to their quantum numbers, LQs couple simultaneously to both quarks and leptons, enabling direct transitions between the two. Consequently, LQs can mediate processes that violate lepton-flavour universality, and were proposed [8–13] as an explanation for measurements of B-meson decays that exhibit deviations from the SM predictions [14–18]. Contributions from a scalar LQ could also account [9,19–21] for the longstanding discrepancy between the measured and the predicted anomalous magnetic moment of the muon $(g-2)_\mu$ [22,23].

In pp collisions at the Large Hadron Collider (LHC), pairs of LQs are mainly produced via gluon–gluon fusion and quark–antiquark annihilation, mediated by the strong interaction. There are also lepton-mediated t- and u-channel production processes that depend on the coupling strength (λ) of

⋆ e-mail: atlas.publications@cern.ch

Published online: 14 August 2024

the quark–lepton–LQ interaction. However, these contributions can usually be neglected in the scenario where LQs couple preferentially to third-generation quarks, since the latter would be required in the initial state. The LQ pair-production cross section can therefore, to a very good approximation, be taken to depend only on the assumed value of the LQ mass (m_{LQ}) for a given LQ spin and centre-of-mass energy [24,25]. Single LQ production in association with a lepton is also possible, but the cross section depends on the strength of the quark–lepton–LQ interaction and it is not considered in this paper.

Most searches [26–40] by the ATLAS and CMS experiments at the LHC have targeted the scenario where LQs only interact with leptons and quarks of the same generation as suggested by the models in Ref. [41]. However, the possibility of flavour-off-diagonal couplings should also be explored as part of a broad and exhaustive LQ search programme. While the simultaneous coupling of a LQ to more than one generation of quarks or to more than one generation of leptons would lead to quark and lepton flavour violation ($K-\bar{K}$ mixing, $\mu \to e\gamma$), the coupling of LQ to a quark from one generation and to a lepton from another one can still preserve the flavour symmetries [42]. The cross-generational LQ search has gained additional interest given the fact that explanations of the B-meson and $(g-2)_\mu$ anomalies require LQs with couplings to quarks of the second or third generation and leptons of the first, second or third generation [43,44].

The ATLAS Collaboration has performed searches for pair production of both scalar and vector LQs. The different ATLAS search results are presented as a function of the LQ mass and the branching ratio into charged leptons ($\mathcal{B}$). In the case of scalar LQs interacting with mixed quark and lepton generation ($\mathrm{LQ}_{\mathrm{mix}}$), two different types were considered: up-type LQs coupling to a third generation quark (top-quark t or b-quark b) and a first or second generation lepton ($\mathrm{LQ}^{\mathrm{u}}_{\mathrm{mix}} \to b\ell^+$ or $t\bar{\nu}$), with $\ell = e, \mu$, and down-type LQs ($\mathrm{LQ}^{\mathrm{d}}_{\mathrm{mix}} \to t\ell^-$ or $b\nu$). The $\mathrm{LQ}^{\mathrm{u}}_{\mathrm{mix}}$ and $\mathrm{LQ}^{\mathrm{d}}_{\mathrm{mix}}$ have fractional electric charges of $+2/3e$ and $-1/3e$, respectively. In the case of vector LQ, the iso-singlet LQ (U_1) carrying electric charge $+2/3e$ with two different coupling scenarios to the SM gauge bosons was considered: the minimal (U_1^{min}) and the Yang–Mills (U_1^{YM}) coupling scenarios. Using the full Run 2 dataset, corresponding to 139 fb^{-1} of pp collisions at $\sqrt{s} = 13$ TeV, these searches have excluded at the 95% confidence level (CL) masses below 1.8 TeV (1.7 TeV) for $\mathrm{LQ}^{\mathrm{u}}_{\mathrm{mix}}$ [29], and below 1.48 TeV (1.47 TeV) for $\mathrm{LQ}^{\mathrm{d}}_{\mathrm{mix}}$ [45], assuming $\mathcal{B} = 1$ into electrons (muons). A dedicated search optimised for $\mathcal{B} = 0.5$ [46] has probed a wide range of scenarios, including both $\mathrm{LQ}^{\mathrm{u}}_{\mathrm{mix}}$ and $\mathrm{LQ}^{\mathrm{d}}_{\mathrm{mix}}$, as well as U_1^{min} and U_1^{YM}. The corresponding mass exclusions for scalar LQs range from 1.37 TeV to 1.46 TeV, whereas for U_1^{min} and U_1^{YM} they range from 1.62 TeV to 1.98 TeV. The CMS Collaboration has also published searches for pair production of scalar LQs decaying into a top-quark and an electron or a muon [47,48], achieving comparable or lower mass exclusions than ATLAS.

This paper presents a dedicated search for the pair production of $\mathrm{LQ}^{\mathrm{d}}_{\mathrm{mix}}$ in the $t\ell^-\bar{t}\ell^+$ decay mode (denoted as $t\ell t\ell$ hereafter), where same-flavour leptons from the $\mathrm{LQ}^{\mathrm{d}}_{\mathrm{mix}}$ decay are considered (denoted as $tete$ and $t\mu t\mu$), and the top-quark pair is required to decay into a final state with one or two leptons as illustrated in Fig. 1. This selection is orthogonal to that used by Ref. [45], where the top-quark pair is required to decay into a final state with jets, and therefore provides additional sensitivity to probe $\mathrm{LQ}^{\mathrm{d}}_{\mathrm{mix}}$. The multi-lepton final state in this analysis takes advantage of the similar top-quark pair branching fraction to final states with at least one lepton compared to those with jets, and of the suppression of SM background processes when selecting events with multiple leptons. Figure 1a, b illustrate the signal processes targeted in this analysis. These decay modes are hereafter indicated without labelling the particle and anti-particle charges. This search uses the full Run 2 dataset of pp collisions at $\sqrt{s} = 13$ TeV recorded with the ATLAS detector and corresponding to an integrated luminosity of 139 fb^{-1}. Events are selected if they have at least two light leptons (electron or muon), and at least two jets, at least one of which must be identified as originating from B-hadrons. Three final states defined by the multiplicity of lepton candidates, 2ℓ with same electric charge (2ℓSS), 3ℓ, and 4ℓ, are considered in the analysis. Each of them is split into multiple event categories. Signal-enriched event categories require at least three leptons and exploit the presence of energetic final-state objects, whereas signal-depleted regions are also defined containing 2ℓSS events.

The composition of background processes varies among the signal-enriched event categories, however the main background contributions arise from SM processes yielding multiple leptons in the final state, such as $t\bar{t}$ production in association with a vector boson and diboson production. In those event categories the final discriminating variable used is the scalar sum of the transverse momenta of all selected leptons, the selected jets and the missing transverse momentum. Higher values of this variable are expected for the signal compared to the background. The rest of the event categories are designed to be enriched in the most relevant backgrounds. A maximum-likelihood fit is performed across event categories to search for the signal and constrain several leading backgrounds simultaneously. This search is performed in the $\mathrm{LQ}^{\mathrm{d}}_{\mathrm{mix}}$ mass range between 1 TeV and 1.9 TeV. The results are also interpreted for the first time in the context of an iso-singlet vector LQ with electric charge $+5/3e$ [41]. This vector LQ has right-handed coupling to a top quark and a charged lepton and is labelled as $\tilde{U}_1$. The mass range consid-

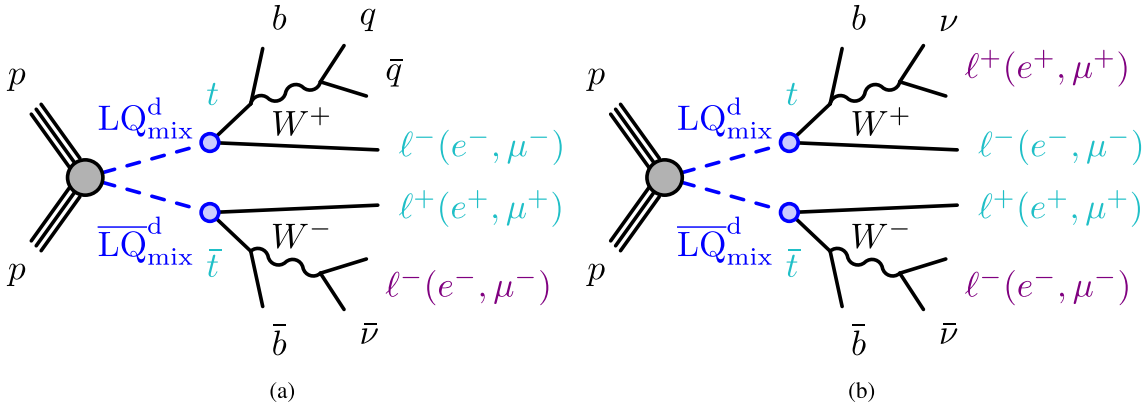

Fig. 1 Signal diagrams of the decay modes of pair-produced scalar leptoquarks LQ^{d}_{mix} targeted in this analysis: **a** 3ℓ and **b** 4ℓ. Decays of the W-boson to an electron or a muon of via a τ-lepton ($W \to \tau\nu \to \ell\nu\nu$) are also considered. The vector leptoquarks $\tilde{U}_1$ production and decay modes can be described with analogous diagrams

ered is between 1 TeV and 2 TeV for two different coupling assumptions with other gauge bosons.

2 ATLAS detector

The ATLAS detector [49] at the LHC covers nearly the entire solid angle around the collision point.[1] It consists of an inner tracking detector surrounded by a thin superconducting solenoid, electromagnetic and hadron calorimeters, and a muon spectrometer incorporating three large superconducting air-core toroidal magnets.

The inner-detector system (ID) is immersed in a 2T axial magnetic field and provides charged-particle tracking in the range $|\eta| < 2.5$. The high-granularity silicon pixel detector covers the vertex region and typically provides four measurements per track, the first hit normally being in the insertable B-layer (IBL) installed before Run 2 [50,51]. It is followed by the silicon microstrip tracker (SCT), which usually provides eight measurements per track. These silicon detectors are complemented by the transition radiation tracker (TRT), which enables radially extended track reconstruction up to $|\eta| = 2.0$. The TRT also provides electron identification information based on the fraction of hits (typically 30 in total) above a higher energy-deposit threshold corresponding to transition radiation.

The calorimeter system covers the pseudorapidity range $|\eta| < 4.9$. Within the region $|\eta| < 3.2$, electromagnetic calorimetry is provided by barrel and endcap high-granularity lead/liquid-argon (LAr) calorimeters, with an additional thin LAr presampler covering $|\eta| < 1.8$ to correct for energy loss in material upstream of the calorimeters. Hadron calorimetry is provided by the steel/scintillator-tile calorimeter, segmented into three barrel structures within $|\eta| < 1.7$, and two copper/LAr hadron endcap calorimeters. The solid angle coverage is completed with forward copper/LAr and tungsten/LAr calorimeter modules optimised for electromagnetic and hadronic energy measurements respectively.

The muon spectrometer (MS) comprises separate trigger and high-precision tracking chambers measuring the deflection of muons in a magnetic field generated by the superconducting air-core toroidal magnets. The field integral of the toroids ranges between 2.0 and 6.0T m across most of the detector. Three layers of precision chambers, each consisting of layers of monitored drift tubes, cover the region $|\eta| < 2.7$, complemented by cathode-strip chambers in the forward region, where the background is highest. The muon trigger system covers the range $|\eta| < 2.4$ with resistive-plate chambers in the barrel, and thin-gap chambers in the endcap regions.

Interesting events are selected by the first-level trigger system implemented in custom hardware, followed by selections made by algorithms implemented in software in the high-level trigger [52]. The first-level trigger accepts events from the 40MHz bunch crossings at a rate below 100kHz, which the high-level trigger further reduces in order to record events to disk at about 1kHz.

An extensive software suite [53] is used in the reconstruction and analysis of real and simulated data, in detector oper-

[1] ATLAS uses a right-handed coordinate system with its origin at the nominal interaction point (IP) in the centre of the detector and the z-axis along the beam pipe. The x-axis points from the IP to the centre of the LHC ring, and the y-axis points upwards. Cylindrical coordinates (r, ϕ) are used in the transverse plane, ϕ being the azimuthal angle around the z-axis. The pseudorapidity is defined in terms of the polar angle θ as $\eta = -\ln\tan(\theta/2)$. Angular distance is measured in units of $\Delta R \equiv \sqrt{(\Delta\eta)^2 + (\Delta\phi)^2}$.

ations, and in the trigger and data acquisition systems of the experiment.

3 Data and simulated event samples

A dataset of pp collisions at $\sqrt{s} = 13$ TeV collected by the ATLAS experiment during 2015–2018 and corresponding to an integrated luminosity of 139 fb^{-1} is used. The number of additional pp interactions per bunch crossing (pile-up) in this dataset ranges from about 8 to 70, with an average of 34. Only events recorded under stable beam conditions and for which all relevant detector subsystems were known to be in a good operating condition are used. Events are selected with a combination of lepton triggers, as discussed in Sect. 5.

Monte Carlo (MC) simulation samples were produced for the different signal and background processes. All simulated samples, except those produced with the SHERPA [54] event generator, utilised EVTGEN 1.2.0 [55] to model the decays of heavy-flavour hadrons. Pile-up was modelled by overlaying the simulated hard-scattering event with inelastic pp events generated with PYTHIA 8.186 [56] using the NNPDF2.3$_{\text{LO}}$ set of parton distribution functions (PDF) [57] and the A3 set of tuned parameters [58] (referred to as the 'tune'). The MC samples were produced using either the detailed ATLAS detector simulation [59] based on GEANT4 [60] or a faster simulation where the full GEANT4 simulation of the calorimeter response is replaced by a parameterisation of the shower shapes [59]. In both cases, the simulated events were processed through the same reconstruction software as the dataset of pp collisions. Corrections were applied to the simulated events so that the particle candidates' selection efficiencies, energy scales and energy resolutions match those determined from data control samples. The simulated samples are normalised to their cross sections, and generated to the highest order available in perturbation theory.

Simulated events with pair-produced scalar LQs were generated at next-to-leading-order (NLO) in quantum chromodynamics (QCD) with MADGRAPH5_AMC@NLO 2.6.0 [61], using the method described in Ref. [62], in which fixed-order NLO QCD calculations [63,64] are interfaced to PYTHIA 8.230 [56] for the parton shower (PS) and hadronisation. Parton luminosities are provided by the five-flavour scheme `NNPDF3.0nlo` [65] PDF set with $\alpha_s = 0.118$ and the underlying event (UE) is modelled with the A14 tune [66]. MADSPIN [67] was used for the decay of the scalar LQ$^{\text{d}}_{\text{mix}}$. The QCD pair production of LQ$^{\text{d}}_{\text{mix}}$ does not depend on the coupling parameter λ to the first order, therefore the choice of this parameter is arbitrary for the production. However, the decay width depends on λ and a narrow width is necessary for on-shell production to dominate [68,69]. A small value ($\lambda = 0.3$) of this parameter was set, resulting in a narrow width of about 0.2% of its mass. The charge of the scalar LQ$^{\text{d}}_{\text{mix}}$ is set to $-1/3e$, allowing decays into either $t\ell^-$ or $b\bar{\nu}$. Samples were generated for masses in the range of 1.0 TeV to 1.9 TeV in 100 GeV steps. The LQ pair-production cross sections were obtained from the calculation of the pair production of supersymmetric partner of top quarks assuming that all other supersymmetric particles are heavier, since the production modes of this process are the same. These cross sections are computed at approximate next-to-next-to-leading-order (NNLO) in QCD with resummation of next-to-next-to-leading logarithmic (NNLL) soft gluon terms [70–73]. The cross sections do not include lepton t-channel contributions, which are neglected in Ref. [62] and may lead to corrections at the percent level [25]. The cross section values range from 6.8 fb to 0.02 fb for the LQ$^{\text{d}}_{\text{mix}}$ mass range considered in this search.

The vector $\tilde{U}_1$ signal samples were generated at leading-order (LO) in QCD with MADGRAPH5_AMC@NLO 2.8.1 and the `NNPDF2.3lo` PDF set using the Boston model [42,74], and matched to PYTHIA 8.244 [56] with A14 tune. The $\tilde{U}_1$ is an isospin singlet, has an electrical charge of $+5/3e$ and can couple to a top quark and a charged lepton [68]. The coupling parameter λ was also set to 0.3. The model introduces a new massive coloured gauge boson known as heavy gluon (g'). There are two main coupling parameters considered for this production, labelled as κ_t and κ_s. The κ_t represents the coupling of the gluon to $\tilde{U}_1$ while κ_s represents the coupling of the heavy gluon g' to $\tilde{U}_1$. The $\kappa_t = \kappa_s = 0$ setup corresponds to the Yang–Mills coupling scenario ($\tilde{U}_1^{\text{YM}}$), whereas the $\kappa_t = \kappa_s = -1$ setup, referred to as the minimal coupling scenario ($\tilde{U}_1^{\text{min}}$), corresponds to the scenario where the Yang–Mills couplings are turned off [42]. The vector leptoquark samples were generated setting the g' mass to zero, where each $\tilde{U}_1$ decays into a top quark and a charged lepton (electron or muon), for masses in the range of 1.0 TeV to 2 TeV in steps of 100 GeV. The corresponding cross section values range from 19.7 fb to 0.02 fb (105 fb to 0.1 fb) for the minimal (Yang–Mills) coupling scenarios.

The sample used to model the $t\bar{t}W$ ($t\bar{t}Z/\gamma^*$) background process was generated using SHERPA 2.2.10 (SHERPA 2.2.11) [75]. The matrix element (ME) was calculated for up to one (zero) additional parton at NLO in QCD and up to two partons at LO in QCD using COMIX [76] and OPENLOOPS [77] and merged with the SHERPA parton shower [78] using the MEPS@NLO prescription [79]. A CKKW merging scale of 30 GeV was used for the $t\bar{t}W$ sample. These samples are generated using the `NNPDF3.0nnlo` [65] PDF set. Both the factorisation and renormalization scales are set to $\mu_R = \mu_F = H_{\text{T}}/2$ in the $t\bar{t}W$ sample, where H_{T} is defined as the scalar sum of the transverse masses $\sqrt{p_{\text{T}}^2 + m^2}$ of all final state particles. The LO $t\bar{t}W$ electroweak (EW) contributions are obtained from a dedicated sample simulated with SHERPA 2.2.10 and are added together with the NLO QCD

sample described above. The invariant mass of the lepton pair ($m_{\ell^+\ell^-}$) in the $t\bar{t}Z/\gamma^*$ sample is set to be greater than 1 GeV. The complete $t\bar{t}W$ simulation is normalised to the total cross section of $\sigma(t\bar{t}W) = 614.7$ fb that comes from the SHERPA configuration outlined above considering NLO QCD and NLO EWK effects, based on a similar strategy as used in Ref. [80]. The $t\bar{t}Z/\gamma^*$ sample is normalised to the cross section $\sigma(t\bar{t}Z/\gamma^*) = 839$ fb calculated at NLO QCD and NLO EW accuracy using MADGRAPH5_AMC@NLO as reported in Ref. [81] and scaled by an off-shell correction estimated at one-loop level in α_s.

Diboson (WZ, ZZ and WW including off-shell productions) background processes are simulated with SHERPA 2.2.2 [75]. The matrix element was calculated using COMIX [76] and OPENLOOPS [77] with NLO accuracy in QCD for up to one additional parton and at LO accuracy for up to three additional partons, and merged with the SHERPA using MEPS@NLO prescription [79]. The `NNPDF3.0nnlo` set of PDFs was used, along with the dedicated set of tuned parton-shower parameters developed by the SHERPA authors. The cross section of $\sigma(VV) = 104$ pb was computed by SHERPA 2.2.2.

Samples for $t\bar{t}H$, $t\bar{t}$, and single top production were generated using the NLO generator POWHEG- BOX [82–87] with `NNPDF3.0nlo` PDF set and interfaced with PYTHIA 8 with the A14 tune. The h_{damp} parameter, which controls the transverse momentum of the first additional emission beyond the Born configuration and therefore regulates the high-p_{T} radiation, is set to $3(m_t + m_{\bar{t}} + m_H)/4$ in the $t\bar{t}H$ sample and to $1.5m_t$ in the $t\bar{t}$ and single top samples, where m_t (m_H) denotes the mass of the top quark (Higgs boson).

A dedicated $t\bar{t}$ sample including relatively rare $t \to Wb\gamma^*(\to \ell^+\ell^-)$ radiative decays, $t\bar{t} \to W^+bW^-\bar{b}\ell^+\ell^-$, is generated using a ME calculated at LO in QCD and requiring $m_{\ell^+\ell^-} > 1$ GeV. In this sample the photon can be radiated from the top quark, the W boson, or the b-quark. Both the $t\bar{t}Z/\gamma^*$ and $t\bar{t} \to W^+bW^-\bar{b}\ell^+\ell^-$ samples are combined and together form the "$t\bar{t}Z$ (high mass)" sample. The contribution from internal photon conversions ($\gamma^* \to \ell^+\ell^-$) with $m_{\ell^+\ell^-} < 1$ GeV are modelled by QED multi-photon radiation via the PS in an inclusive $t\bar{t}$ sample and is referred to as "$t\bar{t}\gamma^*$ (LM)". Dedicated Z+jets samples containing electrons from material photon conversion ($\gamma \to e^+e^-$) or internal photon conversion are generated with POWHEG- BOX and interfaced with Pythia8 for the parton showering and fragmentation. These samples are used to model the data in control regions enriched in material and internal conversion electrons, as explained in Sect. 5.

The production of $t\bar{t}t\bar{t}$ events was modelled using the MADGRAPH5_AMC@NLO v2.6.2 generator that provides matrix elements at NLO in QCD with the `NNPDF3.1nlo` PDF set matched to PYTHIA 8.186 with the A14 tune.

Table 1 shows the configurations used in this analysis, with the samples in parentheses and in bold indicating those used to estimate the systematic uncertainties. Parton shower generator refers to the generator used for parton shower, hadronisation and underlying events. The remaining rare background contributions listed in this table are normalised using their NLO theoretical cross sections, except for the $t\bar{t}t$ process, for which a LO cross section is used.

4 Event reconstruction and object identification

Interaction vertices from the pp collisions are reconstructed from at least two tracks with transverse momentum (p_{T}) larger than 500 MeV that are consistent with originating from the beam collision region in the x–y plane. If more than one primary vertex candidate is found in the event, the candidate for which the associated tracks form the largest sum of squared p_{T} is selected as the hard-scatter primary vertex [91].

Electron candidates are reconstructed from energy clusters in the electromagnetic calorimeter matched to a track in the ID [92]. They are required to satisfy $p_{\text{T}} > 10$ GeV and $|\eta_{\text{cluster}}| < 2.47$, excluding the transition region between the endcap and barrel calorimeters ($1.37 < |\eta_{\text{cluster}}| < 1.52$). Loose and tight electron identification working points are used [92], based on a likelihood discriminant employing calorimeter, tracking and combined variables that provide separation between electrons and jets. The associated track of an electron candidate is required to have at least two hits in the pixel detector and seven hits total in the pixel and silicon-strip detectors combined. For the tight identification working point, one of these pixel hits must be in the innermost layer (or the next-to-innermost layer if the module traversed in the innermost layer is non-operational), and there must be no association with a vertex from a reconstructed photon conversion [93] in the detector material (denoted as 'material conversion' in this paper).

Muon candidates are reconstructed by combining tracks in the ID with tracks in the MS [94]. The resulting muon candidates are re-fitted using the complete track information from both detector systems [95]. They are required to satisfy $p_{\text{T}} > 10$ GeV and $|\eta| < 2.5$. Loose and medium muon identification working points are used [95]. Medium muon candidates with $p_{\text{T}} > 800$ GeV are in addition required to have hits in at least three MS stations (referred to as the 'high-p_{T} working point'), in order to maximise the momentum resolution for the muon track and thus suppress backgrounds with high-p_{T} muons arising from momentum mismeasurements.

Electron (muon) candidates are matched to the primary vertex by requiring the significance of their transverse impact parameter, d_0, satisfies $|d_0/\sigma(d_0)| < 5\,(3)$, where $\sigma(d_0)$ is the measured uncertainty in d_0. Additionally, the longitudinal

Table 1 The configurations used for event generation of signal and background processes. The samples used to estimate the systematic uncertainties are indicated in parentheses. An electroweak boson (W or Z/γ^*) is denoted as V for the associated production sample with Higgs boson. The matrix element order refers to the order in the strong coupling constant of the perturbative calculation. The "$t\bar{t}W$ (EW)" sample includes additionally next-to-leading-order electroweak corrections. Tune refers to the underlying-event tune of the parton shower generator. MG5_aMC refers to MadGraph5_aMC@NLO 2.2, 2.3, or 2.6; MePs@Nlo refers to the method used in Sherpa to match the matrix element to the parton shower. All samples include leading-logarithm photon emission, either modelled by the parton shower generator or by Photos [88]. The mass of the top quark (m_t) and SM Higgs boson were set to 172.5 GeV and 125 GeV, respectively

Process	Generator	ME order	Parton shower	PDF	Tune
$\mathrm{LQ}^{\mathrm{d}}_{\mathrm{mix}}\overline{\mathrm{LQ}}^{\mathrm{d}}_{\mathrm{mix}}$	MG5_aMC	NLO	Pythia 8.230	NNPDF3.0nlo	A14 [66]
$\tilde{U}_1\bar{\tilde{U}}_1$	MG5_aMC	LO	Pythia 8.244	NNPDF2.3lo	A14
$t\bar{t}W$	Sherpa 2.2.10	MePs@Nlo	Sherpa	NNPDF3.0nnlo	Sherpa default
	(MG5_aMC)	**(NLO)**	**(Pythia 8.210)**	**(NNPDF3.0nlo)**	**(A14)**
$t\bar{t}W$ (EW)	Sherpa 2.2.10	LO	Sherpa	NNPDF3.0nnlo	Sherpa default
	(MG5_aMC)	**(LO)**	**(Pythia 8.230)**	**(NNPDF3.0nlo)**	**(A14)**
Diboson, Triboson	Sherpa 2.2.2	MePs@Nlo	Sherpa	NNPDF3.0nnlo	Sherpa default
$t\bar{t}(Z/\gamma^* \to \ell^+\ell^-)$	Sherpa 2.2.11	MePs@Nlo	Sherpa	NNPDF3.0nnlo	Sherpa default
	(MG5_aMC)	**(NLO)**	**(Pythia 8.210)**	**(NNPDF3.0nlo)**	**(A14)**
$t\bar{t}H$	Powheg- BOX	NLO	Pythia 8.230	NNPDF3.0nlo	A14
	(Powheg-BOX)	**(NLO)**	**(Herwig7.0.4** [89]**)**	**(NNPDF3.0nlo)**	**(H7-UE-MMHT** [89]**)**
	(MG5_aMC)	**(NLO)**	**(Pythia 8.230)**	**(NNPDF3.0nlo)**	**(A14)**
$t\bar{t} \to W^+bW^-\bar{b}(\gamma* \to \ell^+\ell^-)$	MG5_aMC	LO	Pythia 8.212	NNPDF3.01o	A14
$t(Z/\gamma^*)$	MG5_aMC	NLO	Pythia 8.230	NNPDF2.3lo	A14
$tW(Z/\gamma^*)$	MG5_aMC	NLO	Pythia 8.212	NNPDF2.3lo	A14
$t\bar{t}$	Powheg- BOX	NLO	Pythia 8.230	NNPDF3.0nlo	A14
	(Powheg-BOX)	**NLO**	**(Herwig7.1.3)**	**(NNPDF3.0nlo)**	**(H7-UE-MMHT)**
$t\bar{t}t$	MG5_aMC	LO	Pythia 8.186	NNPDF2.3lo	A14
$t\bar{t}t\bar{t}$	MG5_aMC	NLO	Pythia 8.186	NNPDF3.1nlo	A14
Single top (t-, Wt-, s-channel)	Powheg- Box	NLO	Pythia 8.230	NNPDF3.0nlo	A14
$Z \to \ell^+\ell^-$	Sherpa 2.2.1	MePs@Nlo	Sherpa	NNPDF3.0nlo	Sherpa default
$Z \to \ell^+\ell^-(\gamma \to e^+e^-)$	Powheg- BOX	NLO	Pythia 8.186	CTEQ6L1nlo [90]	A14
$Z \to \ell^+\ell^-(\gamma* \to e^+e^-)$	Powheg- BOX	NLO	Pythia 8.240	CTEQ6L1nlo	A14
W+jets	Sherpa 2.2.1	MePs@Nlo	Sherpa	NNPDF3.0nlo	Sherpa default
VH	Powheg- BOX	NLO	Pythia 8.186	NNPDF3.0nlo	A14
$t\bar{t}W^+W^-$	MG5_aMC	LO	Pythia 8.186	NNPDF2.3lo	A14
tWH	MG5_aMC	LO	Pythia 8.235	NNPDF2.3lo	A14
$tHjb$	MG5_aMC	LO	Pythia 8.230	NNPDF2.3lo	A14

impact parameter, z_0, satisfies $|z_0 \sin\theta| < 0.5$ mm, where θ is the polar angle of the track.

To further suppress leptons from heavy-flavour hadron decays, misidentified jets, or photon conversions (collectively referred to as 'non-prompt leptons'), lepton candidates are also required to be isolated in the tracker and in the calorimeter. A track-based lepton isolation criterion is defined by calculating the quantity $I_R = \sum p_{\mathrm{T}}^{\mathrm{trk}}$, where the scalar sum includes all tracks (excluding the lepton candidate itself) within the cone defined by $\Delta R < R_{\mathrm{cut}}$ around the direction of the lepton. The value of R_{cut} is the smaller of r_{min} and $10\ \mathrm{GeV}/p_{\mathrm{T}}^{\ell}$, where r_{min} is set to 0.2 (0.3) for electron (muon) candidates and where p_{T}^{ℓ} is the lepton p_{T}. All lepton candidates must satisfy $I_R/p_{\mathrm{T}}^{\ell} < 0.15$. Additionally, electrons (muons) are required to satisfy a calorimeter-based isolation criterion: the sum of the transverse energy within a cone of size $\Delta R = 0.2$ around the lepton, after subtracting the contributions from pile-up and the energy deposit of the lepton itself, is required to be less than 20% (30%) of p_{T}^{ℓ}.

The selection criteria described above largely suppresses the contribution from non-prompt leptons. Additional requirements are applied in the 2ℓSS and 3ℓ categories to further suppress the main non-prompt lepton types. Non-prompt leptons from hadrons decays that contain bottom- and charm-quarks

(denoted as 'heavy-flavour (HF) non-prompt leptons') are further rejected using a boosted decision tree (BDT) discriminant, referred to as the non-prompt-lepton BDT [96]. This BDT discriminant is based on isolation and lifetime information associated with a jet reconstructed from tracks in the ID that matches the selected light lepton. Three exclusive working points (WPs) determined from the BDT score are used: *Tight*, *VeryTight*, and *Tight-not-VeryTight*. The *Tight* WP allows to select prompt-like leptons with an efficiency for muons (barrel/endcap electrons) that satisfy the calorimeter- and track-based isolation criteria of about 60% (60/70%) for $p_{\mathrm{T}} \sim 20$ GeV and reaches a plateau of 95% (95/90%) at $p_{\mathrm{T}} \sim 40$ (40/65) GeV. The prompt lepton efficiency of the *VeryTight* WP for muons (barrel/endcap electrons) that satisfy the calorimeter- and track-based isolation criteria is about 55% (55/60%) for $p_{\mathrm{T}} \sim 20$ GeV and reaches a plateau of 90% (85/83%) at $p_{\mathrm{T}} \sim 40$ (40/65) GeV. The corresponding rejection factor[2] against muons (electrons) from the decay of b-hadrons ranges from 33 to 50 (20 to 50) for the *Tight* WP, and from 50 to 100 (33 to 66) for the *VeryTight* WP, depending on p_{T} and η, after resolving ambiguities between overlapping reconstructed objects. The latter allows to select non-prompt-like leptons and is part of the event selection of the control regions enriched in HF non-prompt lepton background, as described in Sect. 6.

In order to further suppress electrons with incorrect charge assignment, a BDT discriminant based on calorimeter and tracking quantities [97] is used. An efficiency of approximately 96% in the barrel region and 81% in the endcaps is obtained, with rejection factors of 19 in the barrel region and 40 in the endcaps. Material ($\gamma \rightarrow e^+e^-$) and internal ($\gamma^* \rightarrow e^+e^-$) conversion candidates are identified based on a combination of requirements on the invariant mass of tracks and the radius from the reconstructed displaced vertex to the primary vertex. Material conversion candidates have a reconstructed displaced vertex with radius $r > 20$ mm that includes the track associated with the electron.[3] The invariant mass of the associated track and the closest (in $\Delta\eta$) opposite-charge track reconstructed in the silicon detector, calculated at the conversion vertex, is required to be less than 100 MeV. Internal conversion candidates, which correspond to the internal photon conversions (see Sect. 3), are required to fail the criteria for material conversions, but the invariant mass of the two tracks matched to the primary vertex is required to be less than 100 MeV.

After the initial categorisation based on loose leptons (corresponding to L), the most optimal lepton working point to further optimise the event selection is chosen depending on the main background processes and statistics of each category. The medium inclusive (M) lepton working point corresponds to leptons passing the *Tight* non-prompt-lepton BDT WP, whereas the medium exclusive (M_{ex}) lepton working point requires leptons to pass the *Tight-not-VeryTight* non-prompt-lepton BDT WP. The tight (T) lepton working point selects leptons passing the *VeryTight* non-prompt-lepton BDT WP and provides the highest purity of prompt leptons. The various choices can be seen for all categories used in this analysis in Sect. 5. All M, M_{ex}, and T electrons in the analysis are required to not be material nor internal conversion candidates, with the exception of the electron in the control regions enriched with internal and material conversions, denoted as e^*. The various lepton working points used in this analysis are summarised in Table 2.

The constituents for jet reconstruction are identified by combining measurements from both the ID and the calorimeter using a particle flow (PFlow) algorithm [98,99]. Jet candidates are reconstructed from these PFlow objects using the anti-k_t algorithm [100,101] with a radius parameter of $R = 0.4$. They are calibrated using simulation with corrections obtained from in situ techniques in data [99]. Only jet candidates with a $p_{\mathrm{T}} > 25$ GeV and within $|\eta| < 2.5$ are selected. In order to reduce the effect from pile-up, each jet with $p_{\mathrm{T}} < 60$ GeV and $|\eta| < 2.4$ is required to satisfy the "Tight" working point, correspondng to an efficiency of 95–97% depending on jet p_{T} of the Jet Vertex Tagger (JVT) [102] criteria used to identify the jets as originating from the selected primary vertex. A set of quality criteria is also applied to reject events containing at least one jet arising from non-collision sources or detector noise [103].

Jets containing b-hadrons are identified (b-tagged) via an algorithm [104,105] that uses a deep-learning neural network based on the distinctive features of the b-hadrons such as the impact parameters of tracks and the displaced vertices reconstructed in the ID. Additional input to this network is provided by discriminant variables constructed by a recurrent neural network [106], which exploits the spatial and kinematic correlations between tracks originating from the same b-hadron. For each jet, a value for the multivariate b-tagging discriminant is calculated. A jet is b-tagged if the b-tagging score is above a certain threshold, referred to as an operating point (OP). In this search, a jet is considered b-tagged if it passes the OP corresponding to 85% efficiency to tag a b-quark jet, with a light-jet[4] rejection factor of about 40, and a charm-jet (c-jet) rejection factor of about 3, as determined for jets with $p_{\mathrm{T}} > 20$ GeV and $|\eta| < 2.5$ in simulated $t\bar{t}$ events. Correction factors derived from dedicated data samples enriched in b-jets, c-jets, or light jets, are applied to the simulated samples [104,107,108].

[2] The rejection factor is defined as the reciprocal of the efficiency.

[3] The beampipe and insertable B-layer inner radii are 23.5 mm and 33 mm, respectively.

[4] 'Light jet' refers to a jet originating from the hadronisation of a light quark (u, d, s) or a gluon.

Table 2 Description of the loose inclusive (L), medium inclusive (M), medium exclusive (M_{ex}), and tight (T) lepton definitions. The electron e^* is required to fulfil, in addition to the corresponding lepton definition requirements, those corresponding to an internal or material conversion candidate

	e				μ			
Lepton definition	L	M	M_{ex}	T	L	M	M_{ex}	T
Isolation	Yes				Yes			
Non-prompt lepton WP	No	*Tight*	*Tight-not-VeryTight*	*VeryTight*	No	*Tight*	*Tight-not-VeryTight*	*VeryTight*
Identification	Loose	Tight			Loose	Medium		
Electron charge-misassignment veto	No	Yes			N/A			
Electron conversion candidate veto	No	Yes (except e^*)			N/A			
Transverse impact parameter significance $\lvert d_0\rvert/\sigma_{d_0}$	< 5				< 3			
Longitudinal impact parameter $\lvert z_0 \sin\theta\rvert$	< 0.5 mm							

The ambiguities among leptons satisfying the L criteria and selected jets are resolved by following an overlap removal procedure that takes into account whether a jet is b-tagged or not. If two electrons are closer than $\Delta R = 0.1$, only the one with the higher p_{T} is considered. If an electron and a muon overlap within $\Delta R = 0.1$, the muon is rejected if it is reconstructed from a track and calorimeter deposits consistent with a minimum ionising particle (i.e. calo-tagged), else the electron is rejected. If an electron and a selected jet are found within $\Delta R < 0.2$, the jet is rejected if it is not b-tagged[5] or if it has $p_{\mathrm{T}} > 200$ GeV. Muons are required to be separated by $\Delta R > 0.4$ from any jet that is ghost-associated [109] to it. If the jet satisfying the $\Delta R < 0.4$ requirement is not a b-tagged jet and contains less than three tracks with $p_{\mathrm{T}} > 500$ MeV, the overlapping jet is rejected from the event, otherwise, the muon is rejected. If the overlapping jet is b-tagged, the muon is rejected. A lepton lying within a variable-size cone depending on the lepton p_{T} and with a maximum radius of $R = 0.4$ around a selected jet that survived all previous overlap criteria is rejected.

The missing transverse momentum $\vec{p}_{\mathrm{T}}^{\,\mathrm{miss}}$ (with magnitude $E_{\mathrm{T}}^{\mathrm{miss}}$) is defined as the negative vector sum of the p_{T} of all selected and calibrated objects in the event, including a term to account for the momentum from soft particles in the event that are not associated with any of the selected objects [110]. This soft term is calculated from inner-detector tracks matched to the selected primary vertex, which makes it more resilient to contamination from pile-up interactions.

5 Search strategy

This search targets primarily scalar $\mathrm{LQ}^{\mathrm{d}}_{\mathrm{mix}}$ pair production where each $\mathrm{LQ}^{\mathrm{d}}_{\mathrm{mix}}$ decays into te or $t\mu$. In each final state, $tete$ or $t\mu t\mu$, events contain two light leptons from the $\mathrm{LQ}^{\mathrm{d}}_{\mathrm{mix}}$ decays, plus possibly additional leptons from the top-quark(s) decay chain. Additionally, the final state comprises two b-jets from the top-quark decays, and may contain additional light-jets from initial- or final-state radiations or from a hadronically decaying W boson in one of the top-quark decays. The presence of at least three leptons in the signal-enriched event categories is exploited to substantially reduce the SM background and to improve the search sensitivity. This also makes this search orthogonal to a previous ATLAS search [45] with two oppositely charged light leptons, and thus allow for an eventual combination. The analysis channels are sub-divided into different event categories depending on the multiplicity of light leptons and the sign of their electric charges. A maximum-likelihood fit is performed across all event categories to search for the signal and constrain several leading backgrounds simultaneously. The kinematic reconstruction of top quarks and consequently of the LQ is difficult with multiple light leptons and neutrino(s) in the selected events. The decay of a pair of massive LQs results in energetic final state objects. Therefore the effective mass (m_{eff}), defined as the sum of p_{T} of light leptons, jets, and the $E_{\mathrm{T}}^{\mathrm{miss}}$, is chosen as the final discriminant due to its power to discriminate signal against background in the search channels. The results of the search are also interpreted for the vector $\tilde{U}_1$ models for each decay mode ($tete$ or $t\mu t\mu$) of the LQ pair.

[5] For the overlap removal, a jet is considered b-tagged if it passes the 70% working point. However, the choice of the b-tagging working point does not have a sizeable impact on the signal acceptance.

5.1 Event selection

A combination of lepton triggers [111–113], which are based on electron and muon signatures, are used for the events selection. Single-electron (muon) triggers are required to have an electron (muon) satisfying certain identification requirements and with a p_{T} above a certain threshold. For the data collected in 2015, the p_{T} thresholds are 24 GeV, 60 GeV and 120 GeV for the single-electron triggers and 20 GeV and 50 GeV for the single-muon triggers. For the data collected during 2016–2018, the thresholds were raised slightly to 26 GeV, 60 GeV, and 140 GeV for the single-electron triggers and 26 GeV and 50 GeV for the single-muon triggers. The electron identification criteria are relaxed for the higher p_{T} threshold single-electron triggers. Single-lepton triggers with low p_{T} threshold and lepton isolation requirements are combined in a logical OR with the high p_{T} threshold triggers without isolation requirements. The dielectron trigger requires two electrons satisfying loose identification with p_{T} threshold of 12 GeV in 2015, 17 GeV in 2016, and 24 GeV in 2017 and 2018. The dimuon trigger requires two muons with asymmetric p_{T} thresholds of 8 GeV and 18 GeV (8 GeV and 22 GeV) in the 2015 (2016–2018) data period(s). The electron+muon trigger requires events to have an electron candidate satisfying loose identification with a p_{T} threshold of 17 GeV and a muon candidate with a p_{T} threshold of 14 GeV for all data-taking periods. Events are selected using the logical OR of the single-lepton and dilepton triggers.

Events selected by the trigger are required to further satisfy basic preselection requirements. They must have at least one primary vertex candidate. Events are required to contain at least two leptons satisfying the L criteria (see Sect. 4) with $p_{\mathrm{T}} > 10$ GeV. The selected light leptons are required to match, with $\Delta R < 0.15$, the corresponding leptons reconstructed by the trigger and to have a p_{T} exceeding the trigger p_{T} threshold by 1 GeV. Furthermore, two or more jets with $p_{\mathrm{T}} > 25$ GeV must be present in the event. The trigger requirement has an efficiency of 99.9% for signal events satisfying the preselection requirements.

5.2 Event categorisation

Three orthogonal final states, termed "channels", are analysed, defined by the multiplicity of leptons with $p_{\mathrm{T}} > 10$ GeV:

- 2ℓSS: two same-charge light leptons
- 3ℓ: three light leptons
- 4ℓ: at least four leptons

The channels are subdivided into different event categories optimised either to search for the signal (referred to as 'signal regions', or SR), to obtain improved background estimates (referred to as 'control regions', or CR), or to validate the estimated backgrounds (referred to as 'validation regions', or VR). Only SRs and CRs are included in the maximum-likelihood fit.

Signal and control regions are defined in the 3ℓ channels, whereas the 4ℓ (2ℓSS) channel contains only signal (control) regions. Validation regions close to the signal regions are additionally present in the 3ℓ and 4ℓ channels. Important background contributions to this analysis come from $t\bar{t}W$, $t\bar{t}Z$, and diboson processes. The 2ℓSS control regions are enriched in $t\bar{t}W$ and reducible background from non-prompt leptons, while the 3ℓ control regions are dominated by $t\bar{t}Z$, diboson, and the photon conversion backgrounds. Signal events are required to have at least three reconstructed leptons and the SRs are further optimised depending on the lepton multiplicity and kinematics of final-state objects. The signal-to-background ratio and the background compositions are different in the 3ℓ and 4ℓ channels. The 3ℓ SR targets LQ pair signal events where one of the top quarks decays leptonically, whereas the 4ℓ SR is enriched in LQ pair events where both top quarks decay into leptons. Figure 2 illustrates the categorisation and definition of the signal and control regions being fit simultaneously in this analysis.

The variable m_{eff} is powerful in discriminating between the signal and background as shown in Fig. 3a. An additional kinematic variable exploited in the optimisation of SRs is the invariant mass $m_{\ell\ell}^{\mathrm{min}}$, defined as the minimum of all combinations of dilepton-pair invariant masses (see Fig. 3b). The SR labelled as SR-e (SR-μ) is defined for the LQ pair search in the $tete$ ($t\mu t\mu$) channel. A total of 7 CRs are defined to provide background-rich samples that do not overlap with the SRs. The VRs are defined, using cuts on m_{eff} and $m_{\ell\ell}^{\mathrm{min}}$, to be kinematically closer to the SRs but orthogonal to the CRs in order to validate the extrapolation of the background estimation. The definitions of all of these regions is given below.

In the 2ℓSS channel, events contain two same-charge leptons with $p_{\mathrm{T}} > 20$ GeV and at least two jets, of which at least one is b-tagged. A CR enriched in $t\bar{t}W$ is defined by requiring both leptons to satisfy T identification criteria to suppress the contributions from non-prompt leptons. The contribution of $t\bar{t}W$ events in this CR region is more than 50% with negligible signal contamination. To estimate the non-prompt-lepton background in the $t\bar{t}W$ CR, two additional 2ℓSS CRs are defined. These regions are enriched in non-prompt leptons originating from heavy-flavour hadron decays. The M_{ex} identification criteria is applied to at least one of the two leptons in these regions in order to be orthogonal to the signal regions. Events fulfilling the criteria TM_{ex}, $M_{ex}T$, or $M_{ex}M_{ex}$ for the leading and subleading leptons in p_{T} are selected and further split according to the subleading lepton flavour. Additionally, the transverse mass of the leading lepton and the missing transverse energy, $m_T(\ell_0, E_{\mathrm{T}}^{\mathrm{miss}})$,

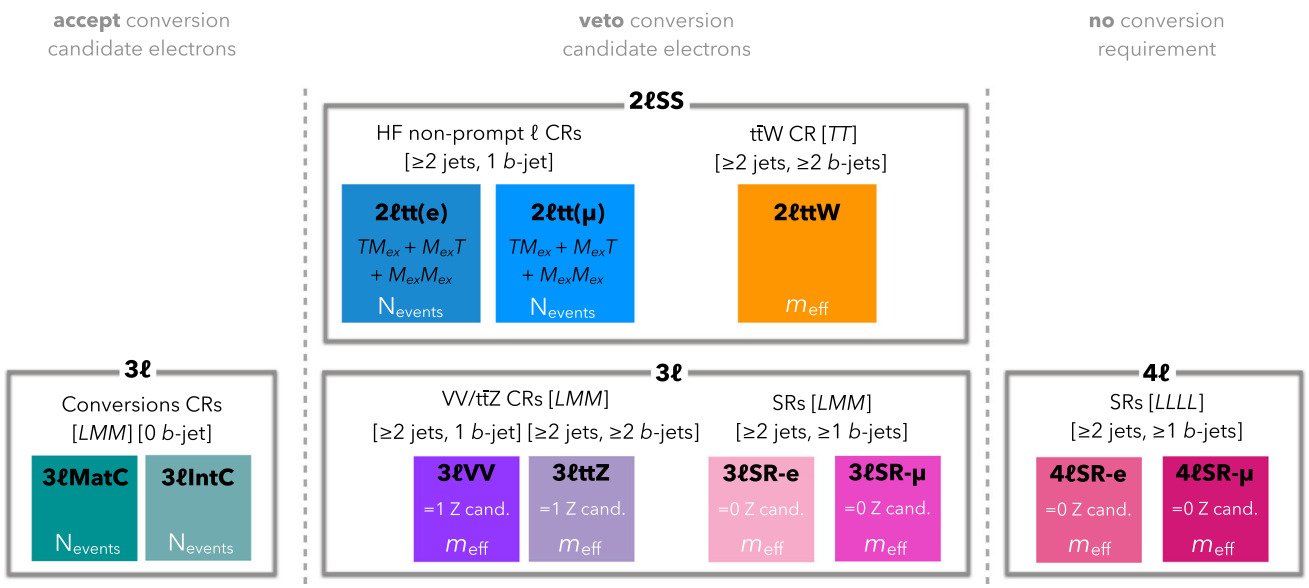

Fig. 2 Illustrative sketch of the definition of the signal and control regions. The corresponding observable used in the simultaneous fit, as described in Sect. 8, is given at the bottom of each region box

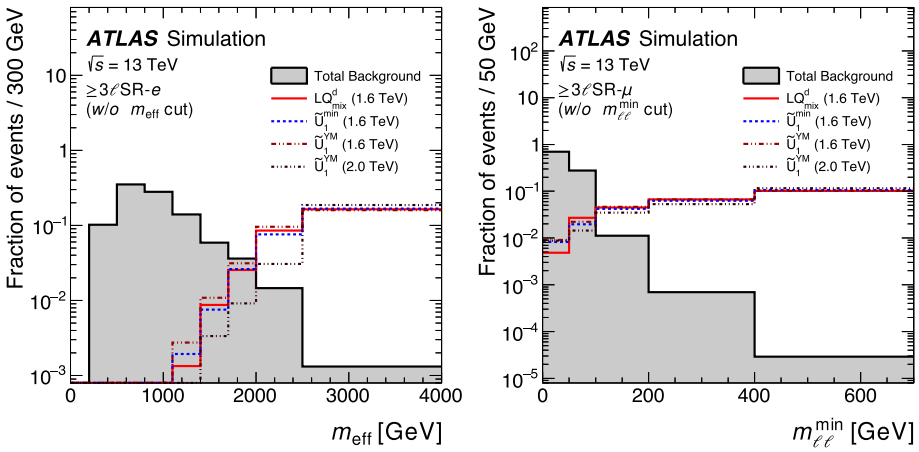

(a) (b)

Fig. 3 Comparison of the distribution of **a** m_{eff} in 3ℓSR-e or 4ℓSR-e region without an m_{eff} requirement, and **b** $m_{\ell\ell}^{\text{min}}$ in 3ℓSR-μ or 4ℓSR-μ region without a $m_{\ell\ell}^{\text{min}}$ requirement, between the total background (shaded histogram) and the various LQ signals. The shapes of these variables (m_{eff} and $m_{\ell\ell}^{\text{min}}$) are very similar in the electron and muon channels. The last bin in each distribution contains the overflow

Table 3 Summary of event categories for the 2ℓSS control regions. All events are required to satisfy preselection requirements. The exclusive medium lepton and tight lepton definitions (see Table 2) are denoted as M_{ex} and T, respectively. The lepton ordering of the e/μ selection and combination rows is based on the lepton p_{T}, with the first one corresponding to the leading lepton. The e internal (material) conversion veto refers to the requirement where the electron candidate fails to fulfil the criteria for the internal (material) photon conversion (see Sect. 4). Dashes (–) refer to cuts that are not applicable

	2ℓSS CRs		
	2ℓtt(e)	2ℓtt(μ)	2ℓttW
e/μ selection	$TM_{ex} \parallel M_{ex}T \parallel M_{ex}M_{ex}$		TT
e/μ combination	$ee/\mu e$	$\mu\mu/e\mu$	$ee/\mu\mu/e\mu/\mu e$
$\ell\ell$ charge	$++$ or $--$		
e internal conversion veto	Yes		
e material conversion veto	Yes		
Number of jets	≥ 2		
Number of b–jets	1		≥ 2
p_{T}^{ℓ} [GeV]	> 20		
$m_{\text{T}}(\ell_0, E_{\text{T}}^{\text{miss}})$ [GeV]	< 250		–

Table 4 Summary of control regions and signal regions categories in the 3ℓ channel. All events are required to satisfy the preselection requirements. The medium and loose lepton definitions (see Table 2) are labelled as M and L, respectively. Same-charge (opposite-charge) lepton pairs are also referred to as same-sign (opposite-sign) with abbreviation SS (OS), and the invariant mass of two same flavour and oppositely charged lepton pair is labelled as $m^{OS-SF}_{\ell^+\ell^-}$. The lepton with opposite-sign charge to that of the other two same-sign leptons is denoted ℓ_0, but is not necessarily the one with highest p_{T}; the remaining SS leptons are denoted ℓ_1 and ℓ_2. The e internal (material) conversion veto refers to the requirement where the electron candidate fails to fulfil the criteria for the internal (material) photon conversion (see Sect. 4). No validation regions are included in the fit. Dashes (–) refer to cuts that are not applicable

	3ℓ						
	CR				VR	SR	
	3ℓVV	3ℓttZ	3ℓIntC	3ℓMatC	3ℓVR	3ℓSR-e	3ℓSR-μ
e/μ selection	M (SS pair), L other						
e/μ combination	$3e$ / $2e1\mu$ / $2\mu1e$ / 3μ					$3e$ / $2e1\mu$	3μ / $2\mu1e$
Total charge	±1		–		±1		
e internal conversion	Yes		Inverted	Yes	Yes		
veto			(ℓ_1 or ℓ_2)	(ℓ_1 and ℓ_2)			
e material conversion	Yes		Yes	Inverted	Yes		
veto			(ℓ_1 and ℓ_2)	(ℓ_1 or ℓ_2)			
Number of jets	≥ 2		≥ 0		≥ 2		
Number of b–jets	1	≥ 2	0		≥ 1		
p^{ℓ}_{T} [GeV]	> 20 (SS pair), > 10 other				> 20		
$m^{OS-SF}_{\ell^+\ell^-}$ [GeV]	> 12						
$\lvert m^{OS-SF}_{\ell^+\ell^-} - m_Z\rvert$ [GeV]	< 10		> 10		> 10		
$\lvert m_{\ell\ell\ell} - m_Z\rvert$ [GeV]	–		< 10		–		
$m^{\mathrm{min}}_{\ell\ell}$ [GeV]	–				< 200	≥ 200	
m_{eff} [GeV]	–				–	≥ 500	

defined as $\sqrt{2E^{\mathrm{miss}}_{\mathrm{T}} p_{T,\ell_0}(1-\cos(\phi_{miss}-\phi_{\ell_0}))}$, is required to be lower than 250 GeV in the TM_{ex} and $M_{ex}T$ regions, in order to reduce the $t\bar{t}W$ contribution in these CRs. The region where the subleading lepton is an electron (muon) is labelled as 2ℓtt(e) (2ℓtt(μ)). The selections applied to these three CRs are given in Table 3.

In the 3ℓ channel, events are required to contain three leptons, where two same-charge leptons satisfy the M identification, and the remaining lepton passes the L identification. Furthermore, events contain one opposite-charge (OS) and same-flavour (SF) pair having invariant mass, $m^{OS-SF}_{\ell^+\ell^-} > 12$ GeV. Selected events fall into seven event categories: two SRs, four CRs and one VR. Regions enriched in diboson and $t\bar{t}Z$ background are defined by requiring $m^{OS-SF}_{\ell^+\ell^-}$ satisfying criteria compatible with a Z boson, $\lvert m^{OS-SF}_{\ell^+\ell^-} - m_Z\rvert < 10$ GeV, differing in the b-jet multiplicity requirement. These regions are labelled as 3ℓVV and 3ℓttZ for the diboson and $t\bar{t}Z$ CRs, respectively. Both CRs have respective event purities of more than 60%. Two additional control regions enriched in photon conversions from $Z \to \mu\mu\gamma^*(\to ee)$ are defined, according to the identification of the electron as a material conversion or internal conversion candidate, and are labelled as 3ℓMatC and 3ℓIntC, respectively. These regions are also required to have invariant mass of three leptons, $m_{\ell\ell\ell}$, compatible with a Z boson, $\lvert m_{\ell\ell\ell} - m_Z\rvert < 10$ GeV, while satisfying $\lvert m^{OS-SF}_{\ell^+\ell^-} - m_Z\rvert > 10$ GeV. Events consisting of three leptons with $p_{\mathrm{T}} > 20$ GeV, at least two jets, and at least one b-tagged jet are split into two SRs depending on the multiplicity of leptons with certain flavour. The 3ℓ SR-e (SR-μ) is characterised by at least two electrons (muons), and additionally has $m^{\mathrm{min}}_{\ell\ell} \geq 200$ GeV and $m_{\mathrm{eff}} \geq 500$ GeV. One VR is defined by removing the m_{eff} requirement and inverting the $m^{\mathrm{min}}_{\ell\ell}$ cut from the SR$-e$ and SR-μ criteria and merging the electron and muon channels. Selection criteria of the 3ℓ CRs, VR and SRs are summarised in Table 4.

In the 4ℓ channel, events are required to have four L identified leptons, at least two jets, and at least one b-tagged jet. Events with an OS and SF lepton pair compatible with a Z boson are vetoed. Selected events are split into two SRs and one VR. The 4ℓSR-e and 4ℓSR-μ are characterised by $m^{\mathrm{min}}_{\ell\ell} \geq 100$ GeV and $m_{\mathrm{eff}} \geq 500$ GeV, while 4ℓVR has $m^{\mathrm{min}}_{\ell\ell} < 100$ GeV, no requirement on m_{eff}, and has the electron and muon regions merged. Table 5 summarises the definitions of the SRs and VR in the 4ℓ channel.

The total signal acceptance $\times$ efficiency in the $tete$ ($t\mu t\mu$) selections ranges from 13.9% to 15.4% (13.3% to 17.5%) depending on the $\mathrm{LQ}^{\mathrm{d}}_{\mathrm{mix}}$ mass. Similar efficiencies are obtained for the $\tilde{U}_1$ signal.

Table 5 Summary of signal regions categories in the 4ℓ channel. All events are required to satisfy the preselection requirements. The loose lepton definition (see Table 2) is labelled as L. In 4ℓ channel the leptons are ordered in p_{T}. The signal region consisting of two electrons and two muons is associated to 4ℓSR-e (4ℓSR-μ), if the leading light lepton in p_{T} is an electron (a muon). No validation regions are included in the fit. Dashes (–) refer to cuts that are not applicable

	4ℓ		
	VR	SR	
	4ℓVR	4ℓSR-e	4ℓSR-μ
e/μ selection	L		
e/μ combination	$4e$ / $3e1\mu$ / $2e2\mu$ / $3\mu1e$ / 4μ	$4e$ / $3e1\mu$ / $2e2\mu$ (lead e)	4μ / $3\mu1e$ / $2\mu2e$ (lead μ)
Total charge	0		
Number of jets	≥ 2		
Number of b–jets	≥ 1		
p_{T}^{ℓ} [GeV]	> 10		
$m_{\ell^+\ell^-}^{OS-SF}$ [GeV]	> 12		
$\lvert m_{\ell^+\ell^-}^{OS-SF} - m_Z\rvert$ [GeV]	> 10		
$m_{\ell\ell}^{\mathrm{min}}$ [GeV]	< 100	≥ 100	
m_{eff} [GeV]	–	≥ 500	

6 Background estimation

The background processes passing the signal region selections are categorised into irreducible and reducible backgrounds. Irreducible backgrounds (Sect. 6.1) have only prompt leptons, i.e. produced in W/Z boson decays, in leptonic τ-lepton decays, or internal conversions. Reducible backgrounds (Sect. 6.2) have prompt leptons with misassigned charge or at least one non-prompt lepton.

All backgrounds with the exception of electrons with misassigned charge (denoted as QMisID) are estimated using the simulated samples described in Sect. 3. In some cases, the simulation is improved using additional corrections derived in data control samples before the simultaneous likelihood fit to data. In particular, the N_{jets} and $N_{b-\mathrm{jets}}$ of the simulated diboson and non-prompt-lepton backgrounds, respectively, require dedicated corrections, whereas the normalisation of the background contribution from simulated $t\bar{t}$ events with at least one additional b-jet ($t\bar{t}$ +≥ 1 b-jet) is scaled to better describe the data. In addition, the yields of some simulated backgrounds, in particular $t\bar{t}W$, $t\bar{t}Z$, diboson and non-prompt-lepton backgrounds, are adjusted via normalisation factors that are determined by performing the likelihood fit to data across all event categories (control and signal regions as defined in Tables 3, 4 and 5), discussed in Sect. 8.

6.1 Irreducible backgrounds

Background contributions with prompt leptons originate from a wide range of physics processes with the relative importance of individual processes varying by channel. The main irreducible backgrounds originate from $t\bar{t}W$, $t\bar{t}Z/\gamma^*$, and diboson (in particular WZ) production, and have final states and kinematic properties similar to the leptoquark signal. Smaller contributions originate from the following rare processes: tZ, tW, tWZ, $t\bar{t}WW$, triboson, $t\bar{t}t$ and $t\bar{t}t\bar{t}$ production.

6.1.1 $t\bar{t}W$ background

The $t\bar{t}W$ background represents the leading background in several event categories. Despite the use of state-of-the-art simulations, accurate modelling of additional QCD and QED radiation in $t\bar{t}W$ production remains challenging. Since the signal leptoquark events populate mostly the 3ℓ and 4ℓ regions, the 2ℓSS region is split based on various combinations of lepton requirements (see Table 2) and b-jet multiplicities in order to create control regions enriched in non-prompt leptons or $t\bar{t}W$. The 2ℓttW control region is required to have exactly two same-sign T leptons and ≥ 2 b-jets. The m_{eff} distribution is the variable fitted in this category and provides additional constrain on this background in the tails of the distribution.

An overall normalisation factor is derived from the final simultaneous likelihood background-only fit that compares the data-MC agreement in this region. The measured normalisation factor is $\hat{\lambda}_{t\bar{t}W} = 1.27 \pm 0.15$, which is compatible with that determined in the ATLAS SM $t\bar{t}t\bar{t}$ analysis [114], and with a previous ATLAS measurement of the $t\bar{t}W$ production cross section [115].

Figure 4a displays the m_{eff} distribution in the 2ℓttW CR after the likelihood fit to data. There is good agreement between data and the background prediction after the fit within the statistical and systematic uncertainty band at high values of the m_{eff} distribution.

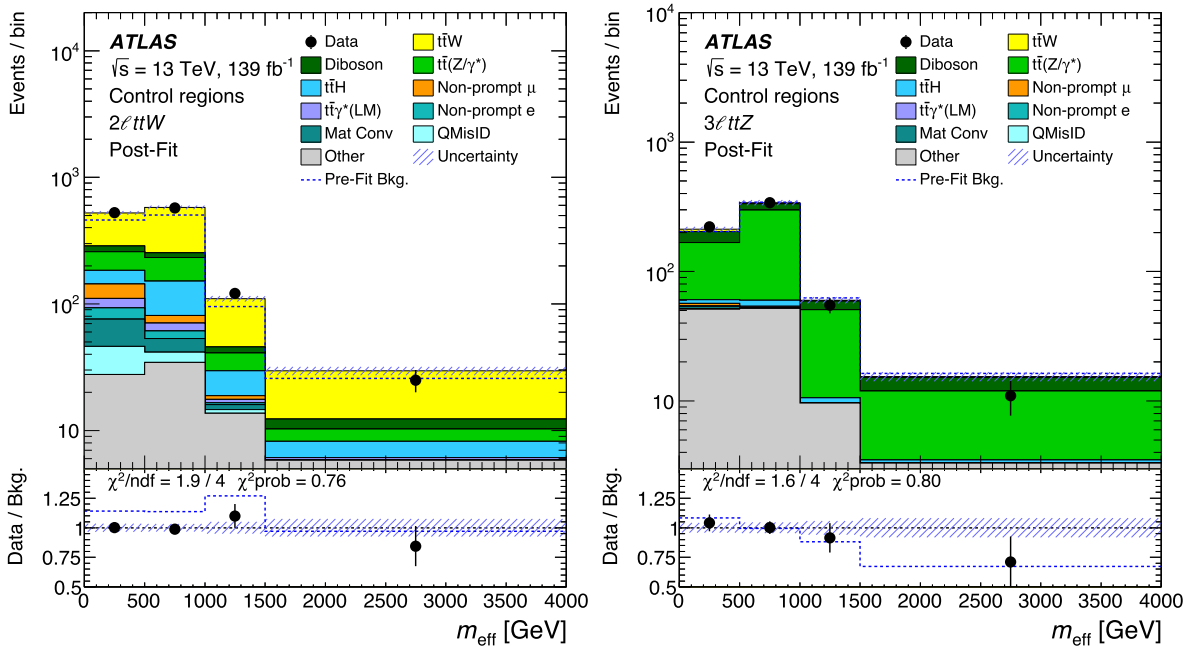

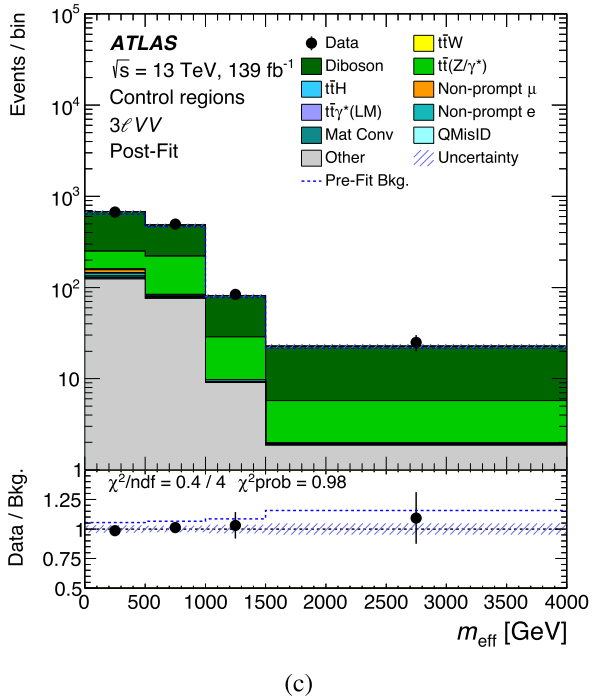

Fig. 4 Comparison between data and the background prediction ("Bkg.") for the m_{eff} distribution in the **a** 2ℓttW, **b** 3ℓttZ, and **c** 3ℓVV CRs. The background contributions after the likelihood fit to data ("Post-Fit") under the background-only hypothesis are shown as filled histograms. The total background prediction before the likelihood fit to data ("Pre-Fit Bkg.") is shown as a dashed blue histogram in the upper panel. The ratio of the data to the background prediction is shown in the lower panel, separately for post-fit background (black points) and pre-fit background (dashed blue line). The size of the combined statistical and systematic uncertainty in the background prediction is indicated by the blue hatched band. The last bin in each figure contains the overflow

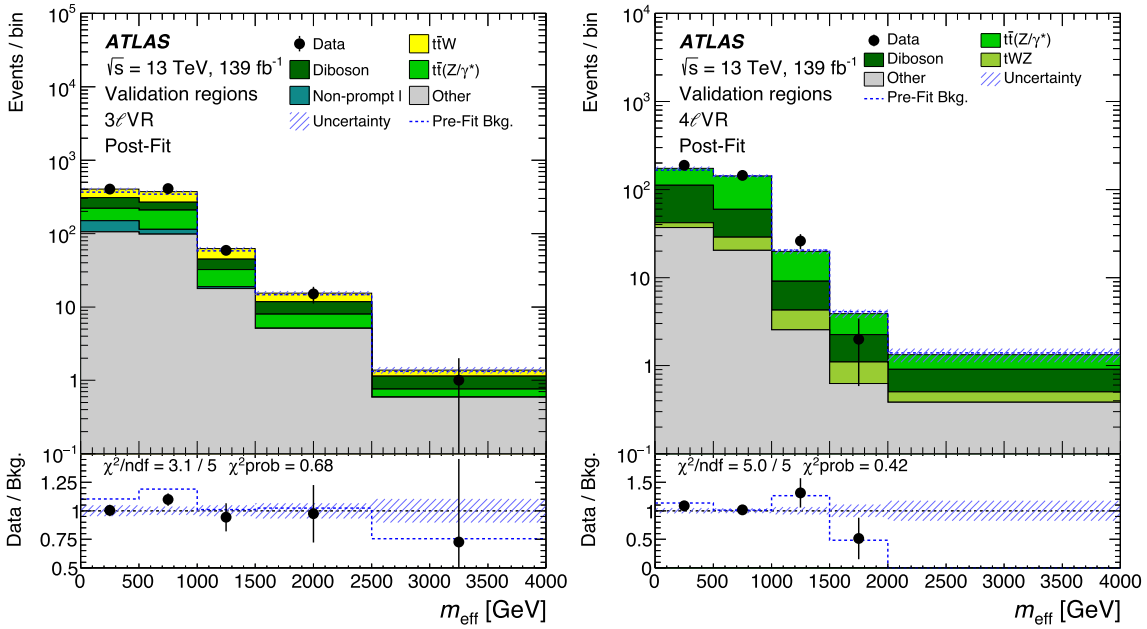

(a) (b)

Fig. 5 Comparison between data and prediction for the m_{eff} distribution used in the validation regions: **a** 3ℓVR, **b** 4ℓVR. The background contributions after the likelihood fit to data ("Post-Fit") under the background-only hypothesis are shown as filled histograms. The total background prediction before the likelihood fit to data ("Pre-Fit Bkg.") is shown as a dashed blue histogram in the upper panel. The ratio of the data to the background ("Bkg.") prediction is shown in the lower panel, separately for post-fit background (black points) and pre-fit background (dashed blue line). The size of the combined statistical and systematic uncertainty in the background prediction is indicated by the blue hatched band. The last bin in each figure contains the overflow

6.1.2 Diboson and $t\bar{t}Z/\gamma^*$ backgrounds

The diboson simulated sample does not correctly model the jet multiplicity spectrum in data. Therefore, a data-driven correction is derived from an inclusive 3ℓ diboson-enriched region with zero b-jets and at least one jet, referred to as 3ℓVV0b region. The events are required to have three leptons passing the (L, M, M) selection, where the second and third are the same-sign lepton pair, and the first lepton is opposite-sign with respect to the other two. The N_{jets} correction values range between 0.99 for diboson events with one additional jet to 0.67 for diboson events with at least seven additional jets.

The 3ℓVV and 3ℓttZ CRs are used in the likelihood fit to improve the prediction of the diboson background contribution with at least one b- or c-jet (denoted as $VV + \text{HF}$) and $t\bar{t}Z/\gamma^*$ processes, respectively. The number of b-jets provides good discrimination between these two processes and is used to build the control regions. The discriminating variable used in the fit is the m_{eff} distribution. The measured normalisation factors from the final simultaneous likelihood background-only fit are: $\hat{\lambda}_{VV+\text{HF}} = 1.21 \pm 0.18$ and $\hat{\lambda}_{t\bar{t}Z} = 0.98 \pm 0.09$.

Figure 4b, c display the m_{eff} distributions in the 3ℓVV and 3ℓttZ CRs after the likelihood fit to data. There is good agreement between data and the background prediction after the fit within the statistical and systematic uncertainty band at high values of the m_{eff} distribution.

6.1.3 Other irreducible backgrounds

The rate of the background from internal conversions with $m(e^+e^-) < 1$ GeV is estimated using the two dedicated CRs (3ℓIntC and 3ℓMatC), where at least one internal or material conversion electron candidate is required, respectively. The total yield in each category is used in the final likelihood background-only fit to determine the following normalisation factor: $\hat{\lambda}_e^{\text{IntC}} = 1.09 \pm 0.24$, where the uncertainty is dominated by the statistical uncertainty.

6.2 Reducible backgrounds

6.2.1 Non-prompt leptons

Non-prompt leptons originate from material conversions, heavy-flavour hadron decays, or the improper reconstruction of other particles, with an admixture strongly depend-

ing on the lepton quality requirements and varying across event categories. These backgrounds are in general small in the 3ℓ SR and are estimated from simulation, with the normalisation determined by the likelihood fit. The non-prompt lepton background contribution in the 4ℓ SR is negligible and is therefore taken from simulation without dedicated data-driven corrections. The main contribution to the non-prompt-lepton background is from $t\bar{t}$ production, followed by much smaller contributions from V+jets and single-top-quark processes. The non-prompt leptons in the simulated samples are labelled according to whether they originate from HF or light-flavour (LF) hadron decays, or from a material conversion candidate. The HF category includes leptons from both bottom and charm decays.

Two corrections are applied to the $t\bar{t}$ and the overall non-prompt lepton background simulation before the fit. First, the $t\bar{t}$ +≥ 1 b-jet contribution is corrected by a factor of 1.3 as measured by a previous ATLAS analysis sensitive to the in-situ measurement of this contribution in the single- and opposite-sign di-lepton final states [116]. Second, the shape of the b-jet multiplicity in the non-prompt lepton background simulation is corrected to match data in an orthogonal 2ℓSS validation region enriched with non-prompt leptons, where one of the leptons in required to pass a looser non-prompt lepton BDT score but not pass the M lepton WP.

Several of the event categories introduced in Sect. 5 were designed to be enriched in specific processes and are used to derive normalisation factors to improve their modelling by the simulation. In three control regions (3ℓMatC, 2ℓtt(e), 2ℓtt(μ)) enriched in $t\bar{t}$ events with non-prompt leptons, the total event yield is used in the likelihood fit to estimate the normalisation factors for these three non-prompt-lepton background contributions. The estimate of non-prompt leptons from heavy-flavour hadron decays or the improper reconstruction of other particles is measured in the 2ℓtt(e) and 2ℓtt(μ) control regions within the simultaneous fit and only affects the same-sign pair in 2ℓSS and 3ℓ. The normalisation factor for HF non-prompt leptons is measured separately for electrons and muons, λ_e^{had} and λ_μ^{had} respectively. An additional normalisation factor is determined for the material conversion background, λ_e^{MatC}. The measured normalisation factors from the final simultaneous likelihood background-only fit are: $\hat{\lambda}_e^{\text{had}} = 0.86 \pm 0.35$, $\hat{\lambda}_\mu^{\text{had}} = 1.05 \pm 0.22$, and $\hat{\lambda}_e^{\text{MatC}} = 1.26 \pm 0.39$, where the uncertainties are dominated by the statistical uncertainty.

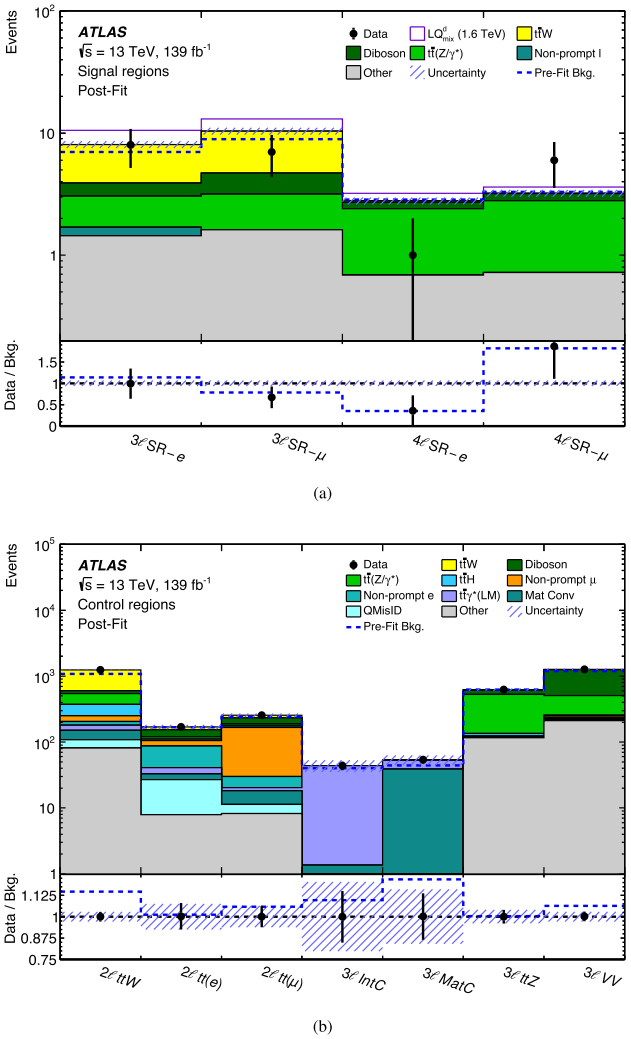

Fig. 6 Comparison between data and the background prediction for the event yields in **a** the four signal region categories and **b** the seven control region categories. The background contributions after the likelihood fit to data ("Post-Fit") under the background-only hypothesis are shown as filled histograms. In **a** the expected $\text{LQ}^{\text{d}}_{\text{mix}}$ ($m_{\text{LQ}^{\text{d}}_{\text{mix}}} = 1.6$ TeV) signal event yields before the fit are added to the background in the upper panel. The signal shown in 3ℓSR –e and 4ℓSR –e (3ℓSR $-\mu$ and 4ℓSR $-\mu$) SRs corresponds to $tete$ ($t\mu t\mu$). The total background prediction before the likelihood fit to data ("Pre-Fit Bkg.") is shown as a dashed blue histogram in the upper panel. The ratio of the data to the background ("Bkg.") prediction is shown in the lower panel, separately for post-fit background (black points) and pre-fit background (dashed blue line). The size of the combined statistical and systematic uncertainty in the background prediction is indicated by the blue hatched band

6.2.2 *Charge misassignment*

The background process containing electrons with the charge incorrectly assigned affects primarily the ≪ channel. This background predominantly arises from $t\bar{t}$ production, with one electron having undergone a hard bremsstrahlung as well as an asymmetric conversion ($e^{\pm} \to e^{\pm}\gamma^* \to e^{\pm}e^+e^-$) or a mismeasured track curvature. The muon charge misassignment rate is negligible in the p_{T} range relevant to this analysis. The electron charge misassignment rate is measured in data using samples of $Z \to e^+e^-$ events reconstructed as same-charge pairs and as opposite-charge pairs. The background in these events is estimated from the sideband of $m_{e^+e^-}$ distribution and subtracted from data.

Table 6 Summary of observed and predicted yields in the four signal region categories. The background prediction is shown after the combined likelihood fit to data under the background-only hypothesis across all control region and signal region categories. The expected signal yields that are obtained by using their theoretical cross sections are also shown with their pre-fit uncertainties, assuming $\mathcal{B}$=1 and μ=1. The uncertainties correspond to the combined statistical and systematic uncertainties in the predicted yields. The "Other" contribution is dominated by $t\bar{t}t\bar{t}$ and $t\bar{t}WW$ in the 3ℓ SRs, whereas it is dominated by tWZ and $t\bar{t}WW$ in the 4ℓ SRs. Dashes refer to components that are negligible or not applicable

	3ℓSR-e	3ℓSR-μ	4ℓSR-e	4ℓSR-μ
Data	8	7	1	6
Total background	8.1 ± 0.6	10.2 ± 0.7	2.8 ± 0.2	3.3 ± 0.2
$t\bar{t}W$	4.2 ± 0.6	5.6 ± 0.8	–	–
Diboson	0.9 ± 0.1	1.5 ± 0.2	0.32 ± 0.05	0.40 ± 0.04
$t\bar{t}Z/\gamma^*$	1.33 ± 0.14	1.55 ± 0.15	1.69 ± 0.18	2.09 ± 0.21
tWZ	–	–	0.23 ± 0.12	0.22 ± 0.12
Non-prompt ℓ	0.25 ± 0.16	–	–	–
Other	1.44 ± 0.22	1.61 ± 0.31	0.53 ± 0.10	0.54 ± 0.12
$\mathrm{LQ}^{\mathrm{d}}_{\mathrm{mix}}$ 1.6 TeV	2.5 ± 0.2	2.7 ± 0.2	0.42 ± 0.11	0.40 ± 0.05
$\tilde{U}_1^{\mathrm{min}}$ 1.6 TeV	4.5 ± 0.2	4.6 ± 0.3	0.7 ± 0.1	0.7 ± 0.1
$\tilde{U}_1^{\mathrm{YM}}$ 1.6 TeV	27 ± 1	29 ± 2	4.4 ± 0.2	4.2 ± 0.3
$\tilde{U}_1^{\mathrm{YM}}$ 2.0 TeV	2.0 ± 0.2	2.0 ± 0.2	0.31 ± 0.08	0.30 ± 0.03

The charge misassignment rate is parameterised as a function of electron p_{T} and $|\eta|$. It varies from about 10^{-5} for low-p_{T} electrons ($17 \leq p_{\mathrm{T}} \leq 50$ GeV) at $|\eta| \leq 1.37$, to about 3×10^{-4} for high-p_{T} electrons ($p_{\mathrm{T}} \geq 100$ GeV) at $1.52 \leq |\eta| \leq 2$. The measured charge misassignment rate is then applied to data events satisfying the requirements of the $\ll$ channels, except that the two leptons are required to be of opposite charge, to estimate the QMisID background in each of the corresponding event categories.

6.3 Validation of background modelling

Two validation regions are defined by requiring lower values of $m_{\ell\ell}^{\mathrm{min}}$ than in the signal regions, as described in Sect. 5.2. Figure 5 shows the m_{eff} distribution in the 3ℓVR and 4ℓVR regions after the likelihood fit to data. The 3ℓVR is composed of 30% $t\bar{t}W$ production, followed by $t\bar{t}Z$ and diboson production, whereas the 4ℓVR is enriched in $t\bar{t}Z$ and diboson processes. There is good agreement between data and the background prediction after the fit within the statistical and systematic uncertainty band.

7 Systematic uncertainties

Systematics uncertainties from the reconstructed objects and from the theoretical modelling of various physics processes can impact the estimated signal and background rates and the shape of the fitted distributions in multiple event categories. The impact of systematic uncertainties in the fit results were found to be very small compared to the statistical uncertainties due to limited number of data events in the signal regions.

The sources of uncertainties due to instrumental effects include data luminosity and pile-up reweighting of reconstructed events in the MC simulations. The uncertainty in the combined 2015–2018 integrated luminosity is 1.7% [117], obtained using the LUCID-2 detector [118] for the primary luminosity measurements. There are also uncertainties associated with the leptons' and jets' energy or momentum scale and resolutions [99,119]. Furthermore, the uncertainties in the scale factors to correct for the differences between data and MC simulation in trigger [111,112], lepton reconstruction, identification and isolation [92,94], jet vertex tagging [120,121] and b-tagging [104,122] efficiencies are taken into account. Some of these uncertainties are split into several components. These uncertainties are treated as correlated across the signal and background in the fit, but uncorrelated among individual components.

The impact of QCD renormalisation (μ_R) and factorisation (μ_F) scale variations by a factor of 0.5 or 2 with respect to the nominal scales, initial-state radiation scale variations and the α_s and `NNPDF3.0nlo` PDFs [123] are evaluated on the signal acceptance in the signal regions. Total theoretical uncertainties on $\mathrm{LQ}^{\mathrm{d}}_{\mathrm{mix}}$ signal acceptance varies from 1% to 10% for low and intermediate masses and from 7% to 19% for high mass ($m_{\mathrm{LQ}^{\mathrm{d}}_{\mathrm{mix}}} \geq 1.7$ TeV) depending on the signal region, with the dominant contributions arising from the initial-state radiation variations and the μ_R and μ_F scale variations. Similar uncertainties are found for the vector $\tilde{U}_1$ signal acceptances in the electron and muon channels.

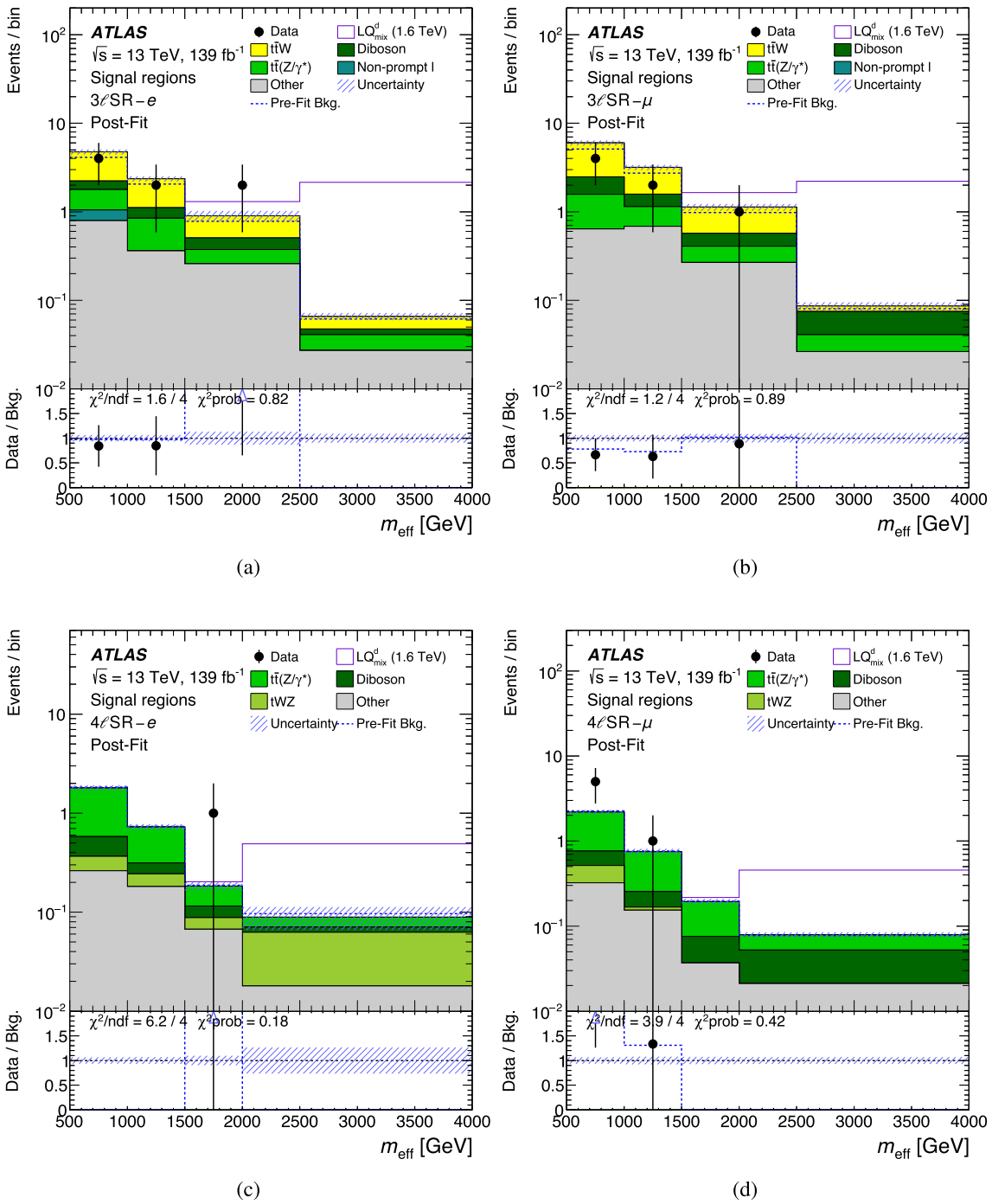

Fig. 7 Comparison between data and prediction for the m_{eff} distribution used in different signal region categories: **a** 3ℓSR –e, **b** 3ℓSR $-\mu$, **c** 4ℓSR –e, and **d** 4ℓSR $-\mu$. The background contributions after the likelihood fit to data ("Post-Fit") under the background-only hypothesis are shown as filled histograms. The total background prediction before the likelihood fit to data ("Pre-Fit Bkg.") is shown as a dashed blue histogram in the upper panel. The ratio of the data to the background ("Bkg.") prediction is shown in the lower panel, separately for post-fit background (black points) and pre-fit background (dashed blue line). The expected $\text{LQ}^{\text{d}}_{\text{mix}}$ ($m_{\text{LQ}^{\text{d}}_{\text{mix}}} = 1.6$ TeV) signal event yields before the fit are added to the background in the upper panel. The signal shown in 3ℓSR –e and 4ℓSR –e (3ℓSR $-\mu$ and 4ℓSR $-\mu$) SRs corresponds to $tete$ ($t\mu t\mu$). The size of the combined statistical and systematic uncertainty in the background prediction is indicated by the blue hatched band. The blue triangles indicate points that are outside the vertical range of the figure. The last bin in each figure contains the overflow

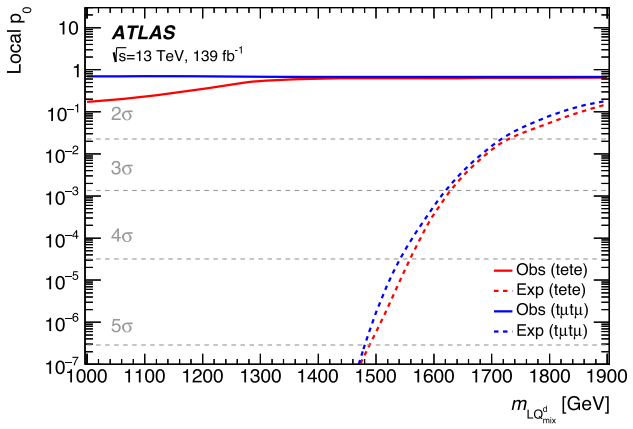

Fig. 8 The observed (solid) local p_0 as a function of $\mathrm{LQ}^{\mathrm{d}}_{\mathrm{mix}}$ mass ($m_{\mathrm{LQ}^{\mathrm{d}}_{\mathrm{mix}}}$) assuming $\mathcal{B} = 1$. The dashed curve shows the expected local p_0 under the hypothesis of a $\mathrm{LQ}^{\mathrm{d}}_{\mathrm{mix}}$ signal at that mass. The horizontal dashed lines indicate the p-values corresponding to significances of 2 to 5 standard deviations

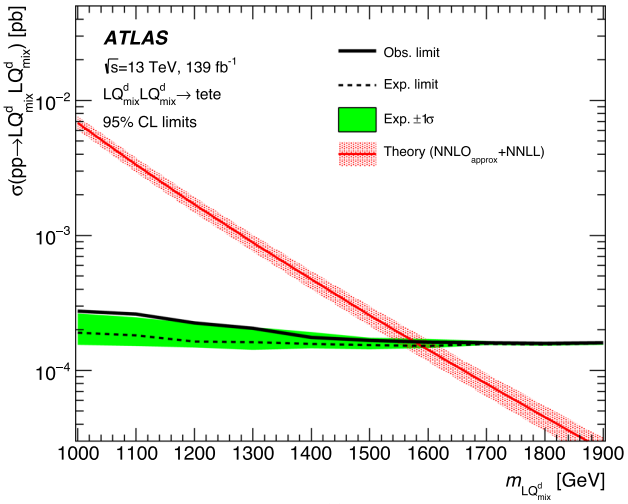

(a)

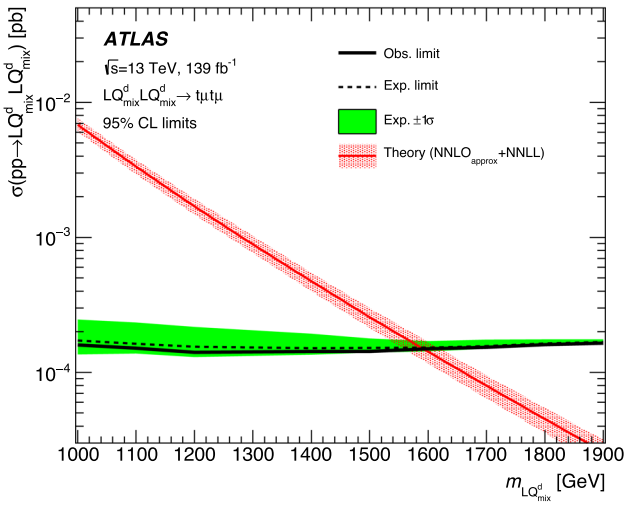

(b)

Fig. 9 Observed (solid line) and expected (dashed line) 95% CL upper limits on the $\mathrm{LQ}^{\mathrm{d}}_{\mathrm{mix}}$ pair production cross section as a function of $m_{\mathrm{LQ}^{\mathrm{d}}_{\mathrm{mix}}}$ for **a** $tete$ and **b** $t\mu t\mu$. The surrounding shaded band corresponds to the ± 1 standard deviation around the combined expected limit. The red line and band show the theoretical prediction and its $\pm 1\,\sigma$ uncertainty

Theoretical uncertainties due to the modelling of various irreducible background are included in the analysis. Modelling uncertainties evaluated by comparing the fit distributions from nominal MC sample to those from the alternative MC generator predictions are estimated for the $t\bar{t}W$, $t\bar{t}Z$, and $t\bar{t}H$ processes, as listed in Table 1. Additional uncertainties are evaluated from renormalisation and factorisation scale variations by a factor of 0.5 and 2, relative to the nominal scales, for the $t\bar{t}W$, $t\bar{t}Z$, $t\bar{t}H$, and diboson samples.

The diboson background contribution with additional light jets has a 2% uncertainty assigned on its cross section, as calculated from the largest statistical uncertainty associated to the data-driven diboson correction in the 3ℓVV0b region, whereas the normalisation of the VV+HF background is determined from the likelihood fit to the data (see Sect. 6.1). Furthermore, an uncertainty derived from the fitted parameters for the jet-multiplicity-dependent diboson correction is additionally applied to diboson processes (see Sect. 6.1). The diboson scale variation uncertainties are uncorrelated between LF and HF, whereas the jet-multiplicity-dependent diboson correction uncertainty is correlated across the LF and HF components.

Various sources of uncertainty in the estimation of the non-prompt leptons, photon conversions and charge misidentified background are taken into account. An extrapolation uncertainty of 20% is assigned to capture possible differences in mismodelling between the T and the M_{ex} lepton definitions. This uncertainty is estimated by comparing the T-over-M non-prompt rate between the nominal POWHEG+PYTHIA8 $t\bar{t}$ sample and the alternative POWHEG+HERWIG7 $t\bar{t}$ sample. The input variables to the non-prompt lepton BDT were studied and non-closure uncertainties were derived for three of them displaying some data and prediction disagreement in the 2ℓSS $T\,M_{ex}$ region. These variables are the relative muon calorimeter cluster energy ($E_{\mathrm{cluster}}/E_{\mathrm{expected}}$), the electron track p_{T} divided by the jet track p_{T}, and the secondary vertex longitudinal significance using tracks with $p_{\mathrm{T}} > 500$ MeV for both electrons and muons. The statistical uncertainty associated to the data-driven correction of the b-jet multiplicity distribution in the non-prompt lepton background is considered as a separate uncertainty. Additionally, a 50% uncertainty is assigned to the $t\bar{t}$ +≥ 1 b/c-jet contribution, although the result is insensitive to this choice and remains unchanged if a 100% uncertainty is assigned instead.

Uncertainties of 50% and 10% are estimated for internal and material conversions, respectively, based on a compari-

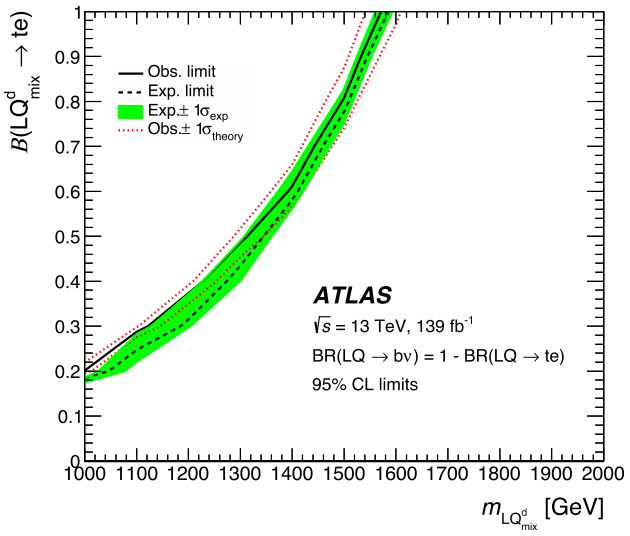

(a)

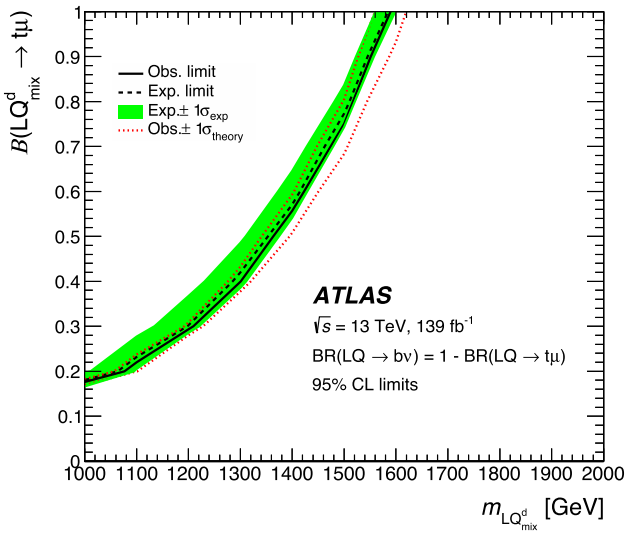

(b)

Fig. 10 Observed (solid line) and expected (dashed line) 95% CL upper limits on $\mathcal{B}$ as a function of $m_{\mathrm{LQ}^{\mathrm{d}}_{\mathrm{mix}}}$, **a** limits resulting from the combination of $tete$ analysis channels, **b** limits resulting from the combination of $t\mu t\mu$ analysis channels. In each analysis, it is assumed that $\mathcal{B}(\mathrm{LQ}^{\mathrm{d}}_{\mathrm{mix}} \to b\nu) = 1 - \mathcal{B}(\mathrm{LQ}^{\mathrm{d}}_{\mathrm{mix}} \to t\ell)$, and there is no acceptance for $\mathrm{LQ}^{\mathrm{d}}_{\mathrm{mix}} \to b\nu$ decays. The surrounding shaded band corresponds to the $\pm 1\,\sigma$ uncertainty around the combined expected limit, as estimated using pseudo-experiments. The dotted red line around the observed limit indicates how the observed limit changes when varying the theoretical prediction for the $\mathrm{LQ}^{\mathrm{d}}_{\mathrm{mix}}$ pair production cross section by its $\pm 1\,\sigma$ uncertainty

son between data and simulation in a dedicated 2ℓSS control sample enhanced in conversion candidate events. This sample is defined by requiring two same-sign T leptons, at least one of which is an electron that fails the internal or material conversion veto requirement, respectively. This uncertainty is applied to all categories, except for 3ℓIntC and 3ℓMatC, as an extrapolation uncertainty.

The electron charge misassignment measurement is validated by a closure test in simulation using same-charge electron pairs, with the observed difference between measured and predicted rates taken as the systematic uncertainty. Additional systematic uncertainties include the statistical uncertainty from the data and the variation in the rates when the Z-peak range definition is varied. The total systematic uncertainty in the charge misassignment background estimate for M electrons is about 30%, with the dominant contribution at low p_{T} originating from the closure tests and at high p_{T} from the statistical uncertainty.

Uncertainties in the modelling of other rare processes (e.g $t\bar{t}t\bar{t}, t(Z/\gamma^*), tW(Z/\gamma^*), t\bar{t}t, t\bar{t}W^+W^-, VH$, triboson) are taken into account by assigning up to 50% uncertainties on the production cross sections. These are conservative uncertainties to account for limited information on the correct modelling of these background processes. The choice of the size of these uncertainties, as well as the $t\bar{t}$ +≥ 1 c-jet uncertainties, have negligible impact on the results.

8 Results

A maximum-likelihood fit is performed for each signal hypothesis ($tete$ and $t\mu t\mu$) on all bins in the 7 control regions and in the corresponding 2 signal regions to simultaneously determine the background and the leptoquark signal yields that are most consistent with the data. For the $tete$ ($t\mu t\mu$) result, the 3ℓSR-e and 4ℓSR-e (3ℓSR-μ and 4ℓSR-μ) signal regions are considered in the fit. All control regions are included in each fit. In the signal regions, as well as in the 2ℓttW, 3ℓttZ, and 3ℓVV control regions, the m_{eff} distribution is fitted, thus ensuring that the main SM background processes are correctly estimated in the tails of high m_{eff} values, as well as maximising the sensitivity to the leptoquark signal. In the remaining control regions 2ℓtt(e), 2ℓtt(μ), 3ℓIntC, and 3ℓMatC, the total event yield (i.e. a single bin) is used.

The likelihood function $\mathcal{L}(\mu, \vec{\lambda}, \vec{\theta})$ is constructed as a product of Poisson probability terms over all bins considered in the search. It depends on the signal-strength parameter, μ, defined as a multiplicative factor applied to the predicted yield for the pair-produced leptoquark signal, $\vec{\lambda}$, the normalisation factors for several backgrounds (see Sect. 6), and $\vec{\theta}$, a set of nuisance parameters (NP) encoding systematic uncertainties in the signal and background expectations [124]. The predicted signal yield depends on the assumed mass $m_{\mathrm{LQ}^{\mathrm{d}}_{\mathrm{mix}}}$ and on the leptoquark being a scalar $\mathrm{LQ}^{\mathrm{d}}_{\mathrm{mix}}$ or a vector $\tilde{U}_1$. Systematic uncertainties can impact the estimated signal and background rates, the migration of events between categories, and the shape of the fitted distributions;

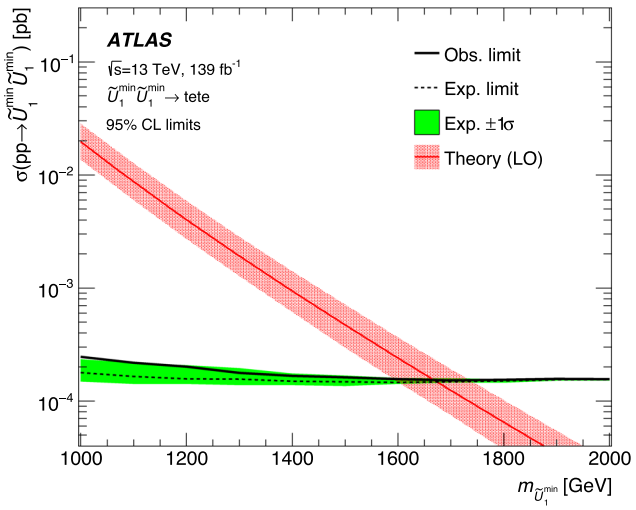

(a)

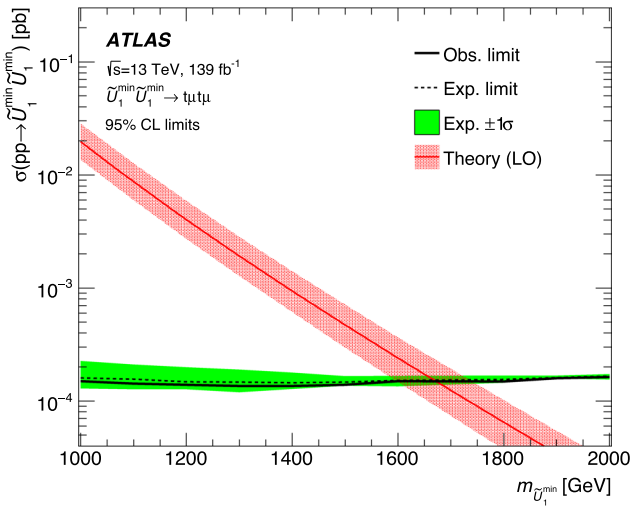

(b)

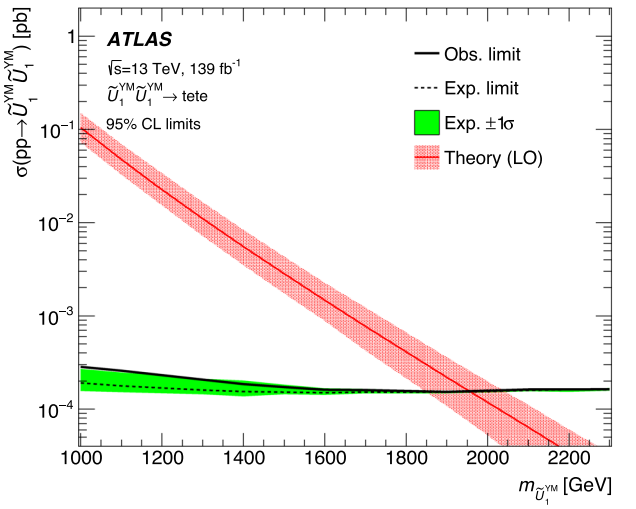

(c)

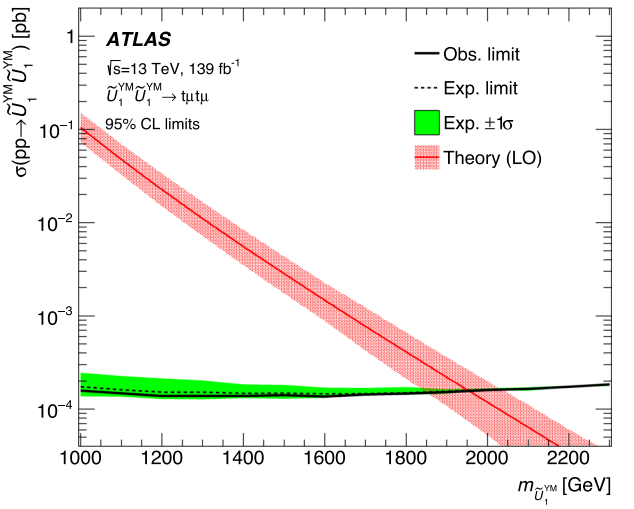

(d)

Fig. 11 Observed (solid line) and expected (dashed line) 95% CL upper limits on the $\tilde{U}_1$ pair production cross section as a function of $m_{\tilde{U}_1}$ for **a** minimal coupling scenario and $\tilde{U}_1^{\min}$ exclusive decay into te, **b** minimal coupling scenario and $\tilde{U}_1^{\min}$ exclusive decay into $t\mu$, **c** Yang–Mills scenario and $\tilde{U}_1^{\mathrm{YM}}$ exclusive decay into te, and **d** Yang–Mills scenario and $\tilde{U}_1^{\mathrm{YM}}$ exclusive decay into $t\mu$. The surrounding shaded band corresponds to the ± 1 standard deviation around the combined expected limit. The red line and band show the theoretical prediction and its $\pm 1\,\sigma$ uncertainty

they are summarised in Sect. 7. Both μ and $\vec{\lambda}$ are treated as free parameters in the likelihood fit. The NPs $\vec{\theta}$ allow variations of the expectations for signal and background according to the systematic uncertainties, subject to Gaussian constraints in the likelihood fit. Their fitted values represent the deviations from the nominal expectations that globally provide the best fit to the data. Statistical uncertainties in each bin due to the limited size of the simulated samples are taken into account by dedicated parameters using the Beeston–Barlow "lite" technique [125].

The test statistic q_μ is defined as the profile likelihood ratio: $q_\mu = -2\ln(\mathcal{L}(\mu, \hat{\hat{\vec{\lambda}}}_\mu, \hat{\hat{\vec{\theta}}}_\mu)/\mathcal{L}(\hat{\mu}, \hat{\hat{\vec{\lambda}}}_{\hat{\mu}}, \hat{\hat{\vec{\theta}}}_{\hat{\mu}}))$, where $\hat{\mu}$, $\hat{\hat{\vec{\lambda}}}_{\hat{\mu}}$, and $\hat{\hat{\vec{\theta}}}_{\hat{\mu}}$ are the values of the parameters that maximise the likelihood function, and $\hat{\hat{\vec{\lambda}}}_\mu$ and $\hat{\hat{\vec{\theta}}}_\mu$ are the values of the parameters that maximise the likelihood function for a given value of μ. The test statistic q_μ is evaluated with the

RooFit package [126]. A related statistic is used to determine the probability that the observed data are compatible with the background-only hypothesis (i.e. the discovery test) by setting $\mu = 0$ in the profile likelihood ratio (q_0). The p-value (referred to as p_0) representing the probability of the data being compatible with the background-only hypothesis is estimated by integrating the distribution of q_0 from background-only pseudo-experiments above the observed value of q_0. Some model dependence exists in the estimation of the p_0, as a given signal scenario needs to be assumed in the calculation of the denominator of q_0, even if the overall signal normalisation is allowed to float and is fitted to data. The observed p_0 is checked for each explored signal scenario. Upper limits on the signal production cross section for each of the signal scenarios considered are derived by using q_μ in the CL_s method [127,128]. For a given signal scenario, values of the production cross section (parameterised by μ) yielding $CL_s < 0.05$, where CL_s is computed using pseudo-experiments, are excluded at $\geq 95\%$ confidence level (CL).

A comparison of the distributions of observed and expected yields in the four SRs and the seven CRs after the combined likelihood fit under the background-only hypothesis is shown in Fig. 6a, b, respectively. The corresponding post-fit yields for the 3ℓ and 4ℓ SRs can be found in Table 6. The systematic uncertainty with the largest impact on the signal strength originates from the lepton identification. The search is dominated by statistical uncertainties. In general, good agreement between the data and predicted background yields is found across all event categories.

The comparison between data and the background prediction for the m_{eff} distributions used in the different SRs is shown in Fig. 7. The binning used for the m_{eff} distributions in the different SRs represents a compromise between preserving enough discrimination in the fit between the background and the signal for the different values of the $m_{\text{LQ}^{\text{d}}_{\text{mix}}}$ considered, and keeping the statistical uncertainty of the background prediction per bin well below 30%. No significant excess is observed in any of the SRs. The observed p_0 is found to be consistent with the background-only hypothesis for all values of $m_{\text{LQ}^{\text{d}}_{\text{mix}}}$ considered. The observed and expected p_0 as a function of $m_{\text{LQ}^{\text{d}}_{\text{mix}}}$ are shown in Fig. 8, assuming the value of $\mathcal{B} = 1$. This illustrates the significant expected sensitivity of the search, which exceeds 5 standard deviations for $m_{\text{LQ}^{\text{d}}_{\text{mix}}} < 1.5$ TeV and 3 standard deviations for $m_{\text{LQ}^{\text{d}}_{\text{mix}}} < 1.6$ TeV.

In the absence of any significant excess above the SM background prediction, 95% CL upper limits are set on the cross section for the $\text{LQ}^{\text{d}}_{\text{mix}}$ pair production as a function of the assumed $m_{\text{LQ}^{\text{d}}_{\text{mix}}}$ and $\mathcal{B}$. Figure 9a, b show the 95% CL upper limits on the $\text{LQ}^{\text{d}}_{\text{mix}}$ pair production cross section as a function of $m_{\text{LQ}^{\text{d}}_{\text{mix}}}$ for $tete$ and $t\mu t\mu$, respectively, assuming $\mathcal{B} = 1$. The deviation in the observed $tete$ limit compared to the expected limit for masses below 1.6 TeV is caused by a slight upward fluctuation in data in the third bin of the m_{eff} distribution and by the leftward shift of the signal population in m_{eff} spectra with the decrease of $m_{\text{LQ}^{\text{d}}_{\text{mix}}}$. The uncertainty in the results is mainly due to limited statistics of selected data events. The size of the $\pm 1\sigma$ uncertainty band around the expected limit shrinks for higher $\text{LQ}^{\text{d}}_{\text{mix}}$ mass hypotheses, for which the sensitivity is driven by m_{eff} bins with very low expected background yield (typically ≤ 0.1 events; see Fig. 7). This uncertainty band, which is computed using pseudo-experiments, has been validated by comparing two independent statistical frameworks.

Assuming $\mathcal{B} = 1$, the observed and expected 95% CL lower limits on scalar $m_{\text{LQ}^{\text{d}}_{\text{mix}}}$ for $tete$ ($t\mu t\mu$) are 1.58 (1.59) TeV and 1.59 (1.59) TeV, respectively. Exclusion limits on the scalar $m_{\text{LQ}^{\text{d}}_{\text{mix}}}$ are also obtained for various values of $\mathcal{B}$ into a charged lepton and top quark (as shown in Fig. 10a, b). As the signal search, with the requirement of at least three leptons, is only sensitive to 100% $\text{LQ}^{\text{d}}_{\text{mix}} \to t\ell$ decay modes, the limits for the alternative $\mathcal{B}$s, in steps of 0.1, are obtained by simply scaling theoretical cross sections by $\mathcal{B}^2$ covering the full plane. Under the assumption of 50% $\mathcal{B}(\text{LQ}^{\text{d}}_{\text{mix}} \to te)$, the lower observed (expected) limit on the $\text{LQ}^{\text{d}}_{\text{mix}}$ is 1.31 (1.35) TeV. In the case of 50% $\mathcal{B}(\text{LQ}^{\text{d}}_{\text{mix}} \to t\mu)$, the lower observed (expected) limit on the $\text{LQ}^{\text{d}}_{\text{mix}}$ is 1.37 (1.36) TeV. These limits are competitive with the previous ATLAS limits established by the complementary dedicated search for $\text{LQ}^{\text{d}}_{\text{mix}}$ in the mixed decay mode ($\text{LQ}^{\text{d}}_{\text{mix}} \to b\nu/t\ell$) with 50% $\mathcal{B}$ [46].

Additionally, 95% CL upper limits are set on the $\tilde{U}_1$ pair production cross section as a function of $m_{\tilde{U}_1}$ in the minimal coupling scenario for $tete$ and $t\mu t\mu$, as shown in Fig. 11a, b, and in the Yang–Mills coupling scenario for $tete$ and $t\mu t\mu$, as shown in Fig. 11c, d. Assuming $\mathcal{B} = 1$, the observed and expected 95% CL lower limits on $m_{\tilde{U}_1^{\text{min}}}$ for minimum coupling scenario in $tete$ ($t\mu t\mu$) are 1.67 (1.67) TeV and 1.67 (1.67) TeV, respectively, whereas analogous lower limits on $m_{\tilde{U}_1^{\text{YM}}}$ for Yang–Mills coupling scenario in $tete$ ($t\mu t\mu$) are 1.95 (1.95) TeV and 1.95 (1.95) TeV, respectively.

9 Conclusion

A search for pair production of cross-generation scalar and vector leptoquarks with a significant branching fraction into a top quark and an electron or muon is presented. The search is based on the full Run 2 dataset recorded with the ATLAS detector at the Large Hadron Collider, which corresponds to 139 fb^{-1} of pp collisions at $\sqrt{s} = 13$ TeV. Events are selected if they have at least two light leptons (electrons or muons), and additional jets. Four signal-enriched categories, defined by the multiplicity and flavour of the lepton candi-

dates, are considered in the analysis in order to search for the leptoquark signal. Additional background-enriched categories are used in the fit to improve the modelling of several leading backgrounds. The signal-enriched categories require at least three light leptons and employ the total effective mass distribution to discriminate between the signal and the background. The search reaches an expected significance of 5 standard deviations for a scalar leptoquark decaying exclusively into $t\ell$ and with mass below about 1.5 TeV. Its sensitivity is improved compared to previous searches with multiple light-leptons in the final state and is also complementary to searches performed with hadronically-decaying top quarks. This results from the sophisticated event selection and categorisation employed, which ensures a high signal acceptance and low background yields. No significant excess above the Standard Model expectation is observed in any of the considered event categories, and 95% CL upper limits are set on the production cross section as a function of the leptoquark mass, for different assumptions of its nature. Scalar leptoquarks decaying exclusively into te ($t\mu$) are excluded up to masses of 1.58 (1.59) TeV. For the vector leptoquarks, the lower mass limit is about 1.67 (1.67) TeV in the minimal coupling scenario, and about 1.95 (1.95) TeV in the Yang–Mills coupling scenario for the decays into te ($t\mu$), respectively.

Acknowledgements We thank CERN for the very successful operation of the LHC and its injectors, as well as the support staff at CERN and at our institutions worldwide without whom ATLAS could not be operated efficiently. The crucial computing support from all WLCG partners is acknowledged gratefully, in particular from CERN, the ATLAS Tier-1 facilities at TRIUMF/SFU (Canada), NDGF (Denmark, Norway, Sweden), CC-IN2P3 (France), KIT/GridKA (Germany), INFN-CNAF (Italy), NL-T1 (Netherlands), PIC (Spain), RAL (UK) and BNL (USA), the Tier-2 facilities worldwide and large non-WLCG resource providers. Major contributors of computing resources are listed in Ref. [129]. We gratefully acknowledge the support of ANPCyT, Argentina; YerPhI, Armenia; ARC, Australia; BMWFW and FWF, Austria; ANAS, Azerbaijan; CNPq and FAPESP, Brazil; NSERC, NRC and CFI, Canada; CERN; ANID, Chile; CAS, MOST and NSFC, China; Minciencias, Colombia; MEYS CR, Czech Republic; DNRF and DNSRC, Denmark; IN2P3-CNRS and CEA-DRF/IRFU, France; SRNSFG, Georgia; BMBF, HGF and MPG, Germany; GSRI, Greece; RGC and Hong Kong SAR, China; ISF and Benoziyo Center, Israel; INFN, Italy; MEXT and JSPS, Japan; CNRST, Morocco; NWO, Netherlands; RCN, Norway; MEiN, Poland; FCT, Portugal; MNE/IFA, Romania; MESTD, Serbia; MSSR, Slovakia; ARRS and MIZŠ, Slovenia; DSI/NRF, South Africa; MICINN, Spain; SRC and Wallenberg Foundation, Sweden; SERI, SNSF and Cantons of Bern and Geneva, Switzerland; MOST, Taipei; TENMAK, Türkiye; STFC, United Kingdom; DOE and NSF, United States of America. Individual groups and members have received support from BCKDF, CANARIE, CRC and DRAC, Canada; PRIMUS 21/SCI/017 and UNCE SCI/013, Czech Republic; COST, ERC, ERDF, Horizon 2020 and Marie Skłodowska-Curie Actions, European Union; Investissements d'Avenir Labex, Investissements d'Avenir Idex and ANR, France; DFG and AvH Foundation, Germany; Herakleitos, Thales and Aristeia programmes co-financed by EU-ESF and the Greek NSRF, Greece; BSF-NSF and MINERVA, Israel; Norwegian Financial Mechanism 2014–2021, Norway; NCN and NAWA, Poland; La Caixa Banking Foundation, CERCA Programme Generalitat de Catalunya and PROMETEO and GenT Programmes Generalitat Valenciana, Spain; Göran Gustafssons Stiftelse, Sweden; The Royal Society and Leverhulme Trust, United Kingdom. In addition, individual members wish to acknowledge support from CERN: European Organization for Nuclear Research (CERN DOCT); Chile: Agencia Nacional de Investigación y Desarrollo (FONDECYT 1190886, FONDECYT 1210400); China: National Natural Science Foundation of China (NSFC – 12175119); EU: H2020 European Research Council (H2020-MSCA-IF-2020: HPOFHIC – 10103); European Union: European Research Council (ERC – 948254), Horizon 2020 Framework Programme (MUCCA – CHIST-ERA-19-XAI-00), Marie Sklodowska-Curie Actions (EU H2020 MSC IF GRANT NO 101033496); France: Agence Nationale de la Recherche (ANR-20-CE31-0013, ANR-21-CE31-0013, ANR-21-CE31-0022), Investissements d'Avenir Idex (ANR-11-LABX-0012); Germany: Deutsche Forschungsgemeinschaft (DFG – CR 312/5-1); Italy: Istituto Nazionale di Fisica Nucleare (FELLINI G.A. n. 754496); Japan: Japan Society for the Promotion of Science (JSPS KAKENHI 22H01227, JSPS KAKENHI JP21H05085, JSPS KAKENHI JP22H04944); Netherlands: Netherlands Organisation for Scientific Research (NWO Veni 2020 – VI.Veni.202.179); Norway: Research Council of Norway (RCN-314472); Poland: Polish National Agency for Academic Exchange (PPN/PPO/2020/1/00002/U/00001), Polish National Science Centre (NCN UMO-2019/34/E/ST2/00393, UMO-2020/37/B/ST2/01043, UMO-2021/40/C/ST2/00187); Slovenia: Slovenian Research Agency (ARIS grant J1-3010); Spain: BBVA Foundation (LEO22-1-603), Generalitat Valenciana (Artemisa, FEDER, IDIFEDER/2018/048), La Caixa Banking Foundation (La Caixa Foundation, LCF/BQ/PI20/11760025), Ministry of Science and Innovation (RYC2019-028510-I), PROMETEO and GenT Programmes Generalitat Valenciana (CIDEGENT/2019/023, CIDEGENT/2019/027, CIDEGENT/2019/029, GVA-SEJI/2020/037); Sweden: Swedish Research Council (SRC – 2017-05160, VR 2017-05092), Knut and Alice Wallenberg Foundation (KAW 2017.0100, KAW 2018.0157, KAW 2019.0447); Switzerland: Swiss National Science Foundation (SNSF – PCEFP2_194658); UAE: Arab Fund for Economic and Social Development (AFESD-2021-994); United Kingdom: Leverhulme Trust (Leverhulme Trust RPG-2020-004).

Data Availability Statement This manuscript has no associated data. [Authors' comment: "All ATLAS scientific output is published in journals, and preliminary results are made available in Conference Notes. All are openly available, without restriction on use by external parties beyond copyright law and the standard conditions agreed by CERN. Data associated with journal publications are also made available: tables and data from plots (e.g. cross section values, likelihood profiles, selection efficiencies, cross section limits, ...) are stored in appropriate repositories such as HEPDATA (http://hepdata.cedar.ac.uk/). ATLAS also strives to make additional material related to the paper available that allows a reinterpretation of the data in the context of new theoretical models. For example, an extended encapsulation of the analysis is often provided for measurements in the framework of RIVET (http://rivet.hepforge.org/). "This information is taken from the ATLAS Data Access Policy, which is a public document that can be downloaded from http://opendata.cern.ch/record/413 [opendata.cern.ch].]

Code Availability Statement This manuscript has no associated code /software. [Authors' comment: "All ATLAS scientific output is published in journals, and preliminary results are made available in Conference Notes. All are openly available, without restriction on use by external parties beyond copyright law and the standard conditions agreed by CERN. Data associated with journal publications are also made available: tables and data from plots (e.g. cross section values, likelihood profiles, selection efficiencies, cross section limits, ...) are stored in appropriate repositories such as HEPDATA (http://hepdata.cedar.ac.uk/). ATLAS also strives to make additional material related to the paper available that allows a reinterpretation of the data in the context of new theoretical models. For example, an extended encapsulation of the anal-

ysis is often provided for measurements in the framework of RIVET (http://rivet.hepforge.org/). " This information is taken from the ATLAS Data Access Policy, which is a public document that can be downloaded from http://opendata.cern.ch/record/413 [opendata.cern.ch].]

Funded by SCOAP[3].

References

1. J.C. Pati, A. Salam, Lepton number as the fourth "color". Phys. Rev. D **10**, 275 (1974). https://doi.org/10.1103/PhysRevD.10.275
2. H. Georgi, S. Glashow, Unity of all elementary-particle forces. Phys. Rev. Lett. **32**, 438 (1974). https://doi.org/10.1103/PhysRevLett.32.438
3. S.K. Dimopoulos, L. Susskind, Mass without scalars. Nucl. Phys. B **155**, 237 (1979). https://doi.org/10.1016/0550-3213(79)90364-X
4. S. Dimopoulos, Technicoloured signatures. Nucl. Phys. B **168**, 69 (1980). https://doi.org/10.1016/0550-3213(80)90277-1
5. E.J. Eichten, K. Lane, Dynamical breaking of weak interaction symmetries. Phys. Lett. B **90**, 125 (1980). https://doi.org/10.1016/0370-2693(80)90065-9
6. V.D. Angelopoulos, J.R. Ellis, H. Kowalski et al., Search for new quarks suggested by the superstring. Nucl. Phys. B **292**, 59 (1987). https://doi.org/10.1016/0550-3213(87)90637-7
7. W. Buchmüller, D. Wyler, Constraints on SU(5)-type leptoquarks. Phys. Lett. B **177**, 377 (1986). https://doi.org/10.1016/0370-2693(86)90771-9
8. M. Freytsis, Z. Ligeti, J.T. Ruderman, Flavor models for $\bar{B} \to D^{(*)}\tau\bar{\nu}$. Phys. Rev. D **92**, 054018 (2015). https://doi.org/10.1103/PhysRevD.92.054018. arXiv:1506.08896 [hep-ph]
9. M. Bauer, M. Neubert, Minimal leptoquark explanation for the $R_{D^{(*)}}$, R_K, and $(g-2)_g$ anomalies. Phys. Rev. Lett. **116**, 141802 (2016). https://doi.org/10.1103/PhysRevLett.116.141802. arXiv:1511.01900 [hep-ph]
10. L. Di Luzio, M. Nardecchia, What is the scale of new physics behind the B-flavour anomalies? Eur. Phys. J. C **77**, 536 (2017). https://doi.org/10.1140/epjc/s10052-017-5118-9. arXiv:1706.01868 [hep-ph]
11. D. Buttazzo, A. Greljo, G. Isidori, D. Marzocca, B-physics anomalies: a guide to combined explanations. JHEP **11**, 044 (2017). https://doi.org/10.1007/JHEP11(2017)044. arXiv:1706.07808 [hep-ph]
12. J.M. Cline, B decay anomalies and dark matter from vectorlike confinement. Phys. Rev. D **97**, 015013 (2018). https://doi.org/10.1103/PhysRevD.97.015013. arXiv:1710.02140 [hep-ph]
13. J. Aebischer, G. Isidori, M. Pesut, B.A. Stefanek, F. Wilsch, Confronting the vector leptoquark hypothesis with new low- and high-energy data. EPJC **83**, 153 (2023). https://doi.org/10.1140/epjc/s10052-023-11304-5
14. BaBar Collaboration, Measurement of an excess of $\bar{B} \to D^{(*)}\tau^-\bar{\nu}_\tau$ decays and implications for charged Higgs bosons. Phys. Rev. D **88**, 072012 (2013). https://doi.org/10.1103/PhysRevD.88.072012. arXiv:1303.0571 [hep-ex]
15. Belle Collaboration, Measurement of the branching ratio of $\bar{B} \to D^{(*)}\tau^-\bar{\nu}_\tau$ relative to $\bar{B} \to D^{(*)}\ell^-\bar{\nu}_\ell$ decays with hadronic tagging at Belle. Phys. Rev. D **92**, 072014 (2015). https://doi.org/10.1103/PhysRevD.92.072014. arXiv:1507.03233 [hep-ex]
16. LHCb Collaboration, Measurement of the ratio of branching fractions $\mathcal{B}(\bar{B}^0 \to D^{*+}\tau^-\bar{\nu}_\tau)/\mathcal{B}(\bar{B}^0 \to D^{*+}\mu^-\bar{\nu}_\mu)$. Phys. Rev. Lett. **115**, 111803 (2015) [Erratum: Phys. Rev. Lett. 115, 159901 (2015)]. https://doi.org/10.1103/PhysRevLett.115.111803. arXiv:1506.08614 [hep-ex]
17. Belle Collaboration, Measurement of the τ lepton polarization and $R(D^*)$ in the decay $\bar{B} \to D^*\tau^-\bar{\nu}_\tau$. Phys. Rev. Lett. **118**, 211801 (2017). https://doi.org/10.1103/PhysRevLett.118.211801. arXiv:1612.00529 [hep-ex]
18. LHCb Collaboration, Measurement of the ratio of branching fractions $\mathcal{B}(B_c^+ \to J/\psi\tau^+\nu_\tau)/\mathcal{B}(B_c^+ \to J/\psi\mu^+\nu_\mu)$. Phys. Rev. Lett. **120**, 121801 (2018). https://doi.org/10.1103/PhysRevLett.120.121801. arXiv:1711.05623 [hep-ex]
19. A. Crivellin, D. Müller, F. Saturnino, Flavor phenomenology of the leptoquark singlet-triplet model. JHEP **06**, 020 (2020). https://doi.org/10.1007/JHEP06(2020)020. arXiv:1912.04224 [hep-ph]
20. V. Gherardi, D. Marzocca, E. Venturini, Low-energy phenomenology of scalar leptoquarks at one-loop accuracy. JHEP **01**, 138 (2021). https://doi.org/10.1007/JHEP01(2021)138. arXiv:2008.09548 [hep-ph]
21. H.M. Lee, Leptoquark option for B-meson anomalies and leptonic signatures. Phys. Rev. D **104**, 015007 (2021). https://doi.org/10.1103/PhysRevD.104.015007. arXiv:2104.02982 [hep-ph]
22. Muon g-2 Collaboration, Final report of the muon E821 anomalous magnetic moment measurement at BNL. Phys. Rev. D **73**, 072003 (2006). https://doi.org/10.1103/PhysRevD.73.072003. arXiv:hep-ex/0602035
23. Muon g-2 Collaboration, Measurement of the Positive Muon Anomalous Magnetic Moment to 0.46 ppm. Phys. Rev. Lett. **126**, 141801 (2021). https://doi.org/10.1103/PhysRevLett.126.141801. arXiv:2104.03281 [hep-ex]
24. J. Blümlein, E. Boos, A. Kryukov, Leptoquark pair production in hadronic interactions. Z. Phys. C **76**, 137 (1997). https://doi.org/10.1007/s002880050538. arXiv:hep-ph/9610408 [hep-ph]
25. C. Borschensky, B. Fuks, A. Kulesza, D. Schwartländer, Scalar leptoquark pair production at hadron colliders. Phys. Rev. D **101**, 115017 (2020). https://doi.org/10.1103/PhysRevD.101.115017. arXiv:2002.08971 [hep-ph]
26. ATLAS Collaboration, Search for scalar leptoquarks in pp collisions at $\sqrt{s} = 13\,TeV$ with the ATLAS experiment. New J. Phys. **18**, 093016 (2016). https://doi.org/10.1088/1367-2630/18/9/093016. arXiv:1605.06035 [hep-ex]
27. ATLAS Collaboration, Searches for third-generation scalar leptoquarks in $\sqrt{s} = 13\,TeV$ pp collisions with the ATLAS detector. JHEP **06**, 144 (2019). https://doi.org/10.1007/JHEP06(2019)144. arXiv:1902.08103 [hep-ex]
28. ATLAS Collaboration, Search for a scalar partner of the top quark in the all-hadronic $t\bar{t}$ plus missing transverse momentum final state at $\sqrt{s} = 13\,TeV$ with the ATLAS detector. Eur. Phys. J. C **80**, 737 (2020). https://doi.org/10.1140/epjc/s10052-020-8102-8. arXiv:2004.14060 [hep-ex]
29. ATLAS Collaboration, Search for pairs of scalar leptoquarks decaying into quarks and electrons or muons in $\sqrt{s} = 13\,TeV$ pp collisions with the ATLAS detector. JHEP **10**, 112 (2020). https://doi.org/10.1007/JHEP10(2020)112. arXiv:2006.05872 [hep-ex]
30. ATLAS Collaboration, Search for pair production of third-generation scalar leptoquarks decaying into a top quark and a τ-lepton in pp collisions at $\sqrt{s} = 13\,TeV$ with the ATLAS detector.

JHEP **06**, 179 (2021). https://doi.org/10.1007/JHEP06(2021)179. arXiv:2101.11582 [hep-ex]
31. ATLAS Collaboration, Search for new phenomena in final states with b-jets and missing transverse momentum in $\sqrt{s} = 13\,TeV$ pp collisions with the ATLAS detector. JHEP **05**, 093 (2021). https://doi.org/10.1007/JHEP05(2021)093. arXiv:2101.12527 [hep-ex]
32. ATLAS Collaboration, Search for new phenomena in pp collisions in final states with tau leptons, b-jets, and missing transverse momentum with the ATLAS detector. Phys. Rev. D **104**, 112005 (2021). https://doi.org/10.1103/PhysRevD.104.112005. arXiv:2108.07665 [hep-ex]
33. CMS Collaboration, Search for third-generation scalar leptoquarks decaying to a top quark and a τ lepton at $\sqrt{s} = 13\,TeV$. Eur. Phys. J. C **78**, 707 (2018). https://doi.org/10.1140/epjc/s10052-018-6143-z. arXiv:1803.02864 [hep-ex]
34. CMS Collaboration, Search for heavy neutrinos or third-generation leptoquarks in final states with two hadronically decaying τ leptons and two jets in proton-proton collisions at $\sqrt{s} = 13\,TeV$. JHEP **03**, 077 (2017). https://doi.org/10.1007/JHEP03(2017)077. arXiv:1612.01190 [hep-ex]
35. CMS Collaboration, Search for third-generation scalar leptoquarks and heavy right-handed neutrinos in final states with two tau leptons and two jets in proton-proton collisions at $\sqrt{s} = 13\,TeV$. JHEP **07**, 121 (2017). https://doi.org/10.1007/JHEP07(2017)121. arXiv:1703.03995 [hep-ex]
36. CMS Collaboration, Search for pair production of second-generation leptoquarks at $\sqrt{s} = 13\,TeV$. Phys. Rev. D **99**, 032014 (2019). https://doi.org/10.1103/PhysRevD.99.032014. arXiv:1808.05082 [hep-ex]
37. CMS Collaboration, Search for pair production of first-generation scalar leptoquarks at $\sqrt{s} = 13\,TeV$. Phys. Rev. D **99**, 052002 (2019). https://doi.org/10.1103/PhysRevD.99.052002. arXiv:1811.01197 [hep-ex]
38. CMS Collaboration, Search for heavy neutrinos and third-generation leptoquarks in hadronic states of two τ leptons and two jets in proton-proton collisions at $\sqrt{s} = 13\,TeV$. JHEP **03**, 170 (2019). https://doi.org/10.1007/JHEP03(2019)170. arXiv:1811.00806 [hep-ex]
39. CMS Collaboration, Search for a singly produced third-generation scalar leptoquark decaying to a τ lepton and a bottom quark in proton-proton collisions at $\sqrt{s} = 13\,TeV$. JHEP **07**, 115 (2018). https://doi.org/10.1007/JHEP07(2018)115. arXiv:1806.03472 [hep-ex]
40. CMS Collaboration, Search for singly and pair-produced leptoquarks coupling to third-generation fermions in proton-proton collisions at $\sqrt{s} = 13\,TeV$. Phys. Lett. B **819**, 136446 (2020). https://doi.org/10.1016/j.physletb.2021.136446. arXiv:2012.04178 [hep-ex]
41. W. Buchmuller, R. Ruckl, D. Wyler, Leptoquarks in lepton-quark collisions. Phys. Lett. B **191**, 442 (1987) [Erratum: Phys. Lett. B 448, 320–320 (1999)]. https://doi.org/10.1016/0370-2693(87)90637-X
42. B. Diaz, M. Schmaltz, Y.-M. Zhong, The leptoquark hunter's guide: pair production. JHEP **10**, 097 (2017). https://doi.org/10.1007/jhep10(2017)097. arXiv:1706.05033 [hep-ph]
43. A. Greljo, P. Stangl, A. Eller Thomsen, A model of muon anomalies. Phys. Lett. B **820**, 136554 (2021). https://doi.org/10.1016/j.physletb.2021.136554
44. C. Cornella, J. Fuentes-Martín, G. Isidori, Revisiting the vector leptoquark explanation of the B-physics anomalies. JHEP **7**, 168 (2019). https://doi.org/10.1007/JHEP07(2019)168
45. ATLAS Collaboration, Search for pair production of scalar leptoquarks decaying into first- or second-generation leptons and top quarks in proton–proton collisions at $\sqrt{s} = 13\,TeV$ with the ATLAS detector. Eur. Phys. J. C **81**, 313 (2021). https://doi.org/10.1140/epjc/s10052-021-09009-8. arXiv:2010.02098 [hep-ex]
46. ATLAS Collaboration, Search for pair-produced scalar and vector leptoquarks decaying into third-generation quarks and first- or second-generation leptons in pp collisions with the ATLAS detector. JHEP **06**, 188 (2022). https://doi.org/10.1007/JHEP06(2023)188. arXiv:2210.04517 [hep-ex]
47. CMS Collaboration, Search for leptoquarks coupled to third-generation quarks in proton-proton collisions at $\sqrt{s} = 13\,TeV$. Phys. Rev. Lett. **121**, 241802 (2018). https://doi.org/10.1103/PhysRevLett.121.241802. arXiv:1809.05558 [hep-ex]
48. CMS Collaboration, Inclusive nonresonant multilepton probes of new phenomena at $\sqrt{s} = 13\,TeV$ (2022). arXiv:2202.08676 [hep-ex]
49. ATLAS Collaboration, The ATLAS experiment at the CERN large hadron collider. JINST **3**, S08003 (2008). https://doi.org/10.1088/1748-0221/3/08/S08003
50. ATLAS Collaboration, ATLAS Insertable B-Layer: Technical Design Report, ATLAS-TDR-19; CERN-LHCC-2010-013 (2010) [Addendum: ATLAS-TDR-19-ADD-1; CERN-LHCC-2012-009, 2012]. https://cds.cern.ch/record/1291633, https://cds.cern.ch/record/1451888
51. B. Abbott et al., Production and integration of the ATLAS Insertable B-Layer. JINST **13**, T05008 (2018). https://doi.org/10.1088/1748-0221/13/05/T05008. arXiv:1803.00844 [physics.ins-det]
52. ATLAS Collaboration, Performance of the ATLAS trigger system. Eur. Phys. J. C **77**(2017), 317 (2015). https://doi.org/10.1140/epjc/s10052-017-4852-3. arXiv:1611.09661 [hep-ex]
53. ATLAS Collaboration, The ATLAS Collaboration Software and Firmware, ATL-SOFT-PUB-2021-001 (2021). https://cds.cern.ch/record/2767187
54. T. Gleisberg et al., Event generation with SHERPA 1.1. JHEP **02**, 007 (2009). https://doi.org/10.1088/1126-6708/2009/02/007. arXiv:0811.4622 [hep-ph]
55. D.J. Lange, The EvtGen particle decay simulation package. Nucl. Instrum. Meth. A **462**, 152 (2001). https://doi.org/10.1016/S0168-9002(01)00089-4
56. T. Sjöstrand, S. Mrenna, P.Z. Skands, A brief introduction to PYTHIA 8.1. Comput. Phys. Commun. **178**, 852 (2008). https://doi.org/10.1016/j.cpc.2008.01.036. arXiv:0710.3820 [hep-ph]
57. R.D. Ball et al., NNPDF Collaboration, Parton distributions with LHC data. Nucl. Phys. B **867**, 244 (2013). https://doi.org/10.1016/j.nuclphysb.2012.10.003. arXiv:1207.1303 [hep-ph]
58. ATLAS Collaboration, The Pythia 8 A3 tune description of ATLAS minimum bias and inelastic measurements incorporating the Donnachie–Landshoff diffractive model, ATL-PHYS-PUB-2016-017 (2016). https://cds.cern.ch/record/2206965
59. ATLAS Collaboration, The ATLAS Simulation Infrastructure. Eur. Phys. J. C **70**, 823 (2010). https://doi.org/10.1140/epjc/s10052-010-1429-9. arXiv:1005.4568 [physics.ins-det]
60. S. Agostinelli et al., GEANT4: a simulation toolkit. Nucl. Instrum. Meth. A **506**, 250 (2003). https://doi.org/10.1016/S0168-9002(03)01368-8
61. J. Alwall et al., The automated computation of tree-level and next-to-leading order differential cross sections, and their matching to parton shower simulations. JHEP **07**, 079 (2014). https://doi.org/10.1007/JHEP07(2014)079. arXiv:1405.0301 [hep-ph]
62. T. Mandal, S. Mitra, S. Seth, Pair production of scalar leptoquarks at the LHC to NLO parton shower accuracy. Phys. Rev. D **93**, 035018 (2016). https://doi.org/10.1103/PhysRevD.93.035018. arXiv:1506.07369 [hep-ph]
63. M. Kramer, T. Plehn, M. Spira, P. Zerwas, Pair production of scalar leptoquarks at the tevatron. Phys. Rev. Lett. **79**, 341 (1997). https://doi.org/10.1103/PhysRevLett.79.341. arXiv:hep-ph/9704322

64. M. Kramer, T. Plehn, M. Spira, P. Zerwas, Pair production of scalar leptoquarks at the CERN LHC. Phys. Rev. D **71**, 057503 (2005). https://doi.org/10.1103/PhysRevD.71.057503. arXiv:hep-ph/0411038
65. R.D. Ball et al., NNPDF Collaboration, Parton distributions for the LHC run II. JHEP **04**, 040 (2015). https://doi.org/10.1007/JHEP04(2015)040. arXiv:1410.8849 [hep-ph]
66. ATLAS Collaboration, ATLAS Pythia 8 tunes to 7 TeV data, ATL-PHYS-PUB-2014-021 (2014). https://cds.cern.ch/record/1966419
67. P. Artoisenet, R. Frederix, O. Mattelaer, R. Rietkerk, Automatic spin-entangled decays of heavy resonances in Monte Carlo simulations. JHEP **03**, 015 (2013). https://doi.org/10.1007/JHEP03(2013)015. arXiv:1212.3460 [hep-ph]
68. W. Buchmüller, R. Rückl, D. Wyler, Leptoquarks in lepton-quark collisions. Phys. Lett. B **191**, 442 (1987). https://doi.org/10.1016/0370-2693(87)90637-X
69. A. Belyaev, C. Leroy, R. Mehdiyev, A. Pukhov, Leptoquark single and pair production at LHC with CalcHEP/CompHEP in the complete model. JHEP **09**, 005 (2005). https://doi.org/10.1088/1126-6708/2005/09/005. arXiv:hep-ph/0502067
70. W. Beenakker, C. Borschensky, M. Krämer, A. Kulesza, E. Laenen, NNLL-fast: predictions for coloured supersymmetric particle production at the LHC with threshold and Coulomb resummation. JHEP **12**, 133 (2016). https://doi.org/10.1007/JHEP12(2016)133. arXiv:1607.07741 [hep-ph]
71. W. Beenakker, M. Kramer, T. Plehn, M. Spira, P. Zerwas, Stop production at hadron colliders. Nucl. Phys. B **515**, 3 (1998). https://doi.org/10.1016/S0550-3213(98)00014-5. arXiv:hep-ph/9710451
72. W. Beenakker et al., Supersymmetric top and bottom squark production at hadron colliders. JHEP **08**, 098 (2010). https://doi.org/10.1007/JHEP08(2010)098. arXiv:1006.4771 [hep-ph]
73. W. Beenakker et al., NNLL resummation for stop pair-production at the LHC. JHEP **05**, 153 (2016). https://doi.org/10.1007/JHEP05(2016)153. arXiv:1601.02954 [hep-ph]
74. M.S. Schmaltz, Y.-M. Zhong, The leptoquark Hunter's guide: large coupling. JHEP **01**, 132 (2019). https://doi.org/10.1007/JHEP01(2019)132. arXiv:1810.10017 [hep-ph]
75. E. Bothmann et al., Event generation with Sherpa 2.2. SciPost Phys. **7**, 034 (2019). https://doi.org/10.21468/SciPostPhys.7.3.034. arXiv:1905.09127 [hep-ph]
76. T. Gleisberg, S. Hoeche, Comix, a new matrix element generator. JHEP **12**, 039 (2008). https://doi.org/10.1088/1126-6708/2008/12/039. arXiv:0808.3674 [hep-ph]
77. F. Cascioli, P. Maierhofer, S. Pozzorini, Scattering amplitudes with open loops. Phys. Rev. Lett. **108**, 111601 (2012). https://doi.org/10.1103/PhysRevLett.108.111601. arXiv:1111.5206 [hep-ph]
78. S. Schumann, F. Krauss, A parton shower algorithm based on Catani–Seymour dipole factorisation. JHEP **03**, 038 (2008). https://doi.org/10.1088/1126-6708/2008/03/038. arXiv:0709.1027 [hep-ph]
79. S. Hoeche, F. Krauss, M. Schonherr, F. Siegert, QCD matrix elements + parton showers: the NLO case. JHEP **04**, 027 (2013). https://doi.org/10.1007/JHEP04(2013)027. arXiv:1207.5030 [hep-ph]
80. R. Frederix, I. Tsinikos, On improving NLO merging for $t\bar{t}W$ production. JHEP **11**, 029 (2021). https://doi.org/10.1007/JHEP11(2021)029. arXiv:2108.07826 [hep-ph]
81. D. de Florian et al., Handbook of LHC Higgs cross sections: 4. Deciphering the nature of the Higgs sector (2016). arXiv:1610.07922 [hep-ph]
82. S. Frixione, P. Nason, G. Ridolfi, A positive-weight next-to-leading-order Monte Carlo for heavy flavour hadroproduction. JHEP **09**, 126 (2007). https://doi.org/10.1088/1126-6708/2007/09/126. arXiv:0707.3088 [hep-ph]
83. P. Nason, A new method for combining NLO QCD with shower Monte Carlo algorithms. JHEP **11**, 040 (2004). https://doi.org/10.1088/1126-6708/2004/11/040. arXiv:hep-ph/0409146
84. S. Frixione, P. Nason, C. Oleari, Matching NLO QCD computations with parton shower simulations: the POWHEG method. JHEP **11**, 070 (2007). https://doi.org/10.1088/1126-6708/2007/11/070. arXiv:0709.2092 [hep-ph]
85. S. Alioli, P. Nason, C. Oleari, E. Re, A general framework for implementing NLO calculations in shower Monte Carlo programs: the POWHEG BOX. JHEP **06**, 043 (2010). https://doi.org/10.1007/JHEP06(2010)043. arXiv:1002.2581 [hep-ph]
86. S. Alioli, P. Nason, C. Oleari, E. Re, NLO single-top production matched with shower in POWHEG: s- and t-channel contributions. JHEP **09**, 111 (2009) [Erratum: JHEP 02 (2010) 011]. https://doi.org/10.1088/1126-6708/2009/09/111. https://doi.org/10.1007/JHEP02(2010)011. arXiv:0907.4076 [hep-ph]
87. E. Re, Single-top Wt-channel production matched with parton showers using the POWHEG method. Eur. Phys. J. C **71**, 1547 (2011). https://doi.org/10.1140/epjc/s10052-011-1547-z. arXiv:1009.2450 [hep-ph]
88. P. Golonka, Z. Was, PHOTOS Monte Carlo: a precision tool for QED corrections in Z and W decays. Eur. Phys. J. C **45**, 97 (2006). https://doi.org/10.1140/epjc/s2005-02396-4. arXiv:hep-ph/0506026
89. J. Bellm et al., Herwig 7.0/Herwig++ 3.0 release note. Eur. Phys. J. **76**, 196 (2016). https://doi.org/10.1140/epjc/s10052-016-4018-8. arXiv:1512.01178 [hep-ph]
90. J. Pumplin et al., New generation of parton distributions with uncertainties from global QCD analysis. JHEP **07**, 012 (2002). https://doi.org/10.1088/1126-6708/2002/07/012. arXiv:hep-ph/0201195
91. ATLAS Collaboration, Development of ATLAS Primary Vertex Reconstruction for LHC Run 3, ATL-PHYS-PUB-2019-015 (2019). https://cds.cern.ch/record/2670380
92. ATLAS Collaboration, Electron and photon performance measurements with the ATLAS detector using the 2015–2017 LHC proton–proton collision data. JINST **14**, P12006 (2019). https://doi.org/10.1088/1748-0221/14/12/P12006. arXiv:1908.00005 [hep-ex]
93. ATLAS Collaboration, Measurement of the photon identification efficiencies with the ATLAS detector using LHC Run 2 data collected in 2015 and 2016. Eur. Phys. J. C **79**, 205 (2019). https://doi.org/10.1140/epjc/s10052-019-6650-6. arXiv:1810.05087 [hep-ex]
94. ATLAS Collaboration, Muon reconstruction and identification efficiency in ATLAS using the full Run 2 pp collision data set at $\sqrt{s} = 13\,TeV$. Eur. Phys. J. C **81**, 578 (2021). https://doi.org/10.1140/epjc/s10052-021-09233-2. arXiv:2012.00578 [hep-ex]
95. ATLAS Collaboration, Muon reconstruction performance of the ATLAS detector in proton–proton collision data at $\sqrt{s} = 13\,TeV$. Eur. Phys. J. C **76**, 292 (2016). https://doi.org/10.1140/epjc/s10052-016-4120-y. arXiv:1603.05598 [hep-ex]
96. ATLAS Collaboration, Evidence for the associated production of the Higgs boson and a top quark pair with the ATLAS detector. Phys. Rev. D **97**, 072003 (2018). https://doi.org/10.1103/PhysRevD.97.072003. arXiv:1712.08891 [hep-ex]
97. ATLAS Collaboration, Electron reconstruction and identification in the ATLAS experiment using the 2015 and 2016 LHC proton–proton collision data at $\sqrt{s} = 13\,TeV$. Eur. Phys. J. C **79**, 639 (2019). https://doi.org/10.1140/epjc/s10052-019-7140-6. arXiv:1902.04655 [physics.ins-det]
98. ATLAS Collaboration, Jet reconstruction and performance using particle flow with the ATLAS Detector. Eur. Phys. J. C **77**, 466

(2017). https://doi.org/10.1140/epjc/s10052-017-5031-2. arXiv:1703.10485 [hep-ex]
99. ATLAS Collaboration, Jet energy scale and resolution measured in proton–proton collisions at $\sqrt{s} = 13\,TeV$ with the ATLAS detector. Eur. Phys. J. C **81**, 689 (2020). https://doi.org/10.1140/epjc/s10052-021-09402-3. arXiv:2007.02645 [hep-ex]
100. M. Cacciari, G.P. Salam, G. Soyez, The anti-k_t jet clustering algorithm. JHEP **04**, 063 (2008). https://doi.org/10.1088/1126-6708/2008/04/063. arXiv:0802.1189 [hep-ph]
101. M. Cacciari, G.P. Salam, G. Soyez, FastJet user manual. Eur. Phys. J. C **72**, 1896 (2012). https://doi.org/10.1140/epjc/s10052-012-1896-2. arXiv:1111.6097 [hep-ph]
102. ATLAS Collaboration, Tagging and suppression of pileup jets with the ATLAS detector, ATLAS-CONF-2014-018 (2014). https://cds.cern.ch/record/1700870
103. ATLAS Collaboration, Selection of jets produced in $13\,TeV$ proton–proton collisions with the ATLAS detector, ATLAS-CONF-2015-029 (2015). https://cds.cern.ch/record/2037702
104. ATLAS Collaboration, ATLAS b-jet identification performance and efficiency measurement with $t\bar{t}$ events in pp collisions at $\sqrt{s} = 13\,TeV$. Eur. Phys. J. C **79**, 970 (2019). https://doi.org/10.1140/epjc/s10052-019-7450-8. arXiv:1907.05120 [hep-ex]
105. ATLAS Collaboration, Optimisation and performance studies of the ATLAS b-tagging algorithms for the 2017-18 LHC run, ATL-PHYS-PUB-2017-013 (2017). https://cds.cern.ch/record/2273281
106. ATLAS Collaboration, Identification of Jets Containing b-Hadrons with Recurrent Neural Networks at the ATLAS Experiment, ATL-PHYS-PUB-2017-003 (2017). https://cds.cern.ch/record/2255226
107. ATLAS Collaboration, Measurement of b-tagging efficiency of c-jets in $t\bar{t}$ events using a likelihood approach with the ATLAS detector, ATLAS-CONF-2018-001 (2018). https://cds.cern.ch/record/2306649
108. ATLAS Collaboration, Calibration of light-flavour b-jet mistagging rates using ATLAS proton–proton collision data at $\sqrt{s} = 13\,TeV$ ATLAS-CONF-2018-006 (2018). https://cds.cern.ch/record/2314418
109. M. Cacciari, G.P. Salam, G. Soyez, The catchment area of jets. JHEP **04**, 005 (2008). https://doi.org/10.1088/1126-6708/2008/04/005. arXiv:0802.1188 [hep-ph]
110. ATLAS Collaboration, Performance of missing transverse momentum reconstruction with the ATLAS detector using proton–proton collisions at $\sqrt{s} = 13\,TeV$. Eur. Phys. J. C **78**, 903 (2018). https://doi.org/10.1140/epjc/s10052-018-6288-9. arXiv:1802.08168 [hep-ex]
111. ATLAS Collaboration, Performance of the ATLAS muon triggers in Run 2. JINST **15**, P09015 (2020). https://doi.org/10.1088/1748-0221/15/09/p09015. arXiv:2004.13447 [physics.ins-det]
112. ATLAS Collaboration, Performance of electron and photon triggers in ATLAS during LHC Run 2. Eur. Phys. J. C **80**, 47 (2020). https://doi.org/10.1140/epjc/s10052-019-7500-2. arXiv:1909.00761 [hep-ex]
113. ATLAS Collaboration, Operation of the ATLAS trigger system in Run 2. JINST **15**, P10004 (2020). https://doi.org/10.1088/1748-0221/15/10/P10004. arXiv:2007.12539 [hep-ex]
114. ATLAS Collaboration, Evidence for $t\bar{t}t\bar{t}$ production in the multilepton final state in proton–proton collisions at $\sqrt{s} = 13$ TeV with the ATLAS detector. Eur. Phys. J. C **80**, 1085 (2020). https://doi.org/10.1140/epjc/s10052-020-08509-3. arXiv:2007.14858 [hep-ex]
115. ATLAS Collaboration, Measurement of the $t\bar{t}Z$ and $t\bar{t}W$ cross sections in proton-proton collisions at $\sqrt{s} = 13$ TeV with the ATLAS detector. Phys. Rev. D **99**, 072009 (2019). https://doi.org/10.1103/PhysRevD.99.072009. arXiv:1901.03584 [hep-ex]
116. ATLAS Collaboration, Measurement of the $t\bar{t}t\bar{t}$ production cross section in pp collisions at $\sqrt{s} = 13\,TeV$ with the ATLAS detector. JHEP **11**, 118 (2021). https://doi.org/10.1007/JHEP11(2021)118. arXiv:2106.11683 [hep-ex]
117. ATLAS Collaboration, Luminosity determination in pp collisions at $\sqrt{s} = 13\,TeV$ using the ATLAS detector at the LHC, ATLAS-CONF-2019-021 (2019). https://cds.cern.ch/record/2677054
118. G. Avoni et al., The new LUCID-2 detector for luminosity measurement and monitoring in ATLAS. JINST **13**, P07017 (2018). https://doi.org/10.1088/1748-0221/13/07/P07017
119. ATLAS Collaboration, Jet energy scale measurements and their systematic uncertainties in proton–proton collisions at $\sqrt{s} = 13\,TeV$ with the ATLAS detector. Phys. Rev. D **96**, 072002 (2017). https://doi.org/10.1103/PhysRevD.96.072002. arXiv:1703.09665 [hep-ex]
120. ATLAS Collaboration, Performance of pile-up mitigation techniques for jets in pp collisions at $\sqrt{s} = 8\,TeV$ using the ATLAS detector. Eur. Phys. J. C **76**, 581 (2016). https://doi.org/10.1140/epjc/s10052-016-4395-z. arXiv:1510.03823 [hep-ex]
121. ATLAS Collaboration, Constituent-level pile-up mitigation techniques in ATLAS, ATLAS-CONF-2017-065 (2017). https://cds.cern.ch/record/2281055
122. ATLAS Collaboration, Measurement of the c-jet mistagging efficiency in $t\bar{t}$ events using pp collision data at $\sqrt{s} = 13\,TeV$ collected with the ATLAS detector. Eur. Phys. J. C **82**, 95 (2022). https://doi.org/10.1140/epjc/s10052-021-09843-w. arXiv:2109.10627 [hep-ex]
123. J. Butterworth et al., PDF4LHC recommendations for LHC Run II. J. Phys. G **43**, 023001 (2016). https://doi.org/10.1088/0954-3899/43/2/023001. arXiv:1510.03865 [hep-ph]
124. K. Cranmer, G. Lewis, L. Moneta, A. Shibata, W. Verkerke, HistFactory: a tool for creating statistical models for use with RooFit and RooStats, CERN-OPEN-2012-016 (2012). https://cds.cern.ch/record/1456844
125. R.J. Barlow, C. Beeston, Fitting using finite Monte Carlo samples. Comput. Phys. Commun. **77**, 219 (1993). https://doi.org/10.1016/0010-4655(93)90005-W
126. W. Verkerke, D.P. Kirkby, The RooFit toolkit for data modeling, eConf C0303241, MOLT007 (2003). arXiv:physics/0306116 [physics.data-an]
127. T. Junk, Confidence level computation for combining searches with small statistics. Nucl. Instrum. Meth. A **434**, 435 (1999). https://doi.org/10.1016/S0168-9002(99)00498-2. arXiv:hep-ex/9902006
128. A.L. Read, Presentation of search results: the CL_S technique. J. Phys. G **28**, 2693 (2002). https://doi.org/10.1088/0954-3899/28/10/313
129. ATLAS Collaboration, ATLAS Computing Acknowledgements, ATL-SOFT-PUB-2023-001 (2023). https://cds.cern.ch/record/2869272

ATLAS Collaboration*

G. Aad[101], B. Abbott[119], D. C. Abbott[102], K. Abeling[55], S. H. Abidi[29], A. Aboulhorma[35e], H. Abramowicz[150], H. Abreu[149], Y. Abulaiti[116], A. C. Abusleme Hoffman[136a], B. S. Acharya[68a,68b,q], B. Achkar[55], C. Adam Bourdarios[4], L. Adamczyk[84a], L. Adamek[154], S. V. Addepalli[26], J. Adelman[114], A. Adiguzel[21c], S. Adorni[56], T. Adye[133], A. A. Affolder[135], Y. Afik[36], M. N. Agaras[13], J. Agarwala[72a,72b], A. Aggarwal[99], C. Agheorghiesei[27c], J. A. Aguilar-Saavedra[129f], A. Ahmad[36], F. Ahmadov[38,ab], W. S. Ahmed[103], S. Ahuja[94], X. Ai[48], G. Aielli[75a,75b], I. Aizenberg[168], M. Akbiyik[99], T. P. A. Åkesson[97], A. V. Akimov[37], K. Al Khoury[41], G. L. Alberghi[23b], J. Albert[164], P. Albicocco[53], S. Alderweireldt[52], M. Aleksa[36], I. N. Aleksandrov[38], C. Alexa[27b], T. Alexopoulos[10], A. Alfonsi[113], F. Alfonsi[23b], M. Alhroob[119], B. Ali[131], S. Ali[147], M. Aliev[37], G. Alimonti[70a], W. Alkakhi[55], C. Allaire[66], B. M. M. Allbrooke[145], P. P. Allport[20], A. Aloisio[71a,71b], F. Alonso[89], C. Alpigiani[137], E. Alunno Camelia[75a,75b], M. Alvarez Estevez[98], M. G. Alviggi[71a,71b], M. Aly[100], Y. Amaral Coutinho[81b], A. Ambler[103], C. Amelung[36], M. Amerl[1], C. G. Ames[108], D. Amidei[105], S. P. Amor Dos Santos[129a], S. Amoroso[48], K. R. Amos[162], V. Ananiev[124], C. Anastopoulos[138], T. Andeen[11], J. K. Anders[36], S. Y. Andrean[47a,47b], A. Andreazza[70a,70b], S. Angelidakis[9], A. Angerami[41,ae], A. V. Anisenkov[37], A. Annovi[73a], C. Antel[56], M. T. Anthony[138], E. Antipov[120], M. Antonelli[53], D. J. A. Antrim[17a], F. Anulli[74a], M. Aoki[82], T. Aoki[152], J. A. Aparisi Pozo[162], M. A. Aparo[145], L. Aperio Bella[48], C. Appelt[18], N. Aranzabal[36], V. Araujo Ferraz[81a], C. Arcangeletti[53], A. T. H. Arce[51], E. Arena[91], J-F. Arguin[107], S. Argyropoulos[54], J.-H. Arling[48], A. J. Armbruster[36], O. Arnaez[154], H. Arnold[113], Z. P. Arrubarrena Tame[108], G. Artoni[74a,74b], H. Asada[110], K. Asai[117], S. Asai[152], N. A. Asbah[61], K. Assamagan[29], R. Astalos[28a], R. J. Atkin[33a], M. Atkinson[161], N. B. Atlay[18], H. Atmani[62b], P. A. Atmasiddha[105], K. Augsten[131], S. Auricchio[71a,71b], A. D. Auriol[20], V. A. Austrup[170], G. Avner[149], G. Avolio[36], K. Axiotis[56], M. K. Ayoub[14c], G. Azuelos[107,aj], D. Babal[28a], H. Bachacou[134], K. Bachas[151,t], A. Bachiu[34], F. Backman[47a,47b], A. Badea[61], P. Bagnaia[74a,74b], M. Bahmani[18], A. J. Bailey[162], V. R. Bailey[161], J. T. Baines[133], C. Bakalis[10], O. K. Baker[171], P. J. Bakker[113], E. Bakos[15], D. Bakshi Gupta[8], S. Balaji[146], R. Balasubramanian[113], E. M. Baldin[37], P. Balek[132], E. Ballabene[70a,70b], F. Balli[134], L. M. Baltes[63a], W. K. Balunas[32], J. Balz[99], E. Banas[85], M. Bandieramonte[128], A. Bandyopadhyay[24], S. Bansal[24], L. Barak[150], E. L. Barberio[104], D. Barberis[57a,57b], M. Barbero[101], G. Barbour[95], K. N. Barends[33a], T. Barillari[109], M-S. Barisits[36], T. Barklow[142], R. M. Barnett[17a], P. Baron[121], D. A. Baron Moreno[100], A. Baroncelli[62a], G. Barone[29], A. J. Barr[125], L. Barranco Navarro[47a,47b], F. Barreiro[98], J. Barreiro Guimarães da Costa[14a], U. Barron[150], M. G. Barros Teixeira[129a], S. Barsov[37], F. Bartels[63a], R. Bartoldus[142], A. E. Barton[90], P. Bartos[28a], A. Basalaev[48], A. Basan[99], M. Baselga[49], I. Bashta[76a,76b], A. Bassalat[66,b], M. J. Basso[154], C. R. Basson[100], R. L. Bates[59], S. Batlamous[35e], J. R. Batley[32], B. Batool[140], M. Battaglia[135], D. Battulga[18], M. Bauce[74a,74b], P. Bauer[24], A. Bayirli[21a], J. B. Beacham[51], T. Beau[126], P. H. Beauchemin[157], F. Becherer[54], P. Bechtle[24], H. P. Beck[19,s], K. Becker[166], A. J. Beddall[21d], V. A. Bednyakov[38], C. P. Bee[144], L. J. Beemster[15], T. A. Beermann[36], M. Begalli[81d], M. Begel[29], A. Behera[144], J. K. Behr[48], C. Beirao Da Cruz E Silva[36], J. F. Beirer[36,55], F. Beisiegel[24], M. Belfkir[158], G. Bella[150], L. Bellagamba[23b], A. Bellerive[34], P. Bellos[20], K. Beloborodov[37], K. Belotskiy[37], N. L. Belyaev[37], D. Benchekroun[35a], F. Bendebba[35a], Y. Benhammou[150], D. P. Benjamin[29], M. Benoit[29], J. R. Bensinger[26], S. Bentvelsen[113], L. Beresford[36], M. Beretta[53], D. Berge[18], E. Bergeaas Kuutmann[160], N. Berger[4], B. Bergmann[131], J. Beringer[17a], S. Berlendis[7], G. Bernardi[5], C. Bernius[142], F. U. Bernlochner[24], T. Berry[94], P. Berta[132], A. Berthold[50], I. A. Bertram[90], S. Bethke[109], A. Betti[74a,74b], A. J. Bevan[93], M. Bhamjee[33c], S. Bhatta[144], D. S. Bhattacharya[165], P. Bhattarai[26], V. S. Bhopatkar[120], R. Bi[29,am], R. M. Bianchi[128], O. Biebel[108], R. Bielski[122], M. Biglietti[76a], T. R. V. Billoud[131], M. Bindi[55], A. Bingul[21b], C. Bini[74a,74b], S. Biondi[23a,23b], A. Biondini[91], C. J. Birch-sykes[100], G. A. Bird[20,133], M. Birman[168], T. Bisanz[36], E. Bisceglie[43a,43b], D. Biswas[169,m], A. Bitadze[100], K. Bjørke[124], I. Bloch[48], C. Blocker[26], A. Blue[59], U. Blumenschein[93], J. Blumenthal[99], G. J. Bobbink[113], V. S. Bobrovnikov[37], M. Boehler[54], D. Bogavac[36], A. G. Bogdanchikov[37], C. Bohm[47a], V. Boisvert[94], P. Bokan[48], T. Bold[84a], M. Bomben[5], M. Bona[93], M. Boonekamp[134], C. D. Booth[94], A. G. Borbély[59], H. M. Borecka-Bielska[107], L. S. Borgna[95], G. Borissov[90], D. Bortoletto[125], D. Boscherini[23b], M. Bosman[13], J. D. Bossio Sola[36], K. Bouaouda[35a], N. Bouchhar[162], J. Boudreau[128], E. V. Bouhova-Thacker[90], D. Boumediene[40], R. Bouquet[5], A. Boveia[118], J. Boyd[36], D. Boye[29], I. R. Boyko[38], J. Bracinik[20], N. Brahimi[62d], G. Brandt[170], O. Brandt[32], F. Braren[48], B. Brau[102],

J. E. Brau[122], K. Brendlinger[48], R. Brener[168], L. Brenner[113], R. Brenner[160], S. Bressler[168], B. Brickwedde[99], D. Britton[59], D. Britzger[109], I. Brock[24], G. Brooijmans[41], W. K. Brooks[136f], E. Brost[29], T. L. Bruckler[125], P. A. Bruckman de Renstrom[85], B. Brüers[48], D. Bruncko[28b,*], A. Bruni[23b], G. Bruni[23b], M. Bruschi[23b], N. Bruscino[74a,74b], L. Bryngemark[142], T. Buanes[16], Q. Buat[137], P. Buchholz[140], A. G. Buckley[59], I. A. Budagov[38,*], M. K. Bugge[124], O. Bulekov[37], B. A. Bullard[61], S. Burdin[91], C. D. Burgard[48], A. M. Burger[40], B. Burghgrave[8], J. T. P. Burr[32], C. D. Burton[11], J. C. Burzynski[141], E. L. Busch[41], V. Büscher[99], P. J. Bussey[59], J. M. Butler[25], C. M. Buttar[59], J. M. Butterworth[95], W. Buttinger[133], C. J. Buxo Vazquez[106], A. R. Buzykaev[37], G. Cabras[23b], S. Cabrera Urbán[162], D. Caforio[58], H. Cai[128], Y. Cai[14a,14d], V. M. M. Cairo[36], O. Cakir[3a], N. Calace[36], P. Calafiura[17a], G. Calderini[126], P. Calfayan[67], G. Callea[59], L. P. Caloba[81b], D. Calvet[40], S. Calvet[40], T. P. Calvet[101], M. Calvetti[73a,73b], R. Camacho Toro[126], S. Camarda[36], D. Camarero Munoz[26], P. Camarri[75a,75b], M. T. Camerlingo[76a,76b], D. Cameron[124], C. Camincher[164], M. Campanelli[95], A. Camplani[42], V. Canale[71a,71b], A. Canesse[103], M. Cano Bret[79], J. Cantero[162], Y. Cao[161], F. Capocasa[26], M. Capua[43a,43b], A. Carbone[70a,70b], R. Cardarelli[75a], J. C. J. Cardenas[8], F. Cardillo[162], T. Carli[36], G. Carlino[71a], J. I. Carlotto[13], B. T. Carlson[128,u], E. M. Carlson[155a,164], L. Carminati[70a,70b], M. Carnesale[74a,74b], S. Caron[112], E. Carquin[136f], S. Carrá[70a], G. Carratta[23a,23b], F. Carrio Argos[33g], J. W. S. Carter[154], T. M. Carter[52], M. P. Casado[13,j], A. F. Casha[154], E. G. Castiglia[171], F. L. Castillo[63a], L. Castillo Garcia[13], V. Castillo Gimenez[162], N. F. Castro[129a,129e], A. Catinaccio[36], J. R. Catmore[124], V. Cavaliere[29], N. Cavalli[23a,23b], V. Cavasinni[73a,73b], E. Celebi[21a], F. Celli[125], M. S. Centonze[69a,69b], K. Cerny[121], A. S. Cerqueira[81a], A. Cerri[145], L. Cerrito[75a,75b], F. Cerutti[17a], A. Cervelli[23b], S. A. Cetin[21d], Z. Chadi[35a], D. Chakraborty[114], M. Chala[129f], J. Chan[169], W. Y. Chan[152], J. D. Chapman[32], B. Chargeishvili[148b], D. G. Charlton[20], T. P. Charman[93], M. Chatterjee[19], S. Chekanov[6], S. V. Chekulaev[155a], G. A. Chelkov[38,a], A. Chen[105], B. Chen[150], B. Chen[164], H. Chen[14c], H. Chen[29], J. Chen[62c], J. Chen[26], S. Chen[152], S. J. Chen[14c], X. Chen[62c], X. Chen[14b,ai], Y. Chen[62a], C. L. Cheng[169], H. C. Cheng[64a], S. Cheong[142], A. Cheplakov[38], E. Cheremushkina[48], E. Cherepanova[113], R. Cherkaoui El Moursli[35e], E. Cheu[7], K. Cheung[65], L. Chevalier[134], V. Chiarella[53], G. Chiarelli[73a], N. Chiedde[101], G. Chiodini[69a], A. S. Chisholm[20], A. Chitan[27b], M. Chitishvili[162], Y. H. Chiu[164], M. V. Chizhov[38], K. Choi[11], A. R. Chomont[74a,74b], Y. Chou[102], E. Y. S. Chow[113], T. Chowdhury[33g], L. D. Christopher[33g], K. L. Chu[64a], M. C. Chu[64a], X. Chu[14a,14d], J. Chudoba[130], J. J. Chwastowski[85], D. Cieri[109], K. M. Ciesla[84a], V. Cindro[92], A. Ciocio[17a], F. Cirotto[71a,71b], Z. H. Citron[168,n], M. Citterio[70a], D. A. Ciubotaru[27b], B. M. Ciungu[154], A. Clark[56], P. J. Clark[52], J. M. Clavijo Columbie[48], S. E. Clawson[100], C. Clement[47a,47b], J. Clercx[48], Y. Coadou[101], M. Cobal[68a,68c], A. Coccaro[57b], R. F. Coelho Barrue[129a], R. Coelho Lopes De Sa[102], S. Coelli[70a], H. Cohen[150], A. E. C. Coimbra[70a,70b], B. Cole[41], J. Collot[60], P. Conde Muiño[129a,129g], M. P. Connell[33c], S. H. Connell[33c], I. A. Connelly[59], E. I. Conroy[125], F. Conventi[71a,ak], H. G. Cooke[20], A. M. Cooper-Sarkar[125], F. Cormier[163], L. D. Corpe[36], M. Corradi[74a,74b], E. E. Corrigan[97], F. Corriveau[103,z], A. Cortes-Gonzalez[18], M. J. Costa[162], F. Costanza[4], D. Costanzo[138], B. M. Cote[118], G. Cowan[94], J. W. Cowley[32], K. Cranmer[116], S. Crépé-Renaudin[60], F. Crescioli[126], M. Cristinziani[140], M. Cristoforetti[77a,77b,d], V. Croft[157], G. Crosetti[43a,43b], A. Cueto[36], T. Cuhadar Donszelmann[159], H. Cui[14a,14d], Z. Cui[7], A. R. Cukierman[142], W. R. Cunningham[59], F. Curcio[43a,43b], P. Czodrowski[36], M. M. Czurylo[63b], M. J. Da Cunha Sargedas De Sousa[62a], J. V. Da Fonseca Pinto[81b], C. Da Via[100], W. Dabrowski[84a], T. Dado[49], S. Dahbi[33g], T. Dai[105], C. Dallapiccola[102], M. Dam[42], G. D'amen[29], V. D'Amico[108], J. Damp[99], J. R. Dandoy[127], M. F. Daneri[30], M. Danninger[141], V. Dao[36], G. Darbo[57b], S. Darmora[6], S. J. Das[29,am], S. D'Auria[70a,70b], C. David[155b], T. Davidek[132], D. R. Davis[51], B. Davis-Purcell[34], I. Dawson[93], K. De[8], R. De Asmundis[71a], M. De Beurs[113], N. De Biase[48], S. De Castro[23a,23b], N. De Groot[112], P. de Jong[113], H. De la Torre[106], A. De Maria[14c], A. De Salvo[74a], U. De Sanctis[75a,75b], A. De Santo[145], J. B. De Vivie De Regie[60], D. V. Dedovich[38], J. Degens[113], A. M. Deiana[44], F. Del Corso[23a,23b], J. Del Peso[98], F. Del Rio[63a], F. Deliot[134], C. M. Delitzsch[49], M. Della Pietra[71a,71b], D. Della Volpe[56], A. Dell'Acqua[36], L. Dell'Asta[70a,70b], M. Delmastro[4], P. A. Delsart[60], S. Demers[171], M. Demichev[38], S. P. Denisov[37], L. D'Eramo[114], D. Derendarz[85], F. Derue[126], P. Dervan[91], K. Desch[24], K. Dette[154], C. Deutsch[24], P. O. Deviveiros[36], F. A. Di Bello[57a,57b], A. Di Ciaccio[75a,75b], L. Di Ciaccio[4], A. Di Domenico[74a,74b], C. Di Donato[71a,71b], A. Di Girolamo[36], G. Di Gregorio[5], A. Di Luca[77a,77b], B. Di Micco[76a,76b], R. Di Nardo[76a,76b], C. Diaconu[101], F. A. Dias[113], T. Dias Do Vale[141], M. A. Diaz[136a,136b], F. G. Diaz Capriles[24], M. Didenko[162], E. B. Diehl[105], L. Diehl[54], S. Díez Cornell[48], C. Diez Pardos[140], C. Dimitriadi[24,160], A. Dimitrievska[17a],

W. Ding[14b], J. Dingfelder[24], I-M. Dinu[27b], S. J. Dittmeier[63b], F. Dittus[36], F. Djama[101], T. Djobava[148b], J. I. Djuvsland[16], C. Doglioni[97,100], J. Dolejsi[132], Z. Dolezal[132], M. Donadelli[81c], B. Dong[62c], J. Donini[40], A. D'Onofrio[14c], M. D'Onofrio[91], J. Dopke[133], A. Doria[71a], M. T. Dova[89], A. T. Doyle[59], M. A. Draguet[125], E. Drechsler[141], E. Dreyer[168], I. Drivas-koulouris[10], A. S. Drobac[157], M. Drozdova[56], D. Du[62a], T. A. du Pree[113], F. Dubinin[37], M. Dubovsky[28a], E. Duchovni[168], G. Duckeck[108], O. A. Ducu[27b], D. Duda[109], A. Dudarev[36], M. D'uffizi[100], L. Duflot[66], M. Dührssen[36], C. Dülsen[170], A. E. Dumitriu[27b], M. Dunford[63a], S. Dungs[49], K. Dunne[47a,47b], A. Duperrin[101], H. Duran Yildiz[3a], M. Düren[58], A. Durglishvili[148b], B. L. Dwyer[114], G. I. Dyckes[17a], M. Dyndal[84a], S. Dysch[100], B. S. Dziedzic[85], Z. O. Earnshaw[145], B. Eckerova[28a], M. G. Eggleston[51], E. Egidio Purcino De Souza[81b], L. F. Ehrke[56], G. Eigen[16], K. Einsweiler[17a], T. Ekelof[160], P. A. Ekman[97], Y. El Ghazali[35b], H. El Jarrari[35e,147], A. El Moussaouy[35a], V. Ellajosyula[160], M. Ellert[160], F. Ellinghaus[170], A. A. Elliot[93], N. Ellis[36], J. Elmsheuser[29], M. Elsing[36], D. Emeliyanov[133], A. Emerman[41], Y. Enari[152], I. Ene[17a], S. Epari[13], J. Erdmann[49,ag], A. Ereditato[19], P. A. Erland[85], M. Errenst[170], M. Escalier[66], C. Escobar[162], E. Etzion[150], G. Evans[129a], H. Evans[67], M. O. Evans[145], A. Ezhilov[37], S. Ezzarqtouni[35a], F. Fabbri[59], L. Fabbri[23a,23b], G. Facini[95], V. Fadeyev[135], R. M. Fakhrutdinov[37], S. Falciano[74a], P. J. Falke[24], S. Falke[36], J. Faltova[132], Y. Fan[14a], Y. Fang[14a,14d], G. Fanourakis[46], M. Fanti[70a,70b], M. Faraj[68a,68b], Z. Farazpay[96], A. Farbin[8], A. Farilla[76a], T. Farooque[106], S. M. Farrington[52], F. Fassi[35e], D. Fassouliotis[9], M. Faucci Giannelli[75a,75b], W. J. Fawcett[32], L. Fayard[66], P. Federicova[130], O. L. Fedin[37,a], G. Fedotov[37], M. Feickert[169], L. Feligioni[101], A. Fell[138], D. E. Fellers[122], C. Feng[62b], M. Feng[14b], Z. Feng[113], M. J. Fenton[159], A. B. Fenyuk[37], L. Ferencz[48], S. W. Ferguson[45], J. Ferrando[48], A. Ferrari[160], P. Ferrari[112,113], R. Ferrari[72a], D. Ferrere[56], C. Ferretti[105], F. Fiedler[99], A. Filipčič[92], E. K. Filmer[1], F. Filthaut[112], M. C. N. Fiolhais[129a,129c,c], L. Fiorini[162], F. Fischer[140], W. C. Fisher[106], T. Fitschen[100], I. Fleck[140], P. Fleischmann[105], T. Flick[170], L. Flores[127], M. Flores[33d,af], L. R. Flores Castillo[64a], F. M. Follega[77a,77b], N. Fomin[16], J. H. Foo[154], B. C. Forland[67], A. Formica[134], A. C. Forti[100], E. Fortin[101], A. W. Fortman[61], M. G. Foti[17a], L. Fountas[9,k], D. Fournier[66], H. Fox[90], P. Francavilla[73a,73b], S. Francescato[61], S. Franchellucci[56], M. Franchini[23a,23b], S. Franchino[63a], D. Francis[36], L. Franco[112], L. Franconi[19], M. Franklin[61], G. Frattari[26], A. C. Freegard[93], P. M. Freeman[20], W. S. Freund[81b], N. Fritzsche[50], A. Froch[54], D. Froidevaux[36], J. A. Frost[125], Y. Fu[62a], M. Fujimoto[117], E. Fullana Torregrosa[162,*], J. Fuster[162], A. Gabrielli[23a,23b], A. Gabrielli[154], P. Gadow[48], G. Gagliardi[57a,57b], L. G. Gagnon[17a], G. E. Gallardo[125], E. J. Gallas[125], B. J. Gallop[133], R. Gamboa Goni[93], K. K. Gan[118], S. Ganguly[152], J. Gao[62a], Y. Gao[52], F. M. Garay Walls[136a,136b], B. Garcia[29], C. García[162], J. E. García Navarro[162], J. A. García Pascual[14a], M. Garcia-Sciveres[17a], R. W. Gardner[39], D. Garg[79], R. B. Garg[142,r], S. Gargiulo[54], C. A. Garner[154], V. Garonne[29], S. J. Gasiorowski[137], P. Gaspar[81b], G. Gaudio[72a], V. Gautam[13], P. Gauzzi[74a,74b], I. L. Gavrilenko[37], A. Gavrilyuk[37], C. Gay[163], G. Gaycken[48], E. N. Gazis[10], A. A. Geanta[27b,27e], C. M. Gee[135], J. Geisen[97], M. Geisen[99], C. Gemme[57b], M. H. Genest[60], S. Gentile[74a,74b], S. George[94], W. F. George[20], T. Geralis[46], L. O. Gerlach[55], P. Gessinger-Befurt[36], M. Ghasemi Bostanabad[164], M. Ghneimat[140], K. Ghorbanian[93], A. Ghosal[140], A. Ghosh[159], A. Ghosh[7], B. Giacobbe[23b], S. Giagu[74a,74b], N. Giangiacomi[154], P. Giannetti[73a], A. Giannini[62a], S. M. Gibson[94], M. Gignac[135], D. T. Gil[84b], A. K. Gilbert[84a], B. J. Gilbert[41], D. Gillberg[34], G. Gilles[113], N. E. K. Gillwald[48], L. Ginabat[126], D. M. Gingrich[2,aj], M. P. Giordani[68a,68c], P. F. Giraud[134], G. Giugliarelli[68a,68c], D. Giugni[70a], F. Giuli[36], I. Gkialas[9,k], L. K. Gladilin[37], C. Glasman[98], G. R. Gledhill[122], M. Glisic[122], I. Gnesi[43b,g], Y. Go[29,am], M. Goblirsch-Kolb[26], B. Gocke[49], D. Godin[107], S. Goldfarb[104], T. Golling[56], M. G. D. Gololo[33g], D. Golubkov[37], J. P. Gombas[106], A. Gomes[129a,129b], G. Gomes Da Silva[140], A. J. Gomez Delegido[162], R. Goncalves Gama[55], R. Gonçalo[129a,129c], G. Gonella[122], L. Gonella[20], A. Gongadze[38], F. Gonnella[20], J. L. Gonski[41], R. Y. González Andana[52], S. González de la Hoz[162], S. Gonzalez Fernandez[13], R. Gonzalez Lopez[91], C. Gonzalez Renteria[17a], R. Gonzalez Suarez[160], S. Gonzalez-Sevilla[56], G. R. Gonzalvo Rodriguez[162], L. Goossens[36], N. A. Gorasia[20], P. A. Gorbounov[37], B. Gorini[36], E. Gorini[69a,69b], A. Gorišek[92], A. T. Goshaw[51], M. I. Gostkin[38], C. A. Gottardo[36], M. Gouighri[35b], V. Goumarre[48], A. G. Goussiou[137], N. Govender[33c], C. Goy[4], I. Grabowska-Bold[84a], K. Graham[34], E. Gramstad[124], S. Grancagnolo[18], M. Grandi[145], V. Gratchev[37,*], P. M. Gravila[27f], F. G. Gravili[69a,69b], H. M. Gray[17a], M. Greco[69a,69b], C. Grefe[24], I. M. Gregor[48], P. Grenier[142], C. Grieco[13], A. A. Grillo[135], K. Grimm[31,o], S. Grinstein[13,w], J.-F. Grivaz[66], E. Gross[168], J. Grosse-Knetter[55], C. Grud[105], A. Grummer[111], J. C. Grundy[125], L. Guan[105], W. Guan[29], C. Gubbels[163], J. G. R. Guerrero Rojas[162], G. Guerrieri[68a,68b], F. Guescini[109], R. Gugel[99], J. A. M. Guhit[105], A. Guida[48], T. Guillemin[4],

E. Guilloton[133,166], S. Guindon[36], F. Guo[14a,14d], J. Guo[62c], L. Guo[66], Y. Guo[105], R. Gupta[48], S. Gurbuz[24], S. S. Gurdasani[54], G. Gustavino[36], M. Guth[56], P. Gutierrez[119], L. F. Gutierrez Zagazeta[127], C. Gutschow[95], C. Guyot[134], C. Gwenlan[125], C. B. Gwilliam[91], E. S. Haaland[124], A. Haas[116], M. Habedank[48], C. Haber[17a], H. K. Hadavand[8], A. Hadef[99], S. Hadzic[109], E. H. Haines[95], M. Haleem[165], J. Haley[120], J. J. Hall[138], G. D. Hallewell[101], L. Halser[19], K. Hamano[164], M. Hamer[24], G. N. Hamity[52], J. Han[62b], K. Han[62a], L. Han[14c], L. Han[62a], S. Han[17a], Y. F. Han[154], K. Hanagaki[82], M. Hance[135], D. A. Hangal[41,ae], H. Hanif[141], M. D. Hank[39], R. Hankache[100], J. B. Hansen[42], J. D. Hansen[42], P. H. Hansen[42], K. Hara[156], D. Harada[56], T. Harenberg[170], S. Harkusha[37], Y. T. Harris[125], N. M. Harrison[118], P. F. Harrison[166], N. M. Hartman[142], N. M. Hartmann[108], Y. Hasegawa[139], A. Hasib[52], S. Haug[19], R. Hauser[106], M. Havranek[131], C. M. Hawkes[20], R. J. Hawkings[36], S. Hayashida[110], D. Hayden[106], C. Hayes[105], R. L. Hayes[163], C. P. Hays[125], J. M. Hays[93], H. S. Hayward[91], F. He[62a], Y. He[153], Y. He[126], M. P. Heath[52], V. Hedberg[97], A. L. Heggelund[124], N. D. Hehir[93,*], C. Heidegger[54], K. K. Heidegger[54], W. D. Heidorn[80], J. Heilman[34], S. Heim[48], T. Heim[17a], J. G. Heinlein[127], J. J. Heinrich[122], L. Heinrich[109,ah], J. Hejbal[130], L. Helary[48], A. Held[169], S. Hellesund[124], C. M. Helling[163], S. Hellman[47a,47b], C. Helsens[36], R. C. W. Henderson[90], L. Henkelmann[32], A. M. Henriques Correia[36], H. Herde[97], Y. Hernández Jiménez[144], L. M. Herrmann[24], M. G. Herrmann[108], T. Herrmann[50], G. Herten[54], R. Hertenberger[108], L. Hervas[36], N. P. Hessey[155a], H. Hibi[83], E. Higón-Rodriguez[162], S. J. Hillier[20], I. Hinchliffe[17a], F. Hinterkeuser[24], M. Hirose[123], S. Hirose[156], D. Hirschbuehl[170], T. G. Hitchings[100], B. Hiti[92], J. Hobbs[144], R. Hobincu[27e], N. Hod[168], M. C. Hodgkinson[138], B. H. Hodkinson[32], A. Hoecker[36], J. Hofer[48], D. Hohn[54], T. Holm[24], M. Holzbock[109], L. B. A. H. Hommels[32], B. P. Honan[100], J. Hong[62c], T. M. Hong[128], J. C. Honig[54], A. Hönle[109], B. H. Hooberman[161], W. H. Hopkins[6], Y. Horii[110], S. Hou[147], A. S. Howard[92], J. Howarth[59], J. Hoya[6], M. Hrabovsky[121], A. Hrynevich[48], T. Hryn'ova[4], P. J. Hsu[65], S.-C. Hsu[137], Q. Hu[41], Y. F. Hu[14a,14d,al], D. P. Huang[95], S. Huang[64b], X. Huang[14c], Y. Huang[62a], Y. Huang[14a], Z. Huang[100], Z. Hubacek[131], M. Huebner[24], F. Huegging[24], T. B. Huffman[125], M. Huhtinen[36], S. K. Huiberts[16], R. Hulsken[103], N. Huseynov[12], J. Huston[106], J. Huth[61], R. Hyneman[142], S. Hyrych[28a], G. Iacobucci[56], G. Iakovidis[29], I. Ibragimov[140], L. Iconomidou-Fayard[66], P. Iengo[71a,71b], R. Iguchi[152], T. Iizawa[56], Y. Ikegami[82], A. Ilg[19], N. Ilic[154], H. Imam[35a], T. Ingebretsen Carlson[47a,47b], G. Introzzi[72a,72b], M. Iodice[76a], V. Ippolito[74a,74b], M. Ishino[152], W. Islam[169], C. Issever[18,48], S. Istin[21a,ao], H. Ito[167], J. M. Iturbe Ponce[64a], R. Iuppa[77a,77b], A. Ivina[168], J. M. Izen[45], V. Izzo[71a], P. Jacka[130,131], P. Jackson[1], R. M. Jacobs[48], B. P. Jaeger[141], C. S. Jagfeld[108], G. Jäkel[170], K. Jakobs[54], T. Jakoubek[168], J. Jamieson[59], K. W. Janas[84a], G. Jarlskog[97], A. E. Jaspan[91], M. Javurkova[102], F. Jeanneau[134], L. Jeanty[122], J. Jejelava[148a,ac], P. Jenni[54,h], C. E. Jessiman[34], S. Jézéquel[4], J. Jia[144], X. Jia[61], X. Jia[14a,14d], Z. Jia[14c], Y. Jiang[62a], S. Jiggins[52], J. Jimenez Pena[109], S. Jin[14c], A. Jinaru[27b], O. Jinnouchi[153], P. Johansson[138], K. A. Johns[7], D. M. Jones[32], E. Jones[166], P. Jones[32], R. W. L. Jones[90], T. J. Jones[91], R. Joshi[118], J. Jovicevic[15], X. Ju[17a], J. J. Junggeburth[36], A. Juste Rozas[13,w], S. Kabana[136e], A. Kaczmarska[85], M. Kado[74a,74b], H. Kagan[118], M. Kagan[142], A. Kahn[41], A. Kahn[127], C. Kahra[99], T. Kaji[167], E. Kajomovitz[149], N. Kakati[168], C. W. Kalderon[29], A. Kamenshchikov[154], S. Kanayama[153], N. J. Kang[135], Y. Kano[110], D. Kar[33g], K. Karava[125], M. J. Kareem[155b], E. Karentzos[54], I. Karkanias[151,f], S. N. Karpov[38], Z. M. Karpova[38], V. Kartvelishvili[90], A. N. Karyukhin[37], E. Kasimi[151,f], C. Kato[62d], J. Katzy[48], S. Kaur[34], K. Kawade[139], K. Kawagoe[88], T. Kawamoto[134], G. Kawamura[55], E. F. Kay[164], F. I. Kaya[157], S. Kazakos[13], V. F. Kazanin[37], Y. Ke[144], J. M. Keaveney[33a], R. Keeler[164], G. V. Kehris[61], J. S. Keller[34], A. S. Kelly[95], D. Kelsey[145], J. J. Kempster[20], K. E. Kennedy[41], P. D. Kennedy[99], O. Kepka[130], B. P. Kerridge[166], S. Kersten[170], B. P. Kerševan[92], S. Keshri[66], L. Keszeghova[28a], S. Ketabchi Haghighat[154], M. Khandoga[126], A. Khanov[120], A. G. Kharlamov[37], T. Kharlamova[37], E. E. Khoda[137], T. J. Khoo[18], G. Khoriauli[165], J. Khubua[148b], Y. A. R. Khwaira[66], M. Kiehn[36], A. Kilgallon[122], D. W. Kim[47a,47b], E. Kim[153], Y. K. Kim[39], N. Kimura[95], A. Kirchhoff[55], D. Kirchmeier[50], C. Kirfel[24], J. Kirk[133], A. E. Kiryunin[109], T. Kishimoto[152], D. P. Kisliuk[154], C. Kitsaki[10], O. Kivernyk[24], M. Klassen[63a], C. Klein[34], L. Klein[165], M. H. Klein[105], M. Klein[91], S. B. Klein[56], U. Klein[91], P. Klimek[36], A. Klimentov[29], F. Klimpel[109], T. Klingl[24], T. Klioutchnikova[36], F. F. Klitzner[108], P. Kluit[113], S. Kluth[109], E. Kneringer[78], T. M. Knight[154], A. Knue[54], D. Kobayashi[88], R. Kobayashi[86], M. Kocian[142], P. Kodyš[132], D. M. Koeck[145], P. T. Koenig[24], T. Koffas[34], M. Kolb[134], I. Koletsou[4], T. Komarek[121], K. Köneke[54], A. X. Y. Kong[1], T. Kono[117], N. Konstantinidis[95], B. Konya[97], R. Kopeliansky[67], S. Koperny[84a], K. Korcyl[85], K. Kordas[151,f], G. Koren[150], A. Korn[95], S. Korn[55], I. Korolkov[13], N. Korotkova[37], B. Kortman[113], O. Kortner[109],

S. Kortner[109], W. H. Kostecka[114], V. V. Kostyukhin[140], A. Kotsokechagia[134], A. Kotwal[51], A. Koulouris[36], A. Kourkoumeli-Charalampidi[72a,72b], C. Kourkoumelis[9], E. Kourlitis[6], O. Kovanda[145], R. Kowalewski[164], W. Kozanecki[134], A. S. Kozhin[37], V. A. Kramarenko[37], G. Kramberger[92], P. Kramer[99], M. W. Krasny[126], A. Krasznahorkay[36], J. A. Kremer[99], T. Kresse[50], J. Kretzschmar[91], K. Kreul[18], P. Krieger[154], F. Krieter[108], S. Krishnamurthy[102], A. Krishnan[63b], M. Krivos[132], K. Krizka[17a], K. Kroeninger[49], H. Kroha[109], J. Kroll[130], J. Kroll[127], K. S. Krowpman[106], U. Kruchonak[38], H. Krüger[24], N. Krumnack[80], M. C. Kruse[51], J. A. Krzysiak[85], O. Kuchinskaia[37], S. Kuday[3a], D. Kuechler[48], J. T. Kuechler[48], S. Kuehn[36], T. Kuhl[48], V. Kukhtin[38], Y. Kulchitsky[37,a], S. Kuleshov[136b,136d], M. Kumar[33g], N. Kumari[101], A. Kupco[130], T. Kupfer[49], A. Kupich[37], O. Kuprash[54], H. Kurashige[83], L. L. Kurchaninov[155a], Y. A. Kurochkin[37], A. Kurova[37], M. Kuze[153], A. K. Kvam[102], J. Kvita[121], T. Kwan[103], K. W. Kwok[64a], N. G. Kyriacou[105], L. A. O. Laatu[101], C. Lacasta[162], F. Lacava[74a,74b], H. Lacker[18], D. Lacour[126], N. N. Lad[95], E. Ladygin[38], B. Laforge[126], T. Lagouri[136e], S. Lai[55], I. K. Lakomiec[84a], N. Lalloue[60], J. E. Lambert[119], S. Lammers[67], W. Lampl[7], C. Lampoudis[151,f], A. N. Lancaster[114], E. Lançon[29], U. Landgraf[54], M. P. J. Landon[93], V. S. Lang[54], R. J. Langenberg[102], A. J. Lankford[159], F. Lanni[36], K. Lantzsch[24], A. Lanza[72a], A. Lapertosa[57a,57b], J. F. Laporte[134], T. Lari[70a], F. Lasagni Manghi[23b], M. Lassnig[36], V. Latonova[130], T. S. Lau[64a], A. Laudrain[99], A. Laurier[34], S. D. Lawlor[94], Z. Lawrence[100], M. Lazzaroni[70a,70b], B. Le[100], B. Leban[92], A. Lebedev[80], M. LeBlanc[36], T. LeCompte[6], F. Ledroit-Guillon[60], A. C. A. Lee[95], G. R. Lee[16], L. Lee[61], S. C. Lee[147], S. Lee[47a,47b], T. F. Lee[91], L. L. Leeuw[33c], H. P. Lefebvre[94], M. Lefebvre[164], C. Leggett[17a], K. Lehmann[141], G. Lehmann Miotto[36], M. Leigh[56], W. A. Leight[102], A. Leisos[151,v], M. A. L. Leite[81c], C. E. Leitgeb[48], R. Leitner[132], K. J. C. Leney[44], T. Lenz[24], S. Leone[73a], C. Leonidopoulos[52], A. Leopold[143], C. Leroy[107], R. Les[106], C. G. Lester[32], M. Levchenko[37], J. Levêque[4], D. Levin[105], L. J. Levinson[168], M. P. Lewicki[85], D. J. Lewis[4], A. Li[5], B. Li[14b], B. Li[62b], C. Li[62a], C-Q. Li[62c], H. Li[62a], H. Li[62b], H. Li[14c], H. Li[62b], J. Li[62c], K. Li[137], L. Li[62c], M. Li[14a,14d], Q. Y. Li[62a], S. Li[14a,14d], S. Li[62c,62d,e], T. Li[62b], X. Li[103], Z. Li[62b], Z. Li[125], Z. Li[103], Z. Li[91], Z. Li[14a,14d], Z. Liang[14a], M. Liberatore[48], B. Liberti[75a], K. Lie[64c], J. Lieber Marin[81b], K. Lin[106], R. A. Linck[67], R. E. Lindley[7], J. H. Lindon[2], A. Linss[48], E. Lipeles[127], A. Lipniacka[16], A. Lister[163], J. D. Little[4], B. Liu[14a], B. X. Liu[141], D. Liu[62c,62d], J. B. Liu[62a], J. K. K. Liu[32], K. Liu[62c,62d], M. Liu[62a], M. Y. Liu[62a], P. Liu[14a], Q. Liu[62c,62d,137], X. Liu[62a], Y. Liu[48], Y. Liu[14c,14d], Y. L. Liu[105], Y. W. Liu[62a], M. Livan[72a,72b], J. Llorente Merino[141], S. L. Lloyd[93], E. M. Lobodzinska[48], P. Loch[7], S. Loffredo[75a,75b], T. Lohse[18], K. Lohwasser[138], M. Lokajicek[130,*], J. D. Long[161], I. Longarini[74a,74b], L. Longo[69a,69b], R. Longo[161], I. Lopez Paz[36], A. Lopez Solis[48], J. Lorenz[108], N. Lorenzo Martinez[4], A. M. Lory[108], A. Lösle[54], X. Lou[47a,47b], X. Lou[14a,14d], A. Lounis[66], J. Love[6], P. A. Love[90], J. J. Lozano Bahilo[162], G. Lu[14a,14d], M. Lu[79], S. Lu[127], Y. J. Lu[65], H. J. Lubatti[137], C. Luci[74a,74b], F. L. Lucio Alves[14c], A. Lucotte[60], F. Luehring[67], I. Luise[144], O. Lukianchuk[66], O. Lundberg[143], B. Lund-Jensen[143], N. A. Luongo[122], M. S. Lutz[150], D. Lynn[29], H. Lyons[91], R. Lysak[130], E. Lytken[97], F. Lyu[14a], V. Lyubushkin[38], T. Lyubushkina[38], H. Ma[29], L. L. Ma[62b], Y. Ma[95], D. M. Mac Donell[164], G. Maccarrone[53], J. C. MacDonald[138], R. Madar[40], W. F. Mader[50], J. Maeda[83], T. Maeno[29], M. Maerker[50], V. Magerl[54], H. Maguire[138], D. J. Mahon[41], C. Maidantchik[81b], A. Maio[129a,129b,129d], K. Maj[84a], O. Majersky[28a], S. Majewski[122], N. Makovec[66], V. Maksimovic[15], B. Malaescu[126], Pa. Malecki[85], V. P. Maleev[37], F. Malek[60], D. Malito[43a,43b], U. Mallik[79], C. Malone[32], S. Maltezos[10], S. Malyukov[38], J. Mamuzic[13], G. Mancini[53], G. Manco[72a,72b], J. P. Mandalia[93], I. Mandić[92], L. Manhaes de Andrade Filho[81a], I. M. Maniatis[151,f], M. Manisha[134], J. Manjarres Ramos[50], D. C. Mankad[168], A. Mann[108], B. Mansoulie[134], S. Manzoni[36], A. Marantis[151,v], G. Marchiori[5], M. Marcisovsky[130], L. Marcoccia[75a,75b], C. Marcon[70a], M. Marinescu[20], M. Marjanovic[119], E. J. Marshall[90], Z. Marshall[17a], S. Marti-Garcia[162], T. A. Martin[166], V. J. Martin[52], B. Martin dit Latour[16], L. Martinelli[74a,74b], M. Martinez[13,w], P. Martinez Agullo[162], V. I. Martinez Outschoorn[102], P. Martinez Suarez[13], S. Martin-Haugh[133], V. S. Martoiu[27b], A. C. Martyniuk[95], A. Marzin[36], S. R. Maschek[109], L. Masetti[99], T. Mashimo[152], J. Masik[100], A. L. Maslennikov[37], L. Massa[23b], P. Massarotti[71a,71b], P. Mastrandrea[73a,73b], A. Mastroberardino[43a,43b], T. Masubuchi[152], T. Mathisen[160], N. Matsuzawa[152], J. Maurer[27b], B. Maček[92], D. A. Maximov[37], R. Mazini[147], I. Maznas[151,f], M. Mazza[106], S. M. Mazza[135], C. Mc Ginn[29], J. P. Mc Gowan[103], S. P. Mc Kee[105], W. P. McCormack[17a], E. F. McDonald[104], A. E. McDougall[113], J. A. Mcfayden[145], G. Mchedlidze[148b], R. P. Mckenzie[33g], T. C. Mclachlan[48], D. J. Mclaughlin[95], K. D. McLean[164], S. J. McMahon[133], P. C. McNamara[104], C. M. Mcpartland[91], R. A. McPherson[164,z], T. Megy[40], S. Mehlhase[108], A. Mehta[91], B. Meirose[45], D. Melini[149], B. R. Mellado Garcia[33g], A. H. Melo[55],

F. Meloni[48], E. D. Mendes Gouveia[129a], A. M. Mendes Jacques Da Costa[20], H. Y. Meng[154], L. Meng[90], S. Menke[109], M. Mentink[36], E. Meoni[43a,43b], C. Merlassino[125], L. Merola[71a,71b], C. Meroni[70a,70b], G. Merz[105], O. Meshkov[37], J. K. R. Meshreki[140], J. Metcalfe[6], A. S. Mete[6], C. Meyer[67], J-P. Meyer[134], M. Michetti[18], R. P. Middleton[133], L. Mijović[52], G. Mikenberg[168], M. Mikestikova[130], M. Mikuž[92], H. Mildner[138], A. Milic[36], C. D. Milke[44], D. W. Miller[39], L. S. Miller[34], A. Milov[168], D. A. Milstead[47a,47b], T. Min[14c], A. A. Minaenko[37], I. A. Minashvili[148b], L. Mince[59], A. I. Mincer[116], B. Mindur[84a], M. Mineev[38], Y. Mino[86], L. M. Mir[13], M. Miralles Lopez[162], M. Mironova[125], M. C. Missio[112], T. Mitani[167], A. Mitra[166], V. A. Mitsou[162], O. Miu[154], P. S. Miyagawa[93], Y. Miyazaki[88], A. Mizukami[82], J. U. Mjörnmark[97], T. Mkrtchyan[63a], T. Mlinarevic[95], M. Mlynarikova[36], T. Moa[47a,47b], S. Mobius[55], K. Mochizuki[107], P. Moder[48], P. Mogg[108], A. F. Mohammed[14a,14d], S. Mohapatra[41], G. Mokgatitswane[33g], B. Mondal[140], S. Mondal[131], K. Mönig[48], E. Monnier[101], L. Monsonis Romero[162], J. Montejo Berlingen[36], M. Montella[118], F. Monticelli[89], N. Morange[66], A. L. Moreira De Carvalho[129a], M. Moreno Llácer[162], C. Moreno Martinez[56], P. Morettini[57b], S. Morgenstern[166], M. Morii[61], M. Morinaga[152], A. K. Morley[36], F. Morodei[74a,74b], L. Morvaj[36], P. Moschovakos[36], B. Moser[36], M. Mosidze[148b], T. Moskalets[54], P. Moskvitina[112], J. Moss[31,p], E. J. W. Moyse[102], O. Mtintsilana[33g], S. Muanza[101], J. Mueller[128], D. Muenstermann[90], R. Müller[19], G. A. Mullier[160], J. J. Mullin[127], D. P. Mungo[154], J. L. Munoz Martinez[13], D. Munoz Perez[162], F. J. Munoz Sanchez[100], M. Murin[100], W. J. Murray[133,166], A. Murrone[70a,70b], J. M. Muse[119], M. Muškinja[17a], C. Mwewa[29], A. G. Myagkov[37,a], A. J. Myers[8], A. A. Myers[128], G. Myers[67], M. Myska[131], B. P. Nachman[17a], O. Nackenhorst[49], A. Nag[50], K. Nagai[125], K. Nagano[82], J. L. Nagle[29,am], E. Nagy[101], A. M. Nairz[36], Y. Nakahama[82], K. Nakamura[82], H. Nanjo[123], R. Narayan[44], E. A. Narayanan[111], I. Naryshkin[37], M. Naseri[34], C. Nass[24], G. Navarro[22a], J. Navarro-Gonzalez[162], R. Nayak[150], A. Nayaz[18], P. Y. Nechaeva[37], F. Nechansky[48], L. Nedic[125], T. J. Neep[20], A. Negri[72a,72b], M. Negrini[23b], C. Nellist[112], C. Nelson[103], K. Nelson[105], S. Nemecek[130], M. Nessi[36,i], M. S. Neubauer[161], F. Neuhaus[99], J. Neundorf[48], R. Newhouse[163], P. R. Newman[20], C. W. Ng[128], Y. S. Ng[18], Y. W. Y. Ng[48], B. Ngair[35e], H. D. N. Nguyen[107], R. B. Nickerson[125], R. Nicolaidou[134], J. Nielsen[135], M. Niemeyer[55], N. Nikiforou[36], V. Nikolaenko[37,a], I. Nikolic-Audit[126], K. Nikolopoulos[20], P. Nilsson[29], H. R. Nindhito[56], A. Nisati[74a], N. Nishu[2], R. Nisius[109], J-E. Nitschke[50], E. K. Nkadimeng[33g], S. J. Noacco Rosende[89], T. Nobe[152], D. L. Noel[32], Y. Noguchi[86], T. Nommensen[146], M. A. Nomura[29], M. B. Norfolk[138], R. R. B. Norisam[95], B. J. Norman[34], J. Novak[92], T. Novak[48], O. Novgorodova[50], L. Novotny[131], R. Novotny[111], L. Nozka[121], K. Ntekas[159], N. M. J. Nunes De Moura Junior[81b], E. Nurse[95], F. G. Oakham[34,aj], J. Ocariz[126], A. Ochi[83], I. Ochoa[129a], S. Oerdek[160], A. Ogrodnik[84a], A. Oh[100], C. C. Ohm[143], H. Oide[82], R. Oishi[152], M. L. Ojeda[48], Y. Okazaki[86], M. W. O'Keefe[91], Y. Okumura[152], A. Olariu[27b], L. F. Oleiro Seabra[129a], S. A. Olivares Pino[136e], D. Oliveira Damazio[29], D. Oliveira Goncalves[81a], J. L. Oliver[159], M. J. R. Olsson[159], A. Olszewski[85], J. Olszowska[85,*], Ö. O. Öncel[54], D. C. O'Neil[141], A. P. O'Neill[19], A. Onofre[129a,129e], P. U. E. Onyisi[11], M. J. Oreglia[39], G. E. Orellana[89], D. Orestano[76a,76b], N. Orlando[13], R. S. Orr[154], V. O'Shea[59], R. Ospanov[62a], G. Otero y Garzon[30], H. Otono[88], P. S. Ott[63a], G. J. Ottino[17a], M. Ouchrif[35d], J. Ouellette[29,am], F. Ould-Saada[124], M. Owen[59], R. E. Owen[133], K. Y. Oyulmaz[21a], V. E. Ozcan[21a], N. Ozturk[8], S. Ozturk[21d], J. Pacalt[121], H. A. Pacey[32], A. Pacheco Pages[13], C. Padilla Aranda[13], G. Padovano[74a,74b], S. Pagan Griso[17a], G. Palacino[67], A. Palazzo[69a,69b], S. Palestini[36], M. Palka[84b], J. Pan[171], T. Pan[64a], D. K. Panchal[11], C. E. Pandini[113], J. G. Panduro Vazquez[94], H. Pang[14b], P. Pani[48], G. Panizzo[68a,68c], L. Paolozzi[56], C. Papadatos[107], S. Parajuli[44], A. Paramonov[6], C. Paraskevopoulos[10], D. Paredes Hernandez[64b], T. H. Park[154], M. A. Parker[32], F. Parodi[57a,57b], E. W. Parrish[114], V. A. Parrish[52], J. A. Parsons[41], U. Parzefall[54], B. Pascual Dias[107], L. Pascual Dominguez[150], V. R. Pascuzzi[17a], F. Pasquali[113], E. Pasqualucci[74a], S. Passaggio[57b], F. Pastore[94], P. Pasuwan[47a,47b], P. Patel[85], J. R. Pater[100], T. Pauly[36], J. Pearkes[142], M. Pedersen[124], R. Pedro[129a], S. V. Peleganchuk[37], O. Penc[36], E. A. Pender[52], C. Peng[64b], H. Peng[62a], K. E. Penski[108], M. Penzin[37], B. S. Peralva[81d], A. P. Pereira Peixoto[60], L. Pereira Sanchez[47a,47b], D. V. Perepelitsa[29,am], E. Perez Codina[155a], M. Perganti[10], L. Perini[70a,70b,*], H. Pernegger[36], A. Perrevoort[112], O. Perrin[40], K. Peters[48], R. F. Y. Peters[100], B. A. Petersen[36], T. C. Petersen[42], E. Petit[101], V. Petousis[131], C. Petridou[151,f], A. Petrukhin[140], M. Pettee[17a], N. E. Pettersson[36], A. Petukhov[37], K. Petukhova[132], A. Peyaud[134], R. Pezoa[136f], L. Pezzotti[36], G. Pezzullo[171], T. M. Pham[169], T. Pham[104], P. W. Phillips[133], M. W. Phipps[161], G. Piacquadio[144], E. Pianori[17a], F. Piazza[70a,70b], R. Piegaia[30], D. Pietreanu[27b], A. D. Pilkington[100], M. Pinamonti[68a,68c], J. L. Pinfold[2], B. C. Pinheiro Pereira[129a], C. Pitman Donaldson[95], D. A. Pizzi[34], L. Pizzimento[75a,75b], A. Pizzini[113], M.-A. Pleier[29], V. Plesanovs[54], V. Pleskot[132], E. Plotnikova[38],

G. Poddar[4], R. Poettgen[97], L. Poggioli[126], I. Pogrebnyak[106], D. Pohl[24], I. Pokharel[55], S. Polacek[132], G. Polesello[72a], A. Poley[141,155a], R. Polifka[131], A. Polini[23b], C. S. Pollard[125], Z. B. Pollock[118], V. Polychronakos[29], E. Pompa Pacchi[74a,74b], D. Ponomarenko[37], L. Pontecorvo[36], S. Popa[27a], G. A. Popeneciu[27d], D. M. Portillo Quintero[155a], S. Pospisil[131], P. Postolache[27c], K. Potamianos[125], I. N. Potrap[38], C. J. Potter[32], H. Potti[1], T. Poulsen[48], J. Poveda[162], M. E. Pozo Astigarraga[36], A. Prades Ibanez[162], M. M. Prapa[46], J. Pretel[54], D. Price[100], M. Primavera[69a], M. A. Principe Martin[98], R. Privara[121], M. L. Proffitt[137], N. Proklova[127], K. Prokofiev[64c], G. Proto[75a,75b], S. Protopopescu[29], J. Proudfoot[6], M. Przybycien[84a], J. E. Puddefoot[138], D. Pudzha[37], P. Puzo[66], D. Pyatiizbyantseva[37], J. Qian[105], D. Qichen[100], Y. Qin[100], T. Qiu[93], A. Quadt[55], M. Queitsch-Maitland[100], G. Quetant[56], G. Rabanal Bolanos[61], D. Rafanoharana[54], F. Ragusa[70a,70b], J. L. Rainbolt[39], J. A. Raine[56], S. Rajagopalan[29], E. Ramakoti[37], K. Ran[14d,48], N. P. Rapheeha[33g], V. Raskina[126], D. F. Rassloff[63a], S. Rave[99], B. Ravina[55], I. Ravinovich[168], M. Raymond[36], A. L. Read[124], N. P. Readioff[138], D. M. Rebuzzi[72a,72b], G. Redlinger[29], K. Reeves[45], J. A. Reidelsturz[170], D. Reikher[150], A. Reiss[99], A. Rej[140], C. Rembser[36], A. Renardi[48], M. Renda[27b], M. B. Rendel[109], F. Renner[48], A. G. Rennie[59], S. Resconi[70a], M. Ressegotti[57a,57b], E. D. Resseguie[17a], S. Rettie[36], J. G. Reyes Rivera[106], B. Reynolds[118], E. Reynolds[17a], M. Rezaei Estabragh[170], O. L. Rezanova[37], P. Reznicek[132], E. Ricci[77a,77b], R. Richter[109], S. Richter[47a,47b], E. Richter-Was[84b], M. Ridel[126], P. Rieck[116], P. Riedler[36], M. Rijssenbeek[144], A. Rimoldi[72a,72b], M. Rimoldi[48], L. Rinaldi[23a,23b], T. T. Rinn[29], M. P. Rinnagel[108], G. Ripellino[143], I. Riu[13], P. Rivadeneira[48], J. C. Rivera Vergara[164], F. Rizatdinova[120], E. Rizvi[93], C. Rizzi[56], B. A. Roberts[166], B. R. Roberts[17a], S. H. Robertson[103,z], M. Robin[48], D. Robinson[32], C. M. Robles Gajardo[136f], M. Robles Manzano[99], A. Robson[59], A. Rocchi[75a,75b], C. Roda[73a,73b], S. Rodriguez Bosca[63a], Y. Rodriguez Garcia[22a], A. Rodriguez Rodriguez[54], A. M. Rodríguez Vera[155b], S. Roe[36], J. T. Roemer[159], A. R. Roepe-Gier[119], J. Roggel[170], O. Røhne[124], R. A. Rojas[164], B. Roland[54], C. P. A. Roland[67], J. Roloff[29], A. Romaniouk[37], E. Romano[72a,72b], M. Romano[23b], A. C. Romero Hernandez[161], N. Rompotis[91], L. Roos[126], S. Rosati[74a], B. J. Rosser[39], E. Rossi[4], E. Rossi[71a,71b], L. P. Rossi[57b], L. Rossini[48], R. Rosten[118], M. Rotaru[27b], B. Rottler[54], D. Rousseau[66], D. Rousso[32], G. Rovelli[72a,72b], A. Roy[161], A. Rozanov[101], Y. Rozen[149], X. Ruan[33g], A. Rubio Jimenez[162], A. J. Ruby[91], V. H. Ruelas Rivera[18], T. A. Ruggeri[1], F. Rühr[54], A. Ruiz-Martinez[162], A. Rummler[36], Z. Rurikova[54], N. A. Rusakovich[38], H. L. Russell[164], J. P. Rutherfoord[7], K. Rybacki[90], M. Rybar[132], E. B. Rye[124], A. Ryzhov[37], J. A. Sabater Iglesias[56], P. Sabatini[162], L. Sabetta[74a,74b], H.F-W. Sadrozinski[135], F. Safai Tehrani[74a], B. Safarzadeh Samani[145], M. Safdari[142], S. Saha[103], M. Sahinsoy[109], M. Saimpert[134], M. Saito[152], T. Saito[152], D. Salamani[36], G. Salamanna[76a,76b], A. Salnikov[142], J. Salt[162], A. Salvador Salas[13], D. Salvatore[43a,43b], F. Salvatore[145], A. Salzburger[36], D. Sammel[54], D. Sampsonidis[151,f], D. Sampsonidou[62c,62d], J. Sánchez[162], A. Sanchez Pineda[4], V. Sanchez Sebastian[162], H. Sandaker[124], C. O. Sander[48], J. A. Sandesara[102], M. Sandhoff[170], C. Sandoval[22b], D. P. C. Sankey[133], A. Sansoni[53], L. Santi[74a,74b], C. Santoni[40], H. Santos[129a,129b], S. N. Santpur[17a], A. Santra[168], K. A. Saoucha[138], J. G. Saraiva[129a,129d], J. Sardain[7], O. Sasaki[82], K. Sato[156], C. Sauer[63b], F. Sauerburger[54], E. Sauvan[4], P. Savard[154,aj], R. Sawada[152], C. Sawyer[133], L. Sawyer[96], I. Sayago Galvan[162], C. Sbarra[23b], A. Sbrizzi[23a,23b], T. Scanlon[95], J. Schaarschmidt[137], P. Schacht[109], D. Schaefer[39], U. Schäfer[99], A. C. Schaffer[66], D. Schaile[108], R. D. Schamberger[144], E. Schanet[108], C. Scharf[18], M. M. Schefer[19], V. A. Schegelsky[37], D. Scheirich[132], F. Schenck[18], M. Schernau[159], C. Scheulen[55], C. Schiavi[57a,57b], Z. M. Schillaci[26], E. J. Schioppa[69a,69b], M. Schioppa[43a,43b], B. Schlag[99], K. E. Schleicher[54], S. Schlenker[36], J. Schmeing[170], M. A. Schmidt[170], K. Schmieden[99], C. Schmitt[99], S. Schmitt[48], L. Schoeffel[134], A. Schoening[63b], P. G. Scholer[54], E. Schopf[125], M. Schott[99], J. Schovancova[36], S. Schramm[56], F. Schroeder[170], H-C. Schultz-Coulon[63a], M. Schumacher[54], B. A. Schumm[135], Ph. Schune[134], A. Schwartzman[142], T. A. Schwarz[105], Ph. Schwemling[134], R. Schwienhorst[106], A. Sciandra[135], G. Sciolla[26], F. Scuri[73a], F. Scutti[104], C. D. Sebastiani[91], K. Sedlaczek[49], P. Seema[18], S. C. Seidel[111], A. Seiden[135], B. D. Seidlitz[41], T. Seiss[39], C. Seitz[48], J. M. Seixas[81b], G. Sekhniaidze[71a], S. J. Sekula[44], L. Selem[4], N. Semprini-Cesari[23a,23b], S. Sen[51], D. Sengupta[56], V. Senthilkumar[162], L. Serin[66], L. Serkin[68a,68b], M. Sessa[76a,76b], H. Severini[119], S. Sevova[142], F. Sforza[57a,57b], A. Sfyrla[56], E. Shabalina[55], R. Shaheen[143], J. D. Shahinian[127], D. Shaked Renous[168], L. Y. Shan[14a], M. Shapiro[17a], A. Sharma[36], A. S. Sharma[163], P. Sharma[79], S. Sharma[48], P. B. Shatalov[37], K. Shaw[145], S. M. Shaw[100], Q. Shen[5,62c], P. Sherwood[95], L. Shi[95], C. O. Shimmin[171], Y. Shimogama[167], J. D. Shinner[94], I. P. J. Shipsey[125], S. Shirabe[60], M. Shiyakova[38,y], J. Shlomi[168], M. J. Shochet[39], J. Shojaii[104], D. R. Shope[124], S. Shrestha[118,an],

E. M. Shrif[33g], M. J. Shroff[164], P. Sicho[130], A. M. Sickles[161], E. Sideras Haddad[33g], A. Sidoti[23b], F. Siegert[50], Dj. Sijacki[15], R. Sikora[84a], F. Sili[89], J. M. Silva[20], M. V. Silva Oliveira[36], S. B. Silverstein[47a], S. Simion[66], R. Simoniello[36], E. L. Simpson[59], N. D. Simpson[97], S. Simsek[21d], S. Sindhu[55], P. Sinervo[154], V. Sinetckii[37], S. Singh[141], S. Singh[154], S. Sinha[48], S. Sinha[33g], M. Sioli[23a,23b], I. Siral[36], S.Yu. Sivoklokov[37,*], J. Sjölin[47a,47b], A. Skaf[55], E. Skorda[97], P. Skubic[119], M. Slawinska[85], V. Smakhtin[168], B. H. Smart[133], J. Smiesko[36], S.Yu. Smirnov[37], Y. Smirnov[37], L. N. Smirnova[37,a], O. Smirnova[97], A. C. Smith[41], E. A. Smith[39], H. A. Smith[125], J. L. Smith[91], R. Smith[142], M. Smizanska[90], K. Smolek[131], A. Smykiewicz[85], A. A. Snesarev[37], H. L. Snoek[113], S. Snyder[29], R. Sobie[164,z], A. Soffer[150], C. A. Solans Sanchez[36], E.Yu. Soldatov[37], U. Soldevila[162], A. A. Solodkov[37], S. Solomon[54], A. Soloshenko[38], K. Solovieva[54], O. V. Solovyanov[37], V. Solovyev[37], P. Sommer[36], A. Sonay[13], W. Y. Song[155b], A. Sopczak[131], A. L. Sopio[95], F. Sopkova[28b], V. Sothilingam[63a], S. Sottocornola[72a,72b], R. Soualah[115b], Z. Soumaimi[35e], D. South[48], S. Spagnolo[69a,69b], M. Spalla[109], F. Spanò[94], D. Sperlich[54], G. Spigo[36], M. Spina[145], S. Spinali[90], D. P. Spiteri[59], M. Spousta[132], E. J. Staats[34], A. Stabile[70a,70b], R. Stamen[63a], M. Stamenkovic[113], A. Stampekis[20], M. Standke[24], E. Stanecka[85], M. V. Stange[50], B. Stanislaus[17a], M. M. Stanitzki[48], M. Stankaityte[125], B. Stapf[48], E. A. Starchenko[37], G. H. Stark[135], J. Stark[101,ad], D. M. Starko[155b], P. Staroba[130], P. Starovoitov[63a], S. Stärz[103], R. Staszewski[85], G. Stavropoulos[46], J. Steentoft[160], P. Steinberg[29], A. L. Steinhebel[122], B. Stelzer[141,155a], H. J. Stelzer[128], O. Stelzer-Chilton[155a], H. Stenzel[58], T. J. Stevenson[145], G. A. Stewart[36], M. C. Stockton[36], G. Stoicea[27b], M. Stolarski[129a], S. Stonjek[109], A. Straessner[50], J. Strandberg[143], S. Strandberg[47a,47b], M. Strauss[119], T. Strebler[101], P. Strizenec[28b], R. Ströhmer[165], D. M. Strom[122], L. R. Strom[48], R. Stroynowski[44], A. Strubig[47a,47b], S. A. Stucci[29], B. Stugu[16], J. Stupak[119], N. A. Styles[48], D. Su[142], S. Su[62a], W. Su[62c,62d,137], X. Su[62a,66], K. Sugizaki[152], V. V. Sulin[37], M. J. Sullivan[91], D. M. S. Sultan[77a,77b], L. Sultanaliyeva[37], S. Sultansoy[3b], T. Sumida[86], S. Sun[105], S. Sun[169], O. Sunneborn Gudnadottir[160], M. R. Sutton[145], M. Svatos[130], M. Swiatlowski[155a], T. Swirski[165], I. Sykora[28a], M. Sykora[132], T. Sykora[132], D. Ta[99], K. Tackmann[48,x], A. Taffard[159], R. Tafirout[155a], J. S. Tafoya Vargas[66], R. H. M. Taibah[126], R. Takashima[87], K. Takeda[83], E. P. Takeva[52], Y. Takubo[82], M. Talby[101], A. A. Talyshev[37], K. C. Tam[64b], N. M. Tamir[150], A. Tanaka[152], J. Tanaka[152], R. Tanaka[66], M. Tanasini[57a,57b], J. Tang[62c], Z. Tao[163], S. Tapia Araya[80], S. Tapprogge[99], A. Tarek Abouelfadl Mohamed[106], S. Tarem[149], K. Tariq[62b], G. Tarna[27b,101], G. F. Tartarelli[70a], P. Tas[132], M. Tasevsky[130], E. Tassi[43a,43b], A. C. Tate[161], G. Tateno[152], Y. Tayalati[35e], G. N. Taylor[104], W. Taylor[155b], H. Teagle[91], A. S. Tee[169], R. Teixeira De Lima[142], P. Teixeira-Dias[94], J. J. Teoh[154], K. Terashi[152], J. Terron[98], S. Terzo[13], M. Testa[53], R. J. Teuscher[154,z], A. Thaler[78], O. Theiner[56], N. Themistokleous[52], T. Theveneaux-Pelzer[18], O. Thielmann[170], D. W. Thomas[94], J. P. Thomas[20], E. A. Thompson[48], P. D. Thompson[20], E. Thomson[127], E. J. Thorpe[93], Y. Tian[55], V. Tikhomirov[37,a], Yu.A. Tikhonov[37], S. Timoshenko[37], E. X. L. Ting[1], P. Tipton[171], S. Tisserant[101], S. H. Tlou[33g], A. Tnourji[40], K. Todome[23a,23b], S. Todorova-Nova[132], S. Todt[50], M. Togawa[82], J. Tojo[88], S. Tokár[28a], K. Tokushuku[82], R. Tombs[32], M. Tomoto[82,110], L. Tompkins[142,r], K. W. Topolnicki[84b], P. Tornambe[102], E. Torrence[122], H. Torres[50], E. Torró Pastor[162], M. Toscani[30], C. Tosciri[39], M. Tost[11], D. R. Tovey[138], A. Traeet[16], I. S. Trandafir[27b], T. Trefzger[165], A. Tricoli[29], I. M. Trigger[155a], S. Trincaz-Duvoid[126], D. A. Trischuk[26], B. Trocmé[60], A. Trofymov[66], C. Troncon[70a], L. Truong[33c], M. Trzebinski[85], A. Trzupek[85], F. Tsai[144], M. Tsai[105], A. Tsiamis[151,f], P. V. Tsiareshka[37], S. Tsigaridas[155a], A. Tsirigotis[151,v], V. Tsiskaridze[144], E. G. Tskhadadze[148a], M. Tsopoulou[151,f], Y. Tsujikawa[86], I. I. Tsukerman[37], V. Tsulaia[17a], S. Tsuno[82], O. Tsur[149], D. Tsybychev[144], Y. Tu[64b], A. Tudorache[27b], V. Tudorache[27b], A. N. Tuna[36], S. Turchikhin[38], I. Turk Cakir[3a], R. Turra[70a], T. Turtuvshin[38,aa], P. M. Tuts[41], S. Tzamarias[151,f], P. Tzanis[10], E. Tzovara[99], K. Uchida[152], F. Ukegawa[156], P. A. Ulloa Poblete[136c], E. N. Umaka[80], G. Unal[36], M. Unal[11], A. Undrus[29], G. Unel[159], J. Urban[28b], P. Urquijo[104], G. Usai[8], R. Ushioda[153], M. Usman[107], Z. Uysal[21b], L. Vacavant[101], V. Vacek[131], B. Vachon[103], K. O. H. Vadla[124], T. Vafeiadis[36], A. Vaitkus[95], C. Valderanis[108], E. Valdes Santurio[47a,47b], M. Valente[155a], S. Valentinetti[23a,23b], A. Valero[162], A. Vallier[101,ad], J. A. Valls Ferrer[162], T. R. Van Daalen[137], P. Van Gemmeren[6], M. Van Rijnbach[36,124], S. Van Stroud[95], I. Van Vulpen[113], M. Vanadia[75a,75b], W. Vandelli[36], M. Vandenbroucke[134], E. R. Vandewall[120], D. Vannicola[150], L. Vannoli[57a,57b], R. Vari[74a], E. W. Varnes[7], C. Varni[17a], T. Varol[147], D. Varouchas[66], L. Varriale[162], K. E. Varvell[146], M. E. Vasile[27b], L. Vaslin[40], G. A. Vasquez[164], F. Vazeille[40], T. Vazquez Schroeder[36], J. Veatch[31], V. Vecchio[100], M. J. Veen[102], I. Veliscek[125], L. M. Veloce[154], F. Veloso[129a,129c], S. Veneziano[74a], A. Ventura[69a,69b], A. Verbytskyi[109], M. Verducci[73a,73b], C. Vergis[24], M. Verissimo De Araujo[81b],

W. Verkerke[113], J. C. Vermeulen[113], C. Vernieri[142], P. J. Verschuuren[94], M. Vessella[102], M. C. Vetterli[141,aj], A. Vgenopoulos[151,f], N. Viaux Maira[136f], T. Vickey[138], O. E. Vickey Boeriu[138], G. H. A. Viehhauser[125], L. Vigani[63b], M. Villa[23a,23b], M. Villaplana Perez[162], E. M. Villhauer[52], E. Vilucchi[53], M. G. Vincter[34], G. S. Virdee[20], A. Vishwakarma[52], C. Vittori[23a,23b], I. Vivarelli[145], V. Vladimirov[166], E. Voevodina[109], F. Vogel[108], P. Vokac[131], J. Von Ahnen[48], E. Von Toerne[24], B. Vormwald[36], V. Vorobel[132], K. Vorobev[37], M. Vos[162], J. H. Vossebeld[91], M. Vozak[113], L. Vozdecky[93], N. Vranjes[15], M. Vranjes Milosavljevic[15], M. Vreeswijk[113], R. Vuillermet[36], O. Vujinovic[99], I. Vukotic[39], S. Wada[156], C. Wagner[102], W. Wagner[170], S. Wahdan[170], H. Wahlberg[89], R. Wakasa[156], M. Wakida[110], V. M. Walbrecht[109], J. Walder[133], R. Walker[108], W. Walkowiak[140], A. M. Wang[61], A. Z. Wang[169], C. Wang[62a], C. Wang[62c], H. Wang[17a], J. Wang[64a], R.-J. Wang[99], R. Wang[61], R. Wang[6], S. M. Wang[147], S. Wang[62b], T. Wang[62a], W. T. Wang[79], X. Wang[14c], X. Wang[161], X. Wang[62c], Y. Wang[62d], Y. Wang[14c], Z. Wang[105], Z. Wang[51,62c,62d], Z. Wang[105], A. Warburton[103], R. J. Ward[20], N. Warrack[59], A. T. Watson[20], H. Watson[59], M. F. Watson[20], G. Watts[137], B. M. Waugh[95], A. F. Webb[11], C. Weber[29], H. A. Weber[18], M. S. Weber[19], S. M. Weber[63a], C. Wei[62a], Y. Wei[125], A. R. Weidberg[125], J. Weingarten[49], M. Weirich[99], C. Weiser[54], C. J. Wells[48], T. Wenaus[29], B. Wendland[49], T. Wengler[36], N. S. Wenke[109], N. Wermes[24], M. Wessels[63a], K. Whalen[122], A. M. Wharton[90], A. S. White[61], A. White[8], M. J. White[1], D. Whiteson[159], L. Wickremasinghe[123], W. Wiedenmann[169], C. Wiel[50], M. Wielers[133], N. Wieseotte[99], C. Wiglesworth[42], L. A. M. Wiik-Fuchs[54], D. J. Wilbern[119], H. G. Wilkens[36], D. M. Williams[41], H. H. Williams[127], S. Williams[32], S. Willocq[102], P. J. Windischhofer[125], F. Winklmeier[122], B. T. Winter[54], J. K. Winter[100], M. Wittgen[142], M. Wobisch[96], R. Wölker[125], J. Wollrath[159], M. W. Wolter[85], H. Wolters[129a,129c], V. W. S. Wong[163], A. F. Wongel[48], S. D. Worm[48], B. K. Wosiek[85], K. W. Woźniak[85], K. Wraight[59], J. Wu[14a,14d], M. Wu[64a], M. Wu[112], S. L. Wu[169], X. Wu[56], Y. Wu[62a], Z. Wu[62a,134], J. Wuerzinger[125], T. R. Wyatt[100], B. M. Wynne[52], S. Xella[42], L. Xia[14c], M. Xia[14b], J. Xiang[64c], X. Xiao[105], M. Xie[62a], X. Xie[62a], S. Xin[14a,14d], J. Xiong[17a], I. Xiotidis[145], D. Xu[14a], H. Xu[62a], H. Xu[62a], L. Xu[62a], R. Xu[127], T. Xu[105], W. Xu[105], Y. Xu[14b], Z. Xu[62b], Z. Xu[14a], B. Yabsley[146], S. Yacoob[33a], N. Yamaguchi[88], Y. Yamaguchi[153], H. Yamauchi[156], T. Yamazaki[17a], Y. Yamazaki[83], J. Yan[62c], S. Yan[125], Z. Yan[25], H. J. Yang[62c,62d], H. T. Yang[62a], S. Yang[62a], T. Yang[64c], X. Yang[62a], X. Yang[14a], Y. Yang[44], Z. Yang[62a,105], W-M. Yao[17a], Y. C. Yap[48], H. Ye[14c], H. Ye[55], J. Ye[44], S. Ye[29], X. Ye[62a], Y. Yeh[95], I. Yeletskikh[38], B. K. Yeo[17a], M. R. Yexley[90], P. Yin[41], K. Yorita[167], S. Younas[27b], C. J. S. Young[54], C. Young[142], M. Yuan[105], R. Yuan[62b,l], L. Yue[95], X. Yue[63a], M. Zaazoua[35e], B. Zabinski[85], E. Zaid[52], T. Zakareishvili[148b], N. Zakharchuk[34], S. Zambito[56], J. A. Zamora Saa[136b,136d], J. Zang[152], D. Zanzi[54], O. Zaplatilek[131], S. V. Zeißner[49], C. Zeitnitz[170], J. C. Zeng[161], D. T. Zenger Jr[26], O. Zenin[37], T. Ženiš[28a], S. Zenz[93], S. Zerradi[35a], D. Zerwas[66], B. Zhang[14c], D. F. Zhang[138], G. Zhang[14b], J. Zhang[62b], J. Zhang[6], K. Zhang[14a,14d], L. Zhang[14c], P. Zhang[14a,14d], R. Zhang[169], S. Zhang[105], T. Zhang[152], X. Zhang[62c], X. Zhang[62b], Y. Zhang[5,62c], Z. Zhang[17a], Z. Zhang[66], H. Zhao[137], P. Zhao[51], T. Zhao[62b], Y. Zhao[135], Z. Zhao[62a], A. Zhemchugov[38], X. Zheng[62a], Z. Zheng[142], D. Zhong[161], B. Zhou[105], C. Zhou[169], H. Zhou[7], N. Zhou[62c], Y. Zhou[7], C. G. Zhu[62b], C. Zhu[14a,14d], H. L. Zhu[62a], H. Zhu[14a], J. Zhu[105], Y. Zhu[62c], Y. Zhu[62a], X. Zhuang[14a], K. Zhukov[37], V. Zhulanov[37], N. I. Zimine[38], J. Zinsser[63b], M. Ziolkowski[140], L. Živković[15], A. Zoccoli[23a,23b], K. Zoch[56], T. G. Zorbas[138], O. Zormpa[46], W. Zou[41], L. Zwalinski[36]

[1] Department of Physics, University of Adelaide, Adelaide, Australia
[2] Department of Physics, University of Alberta, Edmonton, AB, Canada
[3] [(a)]Department of Physics, Ankara University, Ankara, Türkiye; [(b)]Division of Physics, TOBB University of Economics and Technology, Ankara, Türkiye
[4] LAPP, Université Savoie Mont Blanc, CNRS/IN2P3, Annecy, France
[5] APC, Université Paris Cité, CNRS/IN2P3, Paris, France
[6] High Energy Physics Division, Argonne National Laboratory, Argonne, IL, USA
[7] Department of Physics, University of Arizona, Tucson, AZ, USA
[8] Department of Physics, University of Texas at Arlington, Arlington, TX, USA
[9] Physics Department, National and Kapodistrian University of Athens, Athens, Greece
[10] Physics Department, National Technical University of Athens, Zografou, Greece
[11] Department of Physics, University of Texas at Austin, Austin, TX, USA
[12] Institute of Physics, Azerbaijan Academy of Sciences, Baku, Azerbaijan

[13] Institut de Física d'Altes Energies (IFAE), Barcelona Institute of Science and Technology, Barcelona, Spain
[14] [(a)]Institute of High Energy Physics, Chinese Academy of Sciences, Beijing, China; [(b)]Physics Department, Tsinghua University, Beijing, China; [(c)]Department of Physics, Nanjing University, Nanjing, China; [(d)]University of Chinese Academy of Science (UCAS), Beijing, China
[15] Institute of Physics, University of Belgrade, Belgrade, Serbia
[16] Department for Physics and Technology, University of Bergen, Bergen, Norway
[17] [(a)]Physics Division, Lawrence Berkeley National Laboratory, Berkeley, CA, USA; [(b)]University of California, Berkeley, CA, USA
[18] Institut für Physik, Humboldt Universität zu Berlin, Berlin, Germany
[19] Albert Einstein Center for Fundamental Physics and Laboratory for High Energy Physics, University of Bern, Bern, Switzerland
[20] School of Physics and Astronomy, University of Birmingham, Birmingham, UK
[21] [(a)]Department of Physics, Bogazici University, Istanbul, Türkiye; [(b)]Department of Physics Engineering, Gaziantep University, Gaziantep, Türkiye; [(c)]Department of Physics, Istanbul University, Istanbul, Türkiye; [(d)]Istinye University, Sariyer, Istanbul, Türkiye
[22] [(a)]Facultad de Ciencias y Centro de Investigaciónes, Universidad Antonio Nariño, Bogotá, Colombia; [(b)]Departamento de Física, Universidad Nacional de Colombia, Bogotá, Colombia
[23] [(a)]Dipartimento di Fisica e Astronomia A. Righi, Università di Bologna, Bologna, Italy; [(b)]INFN Sezione di Bologna, Bologna, Italy
[24] Physikalisches Institut, Universität Bonn, Bonn, Germany
[25] Department of Physics, Boston University, Boston, MA, USA
[26] Department of Physics, Brandeis University, Waltham, MA, USA
[27] [(a)]Transilvania University of Brasov, Brasov, Romania; [(b)]Horia Hulubei National Institute of Physics and Nuclear Engineering, Bucharest, Romania; [(c)]Department of Physics, Alexandru Ioan Cuza University of Iasi, Iasi, Romania; [(d)]Physics Department, National Institute for Research and Development of Isotopic and Molecular Technologies, Cluj-Napoca, Romania; [(e)]National University of Science and Technology Politechnica, Bucharest, Romania; [(f)]West University in Timisoara, Timisoara, Romania; [(g)]Faculty of Physics, University of Bucharest, Bucharest, Romania
[28] [(a)]Faculty of Mathematics, Physics and Informatics, Comenius University, Bratislava, Slovakia; [(b)]Department of Subnuclear Physics, Institute of Experimental Physics of the Slovak Academy of Sciences, Kosice, Slovak Republic
[29] Physics Department, Brookhaven National Laboratory, Upton, NY, USA
[30] Departamento de Física, y CONICET, Facultad de Ciencias Exactas y Naturales, Instituto de Física de Buenos Aires (IFIBA), Universidad de Buenos Aires, Buenos Aires, Argentina
[31] California State University, Los Angeles, CA, USA
[32] Cavendish Laboratory, University of Cambridge, Cambridge, UK
[33] [(a)]Department of Physics, University of Cape Town, Cape Town, South Africa; [(b)]iThemba Labs, Western Cape, South Africa; [(c)]Department of Mechanical Engineering Science, University of Johannesburg, Johannesburg, South Africa; [(d)] National Institute of Physics, University of the Philippines, Diliman, Philippines; [(e)]Department of Physics, University of South Africa, Pretoria, South Africa; [(f)]University of Zululand, KwaDlangezwa, South Africa; [(g)]School of Physics, University of the Witwatersrand, Johannesburg, South Africa
[34] Department of Physics, Carleton University, Ottawa, ON, Canada
[35] [(a)]Faculté des Sciences Ain Chock, Réseau Universitaire de Physique des Hautes Energies-Université Hassan II, Casablanca, Morocco; [(b)]Faculté des Sciences, Université Ibn-Tofail, Kénitra, Morocco; [(c)]Faculté des Sciences Semlalia, Université Cadi Ayyad, LPHEA-Marrakech, Morocco; [(d)]LPMR, Faculté des Sciences, Université Mohamed Premier, Oujda, Morocco; [(e)]Faculté des sciences, Université Mohammed V, Rabat, Morocco; [(f)]Institute of Applied Physics, Mohammed VI Polytechnic University, Ben Guerir, Morocco
[36] CERN, Geneva, Switzerland
[37] Affiliated with an Institute Covered by a Cooperation Agreement with CERN, Geneva, Switzerland
[38] Affiliated with an International Laboratory Covered by a Cooperation Agreement with CERN, Geneva, Switzerland
[39] Enrico Fermi Institute, University of Chicago, Chicago, IL, USA
[40] LPC, Université Clermont Auvergne, CNRS/IN2P3, Clermont-Ferrand, France
[41] Nevis Laboratory, Columbia University, Irvington, NY, USA

[42] Niels Bohr Institute, University of Copenhagen, Copenhagen, Denmark
[43] [(a)]Dipartimento di Fisica, Università della Calabria, Rende, Italy; [(b)]INFN Gruppo Collegato di Cosenza, Laboratori Nazionali di Frascati, Frascati, Italy
[44] Physics Department, Southern Methodist University, Dallas, TX, USA
[45] Physics Department, University of Texas at Dallas, Richardson, TX, USA
[46] National Centre for Scientific Research "Demokritos", Agia Paraskevi, Greece
[47] [(a)]Department of Physics, Stockholm University, Stockholm, Sweden; [(b)]Oskar Klein Centre, Stockholm, Sweden
[48] Deutsches Elektronen-Synchrotron DESY, Hamburg and Zeuthen, Germany
[49] Fakultät Physik , Technische Universität Dortmund, Dortmund, Germany
[50] Institut für Kern- und Teilchenphysik, Technische Universität Dresden, Dresden, Germany
[51] Department of Physics, Duke University, Durham, NC, USA
[52] SUPA-School of Physics and Astronomy, University of Edinburgh, Edinburgh, UK
[53] INFN e Laboratori Nazionali di Frascati, Frascati, Italy
[54] Physikalisches Institut, Albert-Ludwigs-Universität Freiburg, Freiburg, Germany
[55] II. Physikalisches Institut, Georg-August-Universität Göttingen, Göttingen, Germany
[56] Département de Physique Nucléaire et Corpusculaire, Université de Genève, Geneva, Switzerland
[57] [(a)]Dipartimento di Fisica, Università di Genova, Genoa, Italy; [(b)]INFN Sezione di Genova, Genoa, Italy
[58] II. Physikalisches Institut, Justus-Liebig-Universität Giessen, Giessen, Germany
[59] SUPA-School of Physics and Astronomy, University of Glasgow, Glasgow, UK
[60] LPSC, Université Grenoble Alpes, CNRS/IN2P3, Grenoble INP, Grenoble, France
[61] Laboratory for Particle Physics and Cosmology, Harvard University, Cambridge, MA, USA
[62] [(a)]Department of Modern Physics and State Key Laboratory of Particle Detection and Electronics, University of Science and Technology of China, Hefei, China; [(b)]Institute of Frontier and Interdisciplinary Science and Key Laboratory of Particle Physics and Particle Irradiation (MOE), Shandong University, Qingdao, China; [(c)]School of Physics and Astronomy, Shanghai Jiao Tong University, Key Laboratory for Particle Astrophysics and Cosmology (MOE), SKLPPC, Shanghai, China; [(d)]Tsung-Dao Lee Institute, Shanghai, China
[63] [(a)]Kirchhoff-Institut für Physik, Ruprecht-Karls-Universität Heidelberg, Heidelberg, Germany; [(b)]Physikalisches Institut, Ruprecht-Karls-Universität Heidelberg, Heidelberg, Germany
[64] [(a)]Department of Physics, Chinese University of Hong Kong, Shatin, N.T., Hong Kong, China; [(b)]Department of Physics, University of Hong Kong, Hong Kong, China; [(c)]Department of Physics and Institute for Advanced Study, Hong Kong University of Science and Technology, Clear Water Bay, Kowloon, Hong Kong, China
[65] Department of Physics, National Tsing Hua University, Hsinchu, Taiwan
[66] IJCLab, Université Paris-Saclay, CNRS/IN2P3, 91405 Orsay, France
[67] Department of Physics, Indiana University, Bloomington, IN, USA
[68] [(a)]INFN Gruppo Collegato di Udine, Sezione di Trieste, Udine, Italy; [(b)]ICTP, Trieste, Italy; [(c)]Dipartimento Politecnico di Ingegneria e Architettura, Università di Udine, Udine, Italy
[69] [(a)]INFN Sezione di Lecce, Lecce, Italy; [(b)]Dipartimento di Matematica e Fisica, Università del Salento, Lecce, Italy
[70] [(a)]INFN Sezione di Milano, Milan, Italy; [(b)]Dipartimento di Fisica, Università di Milano, Milan, Italy
[71] [(a)]INFN Sezione di Napoli, Naples, Italy; [(b)]Dipartimento di Fisica, Università di Napoli, Naples, Italy
[72] [(a)]INFN Sezione di Pavia, Pavia, Italy; [(b)]Dipartimento di Fisica, Università di Pavia, Pavia, Italy
[73] [(a)]INFN Sezione di Pisa, Pisa, Italy; [(b)]Dipartimento di Fisica E. Fermi, Università di Pisa, Pisa, Italy
[74] [(a)]INFN Sezione di Roma, Rome, Italy; [(b)]Dipartimento di Fisica, Sapienza Università di Roma, Rome, Italy
[75] [(a)]INFN Sezione di Roma Tor Vergata, Rome, Italy; [(b)]Dipartimento di Fisica, Università di Roma Tor Vergata, Rome, Italy
[76] [(a)]INFN Sezione di Roma Tre, Rome, Italy; [(b)]Dipartimento di Matematica e Fisica, Università Roma Tre, Rome, Italy
[77] [(a)]INFN-TIFPA, Povo, Italy; [(b)]Università degli Studi di Trento, Trento, Italy
[78] Department of Astro and Particle Physics, Universität Innsbruck, Innsbruck, Austria
[79] University of Iowa, Iowa City, IA, USA
[80] Department of Physics and Astronomy, Iowa State University, Ames, IA, USA
[81] [(a)]Departamento de Engenharia Elétrica, Universidade Federal de Juiz de Fora (UFJF), Juiz de Fora, Brazil; [(b)]Universidade Federal do Rio De Janeiro COPPE/EE/IF, Rio de Janeiro, Brazil; [(c)]Instituto de Física, Universidade de São Paulo, São Paulo, Brazil; [(d)]Rio de Janeiro State University, Rio de Janeiro, Brazil
[82] KEK, High Energy Accelerator Research Organization, Tsukuba, Japan

[83] Graduate School of Science, Kobe University, Kobe, Japan
[84] [(a)]AGH University of Krakow, Faculty of Physics and Applied Computer Science, Krakow, Poland; [(b)]Marian Smoluchowski Institute of Physics, Jagiellonian University, Krakow, Poland
[85] Institute of Nuclear Physics Polish Academy of Sciences, Krakow, Poland
[86] Faculty of Science, Kyoto University, Kyoto, Japan
[87] Kyoto University of Education, Kyoto, Japan
[88] Research Center for Advanced Particle Physics and Department of Physics, Kyushu University, Fukuoka, Japan
[89] Instituto de Física La Plata, Universidad Nacional de La Plata and CONICET, La Plata, Argentina
[90] Physics Department, Lancaster University, Lancaster, UK
[91] Oliver Lodge Laboratory, University of Liverpool, Liverpool, UK
[92] Department of Experimental Particle Physics, Jožef Stefan Institute and Department of Physics, University of Ljubljana, Ljubljana, Slovenia
[93] School of Physics and Astronomy, Queen Mary University of London, London, UK
[94] Department of Physics, Royal Holloway University of London, Egham, UK
[95] Department of Physics and Astronomy, University College London, London, UK
[96] Louisiana Tech University, Ruston, LA, USA
[97] Fysiska institutionen, Lunds universitet, Lund, Sweden
[98] Departamento de Física Teorica C-15 and CIAFF, Universidad Autónoma de Madrid, Madrid, Spain
[99] Institut für Physik, Universität Mainz, Mainz, Germany
[100] School of Physics and Astronomy, University of Manchester, Manchester, UK
[101] CPPM, Aix-Marseille Université, CNRS/IN2P3, Marseille, France
[102] Department of Physics, University of Massachusetts, Amherst, MA, USA
[103] Department of Physics, McGill University, Montreal, QC, Canada
[104] School of Physics, University of Melbourne, Victoria, Australia
[105] Department of Physics, University of Michigan, Ann Arbor, MI, USA
[106] Department of Physics and Astronomy, Michigan State University, East Lansing, MI, USA
[107] Group of Particle Physics, University of Montreal, Montreal, QC, Canada
[108] Fakultät für Physik, Ludwig-Maximilians-Universität München, Munich, Germany
[109] Max-Planck-Institut für Physik (Werner-Heisenberg-Institut), Munich, Germany
[110] Graduate School of Science and Kobayashi-Maskawa Institute, Nagoya University, Nagoya, Japan
[111] Department of Physics and Astronomy, University of New Mexico, Albuquerque, NM, USA
[112] Institute for Mathematics, Astrophysics and Particle Physics, Radboud University/Nikhef, Nijmegen, The Netherlands
[113] Nikhef National Institute for Subatomic Physics and University of Amsterdam, Amsterdam, The Netherlands
[114] Department of Physics, Northern Illinois University, DeKalb, IL, USA
[115] [(a)]New York University Abu Dhabi, Abu Dhabi, United Arab Emirates; [(b)]University of Sharjah, Sharjah, United Arab Emirates
[116] Department of Physics, New York University, New York, NY, USA
[117] Ochanomizu University, Otsuka, Bunkyo-ku, Tokyo, Japan
[118] Ohio State University, Columbus, OH, USA
[119] Homer L. Dodge Department of Physics and Astronomy, University of Oklahoma, Norman, OK, USA
[120] Department of Physics, Oklahoma State University, Stillwater, OK, USA
[121] Palacký University, Joint Laboratory of Optics, Olomouc, Czech Republic
[122] Institute for Fundamental Science, University of Oregon, Eugene, OR, USA
[123] Graduate School of Science, Osaka University, Osaka, Japan
[124] Department of Physics, University of Oslo, Oslo, Norway
[125] Department of Physics, Oxford University, Oxford, UK
[126] LPNHE, Sorbonne Université, Université Paris Cité, CNRS/IN2P3, Paris, France
[127] Department of Physics, University of Pennsylvania, Philadelphia, PA, USA
[128] Department of Physics and Astronomy, University of Pittsburgh, Pittsburgh, PA, USA
[129] [(a)]Laboratório de Instrumentação e Física Experimental de Partículas-LIP, Lisbon, Portugal; [(b)]Departamento de Física, Faculdade de Ciências, Universidade de Lisboa, Lisbon, Portugal; [(c)]Departamento de Física, Universidade de Coimbra, Coimbra, Portugal; [(d)]Centro de Física Nuclear da Universidade de Lisboa, Lisbon, Portugal; [(e)]Departamento de Física,

Universidade do Minho, Braga, Portugal; [f]Departamento de Física Teórica y del Cosmos, Universidad de Granada, Granada, Spain; [g]Departamento de Física, Instituto Superior Técnico, Universidade de Lisboa, Lisbon, Portugal
[130] Institute of Physics of the Czech Academy of Sciences, Prague, Czech Republic
[131] Czech Technical University in Prague, Prague, Czech Republic
[132] Charles University, Faculty of Mathematics and Physics, Prague, Czech Republic
[133] Particle Physics Department, Rutherford Appleton Laboratory, Didcot, UK
[134] IRFU, CEA, Université Paris-Saclay, Gif-sur-Yvette, France
[135] Santa Cruz Institute for Particle Physics, University of California Santa Cruz, Santa Cruz, CA, USA
[136] [a]Departamento de Física, Pontificia Universidad Católica de Chile, Santiago, Chile; [b]Millennium Institute for Subatomic physics at high energy frontier (SAPHIR), Santiago, Chile; [c]Instituto de Investigación Multidisciplinario en Ciencia y Tecnología y Departamento de Física, Universidad de La Serena, La Serena, Chile; [d]Department of Physics, Universidad Andres Bello, Santiago, Chile; [e]Instituto de Alta Investigación, Universidad de Tarapacá, Arica, Chile; [f]Departamento de Física, Universidad Técnica Federico Santa María, Valparaíso, Chile
[137] Department of Physics, University of Washington, Seattle, WA, USA
[138] Department of Physics and Astronomy, University of Sheffield, Sheffield, UK
[139] Department of Physics, Shinshu University, Nagano, Japan
[140] Department Physik, Universität Siegen, Siegen, Germany
[141] Department of Physics, Simon Fraser University, Burnaby, BC, Canada
[142] SLAC National Accelerator Laboratory, Stanford, CA, USA
[143] Department of Physics, Royal Institute of Technology, Stockholm, Sweden
[144] Departments of Physics and Astronomy, Stony Brook University, Stony Brook, NY, USA
[145] Department of Physics and Astronomy, University of Sussex, Brighton, UK
[146] School of Physics, University of Sydney, Sydney, Australia
[147] Institute of Physics, Academia Sinica, Taipei, Taiwan
[148] [a]E. Andronikashvili Institute of Physics, Iv. Javakhishvili Tbilisi State University, Tbilisi, Georgia; [b]High Energy Physics Institute, Tbilisi State University, Tbilisi, Georgia; [c]University of Georgia, Tbilisi, Georgia
[149] Department of Physics, Technion, Israel Institute of Technology, Haifa, Israel
[150] Raymond and Beverly Sackler School of Physics and Astronomy, Tel Aviv University, Tel Aviv, Israel
[151] Department of Physics, Aristotle University of Thessaloniki, Thessaloniki, Greece
[152] International Center for Elementary Particle Physics and Department of Physics, University of Tokyo, Tokyo, Japan
[153] Department of Physics, Tokyo Institute of Technology, Tokyo, Japan
[154] Department of Physics, University of Toronto, Toronto, ON, Canada
[155] [a]TRIUMF, Vancouver, BC, Canada; [b]Department of Physics and Astronomy, York University, Toronto, ON, Canada
[156] Division of Physics and Tomonaga Center for the History of the Universe, Faculty of Pure and Applied Sciences, University of Tsukuba, Tsukuba, Japan
[157] Department of Physics and Astronomy, Tufts University, Medford, MA, USA
[158] United Arab Emirates University, Al Ain, United Arab Emirates
[159] Department of Physics and Astronomy, University of California Irvine, Irvine, CA, USA
[160] Department of Physics and Astronomy, University of Uppsala, Uppsala, Sweden
[161] Department of Physics, University of Illinois, Urbana, IL, USA
[162] Instituto de Física Corpuscular (IFIC), Centro Mixto Universidad de Valencia-CSIC, Valencia, Spain
[163] Department of Physics, University of British Columbia, Vancouver, BC, Canada
[164] Department of Physics and Astronomy, University of Victoria, Victoria, BC, Canada
[165] Fakultät für Physik und Astronomie, Julius-Maximilians-Universität Würzburg, Würzburg, Germany
[166] Department of Physics, University of Warwick, Coventry, UK
[167] Waseda University, Tokyo, Japan
[168] Department of Particle Physics and Astrophysics, Weizmann Institute of Science, Rehovot, Israel
[169] Department of Physics, University of Wisconsin, Madison, WI, USA
[170] Fakultät für Mathematik und Naturwissenschaften, Fachgruppe Physik, Bergische Universität Wuppertal, Wuppertal, Germany
[171] Department of Physics, Yale University, New Haven, CT, USA

[a] Also Affiliated with an Institute Covered by a Cooperation Agreement with CERN, Geneva, Switzerland

[b] Also at An-Najah National University, Nablus, Palestine
[c] Also at Borough of Manhattan Community College, City University of New York, New York, NY, USA
[d] Also at Bruno Kessler Foundation, Trento, Italy
[e] Also at Center for High Energy Physics, Peking University, China
[f] Also at Center for Interdisciplinary Research and Innovation (CIRI-AUTH), Thessaloniki, Greece
[g] Also at Centro Studi e Ricerche Enrico Fermi, Rome, Italy
[h] Also at CERN, Geneva, Switzerland
[i] Also at Département de Physique Nucléaire et Corpusculaire, Université de Genève, Geneva, Switzerland
[j] Also at Departament de Fisica de la Universitat Autonoma de Barcelona, Barcelona, Spain
[k] Also at Department of Financial and Management Engineering, University of the Aegean, Chios, Greece
[l] Also at Department of Physics and Astronomy, Michigan State University, East Lansing, MI, USA
[m] Also at Department of Physics and Astronomy, University of Louisville, Louisville, KY, USA
[n] Also at Department of Physics, Ben Gurion University of the Negev, Beer Sheva, Israel
[o] Also at Department of Physics, California State University, East Bay, USA
[p] Also at Department of Physics, California State University, Sacramento, USA
[q] Also at Department of Physics, King's College London, London, UK
[r] Also at Department of Physics, Stanford University, Stanford, CA, USA
[s] Also at Department of Physics, University of Fribourg, Fribourg, Switzerland
[t] Also at Department of Physics, University of Thessaly, Volos, Greece
[u] Also at Department of Physics, Westmont College, Santa Barbara, USA
[v] Also at Hellenic Open University, Patras, Greece
[w] Also at Institucio Catalana de Recerca i Estudis Avancats, ICREA, Barcelona, Spain
[x] Also at Institut für Experimentalphysik, Universität Hamburg, Hamburg, Germany
[y] Also at Institute for Nuclear Research and Nuclear Energy (INRNE) of the Bulgarian Academy of Sciences, Sofia, Bulgaria
[z] Also at Institute of Particle Physics (IPP), Toronto, Canada
[aa] Also at Institute of Physics and Technology, Mongolian Academy of Sciences, Ulaanbaatar, Mongolia
[ab] Also at Institute of Physics, Azerbaijan Academy of Sciences, Baku, Azerbaijan
[ac] Also at Institute of Theoretical Physics, Ilia State University, Tbilisi, Georgia
[ad] Also at L2IT, Université de Toulouse, CNRS/IN2P3, UPS, Toulouse, France
[ae] Also at Lawrence Livermore National Laboratory, Livermore, USA
[af] Also at National Institute of Physics, University of the Philippines, Diliman, Philippines
[ag] Also at RWTH Aachen University, III. Physikalisches Institut A, Aachen, Germany
[ah] Also at Technical University of Munich, Munich, Germany
[ai] Also at The Collaborative Innovation Center of Quantum Matter (CICQM), Beijing, China
[aj] Also at TRIUMF, Vancouver, BC, Canada
[ak] Also at Università di Napoli Parthenope, Naples, Italy
[al] Also at University of Chinese Academy of Sciences (UCAS), Beijing, China
[am] Also at Department of Physics, University of Colorado, Boulder, CO, USA
[an] Also at Washington College, Chestertown, MD, USA
[ao] Also at Yeditepe University, Physics Department, Istanbul, Türkiye
[*] Deceased